EPA/600/7-87/027
December 1987

FUNDAMENTAL COMBUSTION RESEARCH APPLIED TO POLLUTION FORMATION

Volume IV: Engineering Analysis

Prepared By:

C. J. Kau, M. P. Heap, W. R. Seeker, T. J. Tyson

Energy and Environmental Research Corporation
18 Mason
Irvine, California 92718

EPA Contract 68-02-2631

EPA Project Officer W. Steven Lanier
Air and Energy Engineering Research Laboratory
Research Triangle Park, North Carolina 27711

AIR AND ENERGY ENGINEERING RESEARCH LABORATORY
OFFICE OF RESEARCH AND DEVELOPMENT
U.S. ENVIRONMENTAL PROTECTION AGENCY
RESEARCH TRIANGLE PARK, NC 27711

TECHNICAL REPORT DATA
(Please read Instructions on the reverse before completing)

1. REPORT NO.	2.	3. RECIPIENT'S ACCESSION NO.
EPA/600/7-87/-27		PB88 144001/AS

4. TITLE AND SUBTITLE	5. REPORT DATE
Fundamental Combustion Research Applied to Pollution Formation; Volume IV. Engineering Analysis	December 1987
	6. PERFORMING ORGANIZATION CODE
7. AUTHOR(S)	8. PERFORMING ORGANIZATION REPORT NO.
C. J. Kau, M. P. Heap, W. R. Seeker, and T. J. Tyson	
9. PERFORMING ORGANIZATION NAME AND ADDRESS	10. PROGRAM ELEMENT NO.
Energy and Environmental Research Corporation 18 Mason Irvine, California 92718	11. CONTRACT/GRANT NO. 68-02-2631
12. SPONSORING AGENCY NAME AND ADDRESS	13. TYPE OF REPORT AND PERIOD COVERED
EPA, Office of Research and Development Air and Energy Engineering Research Laboratory **Research Triangle Park, NC 27711**	Final; 1/77 - 9/80 14. SPONSORING AGENCY CODE **EPA/600/13**

15. SUPPLEMENTARY NOTES AEERL project officer W. Steven Lanier is no longer with the Agency. For details contact William P. Linak, Mail Drop 65, 919/541-5792. Volume I of this series is EPA-600/7-85-048.

16. ABSTRACT The report is the fourth and final volume in a series documenting research activities under the EPA's Fundamental Combustion Research (FCR) program applied to pollution formation. The FCR program had three major objectives: (1) to generate an understanding of combustion behavior necessary to help develop control strategies to minimize NOx emissions from stationary sources, (2) to develop engineering models which would allow effective utilization of a large body of fundamental information in the development of new NOx control techniques, and (3) to identify critical information necessary for low-NOx combustor development and to generate it in a time frame consistent with the needs of EPA's technology development programs. The report documents FCR program efforts to develop engineering design models. Six modeling studies were conducted in support of FCR: (1) a computer program for general flame analysis, (2) mathematical modeling of microscale combustion of a coal particle, (3) data analysis through inverse techniques, (4) microscale mixing in turbulent diffusion flames, (5) a numerical model for a two-phase one-dimensional flow reactor, and (6) generation of elliptic-code test cases.

17. KEY WORDS AND DOCUMENT ANALYSIS

a. DESCRIPTORS	b. IDENTIFIERS/OPEN ENDED TERMS	c. COSATI Field/Group
Pollution Mathematical Models Combustion Research Nitrogen Oxides Flames Analyzing Coal Turbulent Diffusion	Pollution Control Stationary Sources	13B 14B 12A 21B 21B 14F 14G 07B

18. DISTRIBUTION STATEMENT	19. SECURITY CLASS *(This Report)*	21. NO. OF PAGES
Release to Public	**Unclassified**	210
	20. SECURITY CLASS *(This page)* **Unclassified**	22. PRICE

EPA Form 2220-1 (9-73)

NOTICE

This document has been reviewed in accordance with U.S. Environmental Protection Agency policy and approved for publication. Mention of trade names or commercial products does not constitute endorsement or recommendation for use.

ABSTRACT

This document is the final volume in a four volume series describing research work performed under the Fundamental Combustion Research (FCR) Applied to Pollution Control Program (EPA contract 68-02-2631). Volumes I, II, and III in the report series document a wide range of experimental research efforts conducted as part of FCR. Volume IV reports on six numerical modeling studies performed in support of the overall FCR effort. Part 1 documents development of "A Computer Program for General Flame Analysis" which is a code for analyzing detailed chemistry in various types of premixed and simple diffusional flames. Part 2 is entitled "Mathematical Modeling of Microscale Combustion of a Coal Particle." This code was developed in support of experimental FCR program studies to better understand details of coal particle devolatilization and burnout. Part 3 documents attempts to develop a computer code to extract information on turbulent diffusivity and pollutant formation rates based on limited data collected from complex furnace flames. Part 4 addresses modeling of turbulent diffusion flames and documents a computational procedure describing chemical reaction processes in large-scale coherent turbulent structures. Part 5 describes a computer procedure developed to model coal-fired well-stirred reactors. This effort was in direct support of one of the FCR program experimental activities. The final part of Volume IV is entitled "Generation of Elliptic-Code Test Cases." It describes a series of critical test cases which can be used to evaluate the numerical procedures incorporated into fluid mechanics codes for solving the elliptic Navier-Stokes equations.

TABLE OF CONTENTS*

FIGURES*

(*)Each part of this volume is accompanied by detailed table of contents, list of figures, and list of tables.

EXECUTIVE SUMMARY

The Fundamental Combustion Research Applied to Pollution Control Program (FCR) had three major objectives. These were:

- To generate an understanding of combustor behavior necessary to aid the Combustion Research Branch (CRB) in development of control strategies to minimize NO_x emissions from stationary sources.
- To develop engineering models which would allow effective utilization of a large body of fundamental information in the development of new NO_x control techniques.
- To identify critical information necessary for low-NO_x combustor development and to generate it in a time frame which was consistent with the needs of the CRB technology development programs.

The overall goal of the CRB, and hence FCR, was to provide the technology for maximum control of NO_x emissions from stationary sources. The intent of FCR was to develop a focused program directed at important issues relevant to the CRB so that the results could be applied in a relatively short time period. The program plan emphasized well defined priority target areas, and the ensuing research effort was always guided towards engineering solutions to specific problems. There was a conscious effort to avoid projects that did not provide information critical to the needs of the CRB. Consequently, it was necessary to isolate relevant issues and direct the program away from the studies of physics and chemistry of combustion which were not relevant to the goals of the CRB.

Fifty-six percent of the annual emission of nitrogen oxides from stationary sources in this country emanate from the single combustor category of boilers firing coal or oil. The dominant characteristics of combustors can be described as follows:

- The flames are large, with energy release zones whose dimensions are on the order of tens of feet.
- The time mean motion is in steady state.
- Pressure is atmospheric.
- Radiation heat transfer dominates exchange from the heat release zone to the cold confining walls.
- Mass and thermal transport is turbulent.

- Fuel/air contacting occurs by diffusion and particle penetration.
- Fuels are injected as solids or liquids giving rise to two-phase transport and both homogeneous and heterogeneous reactions.
- The high fuel-bound nitrogen content of coal and residual fuel generally requires that NO_x emissions be minimized by the application of staged combustion.

Thus, the primary initial objective of FCR was to immediately establish a subcontractor-oriented program of fundamental investigations that focused on the control of NO_x from large, confined, one-atmosphere turbulent diffusion flames burning heavy residual oil and pulverized coal. This section describes the FCR programming structure and describes the goals of Volume 4.

The combustion of pulverized coal and oil in stationary combustors involves the use of burners, of which there are many commercial designs. For the purposes of this discussion, a burner will be considered a device which allows fuel and air to be injected in such a way as to provide a stable flame whose characteristics are suited to a given combustion chamber. Pulverized coal is injected either through annular or axial nozzles with spreading devices. Liquid fuels are normally broken into droplets by atomizers of many different designs which produce different fuel spray characteristics (spray angle, spray type, drop size). Depending upon the fuel and air injection parameters, two different types of flames can be readily distinguished, both of which are shown in Figure 1. The top half of the sketch shows a near-field dominated burner stabilized flame. This is a relatively short, high-intensity flame typical of wall-fired boilers produced with rapid fuel/air mixing. Each flame is stabilized independently, although there is some flame/flame interaction. The second class of flames is typified by flames in cement kilns or corner-fired boilers where air is injected completely axially, producing a long, simple jet flame (see the bottom half sketch in Figure 1). In a corner-fired boiler these jet flames intersect on a firing circle and mix in a fireball which occupies a significant fraction of a combustion chamber. Regardless of the type of flame, the liquid droplets exhibit the same behavior as pulverized coal particles in that potential chemical energy in the fuel is converted to thermal energy in the combustion products.

A simplified description of the phenomena occurring to solid particles and

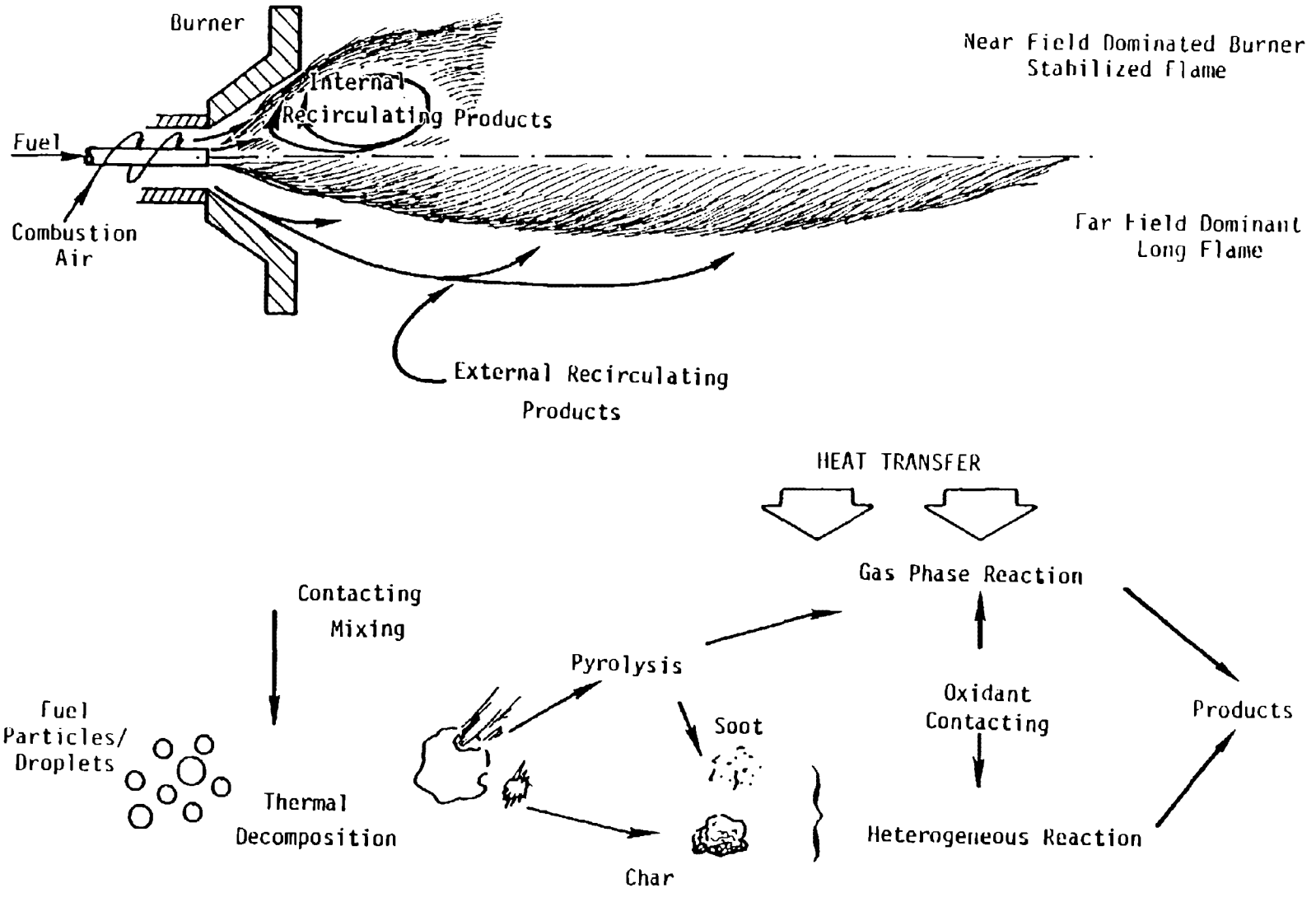

Figure 1 Solid Liquid Fuel Processing in Turbulent Diffusion Flames.

liquid droplets of fuels in turbulent diffusion flames is illustrated in Figure 1. The fuels first decompose, giving a vapor and a solid product. The vapor may be ejected from the solid as a single jet from a blowhole or may vaporize uniformly from the particle or droplets. This vapor will then either undergo pyrolysis, producing soot particles, or undergo gas phase oxidation. The solid remaining after devolatilization of coal is normally referred to as char. The char and soot may then undergo heterogeneous reaction which includes oxidation (burnout) and possible reaction with gaseous nitrogen species. Throughout this sequence of events the droplets and particles of fuel and their products must be brought into contact with oxidant and the high temperature combustion products in order to cause decomposition and subsequent reaction. This contacting is important on a macroscale because it dictates the major flame characteristics (i.e., near-field dominated burner stability or far-field dominated jet flame), and on a microscale because it ultimately dictates the production of pollutant species. FCR has been primarily concerned with the phenomena associated with conversion of nitrogen in droplets and particles of fuel to the ultimate nitrogen oxide released from the combustion chamber.

FCR was divided into three program areas. These were concerned with (1) transport processes in reacting systems; (2) gas phase chemistry; and (3) the physics and chemistry of two-phase systems. Figure 2 presents an overall view of the program structure, which is divided into major program areas, specific program elements and support areas. This program structure was planned to lead to two major program outputs. These were:

- A description of the chemical limits of NO production in order to ascertain the lower bounds of both fuel NO and thermal NO production under a series of process constraints which were not limited in any way by fuel/air contacting.

- A description of fuel NO formation in turbulent diffusion flames for gas, liquid and pulverized coal systems.

This overall program was planned as a combined in-house and subcontract project effort. EER took responsibility for program planning, management and synthesis of the overall program, and subcontracted separate projects within the

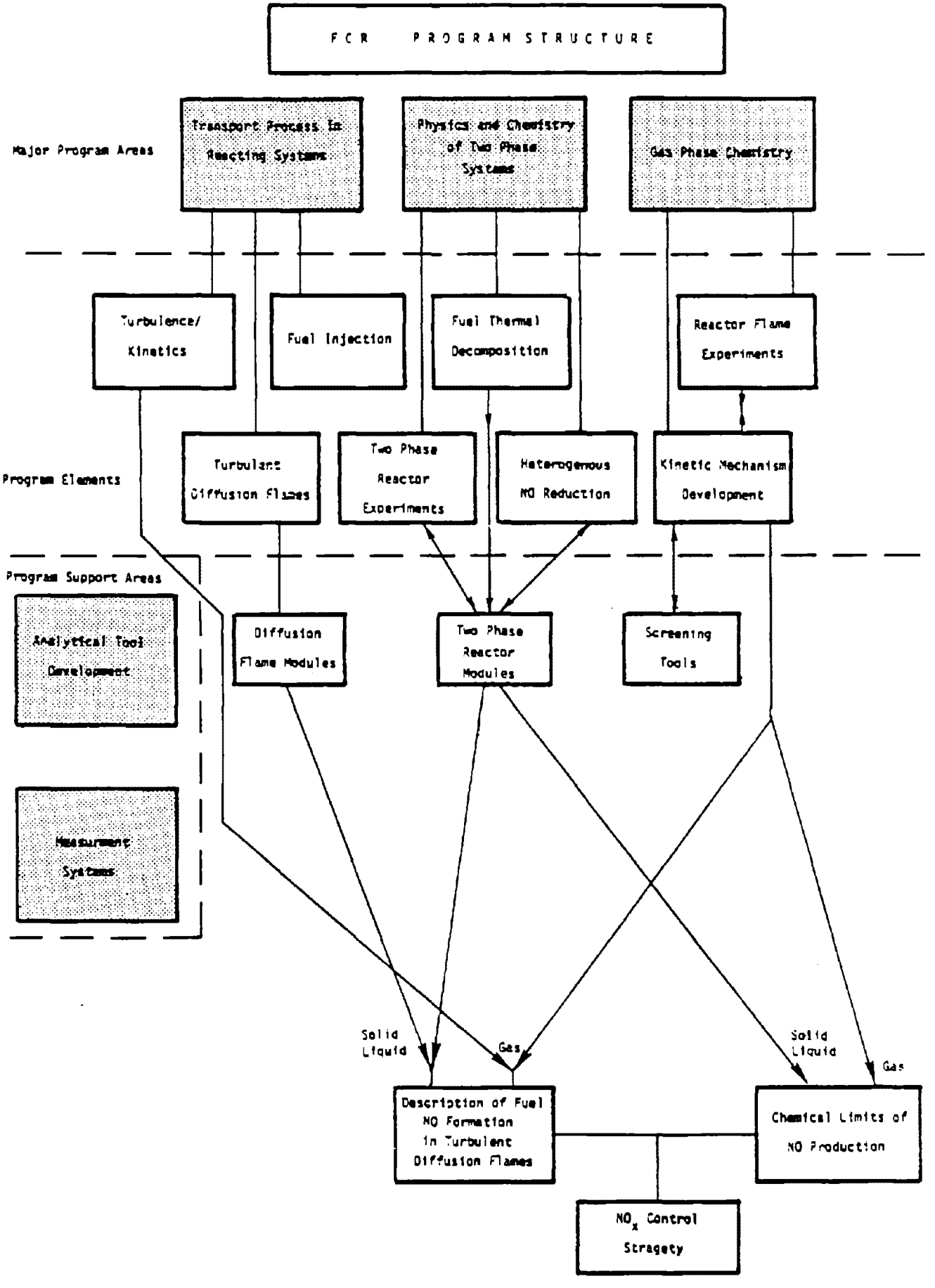

Figure 2. FCR Program Structure.

program elements to various organizations. Subcontracts accounted for 70 percent of the program and were used to ensure that FCR had the benefit of the best scientific talent available. Every effort was made to use subcontractors who had the necessary experience, and in many cases, equipment. The main synthesis role was accomplished by EER using analytical tools developed in major program areas.

The reasoning behind the division of the total program into three major program areas can most easily be described by consideration of the phenomena occurring to solid and liquid fuels in turbulent diffusion flames. When a pulverized coal particle is heated and decomposes, the fuel-bound nitrogen component is divided between that which stays with the solid (char) and that which is evolved with the volatile gases. The processes that lead to the division of fuel nitrogen are governed by the physics and chemistry of two-phase systems, as are the subsequent reactions of the solid phase. Thus, two of the program elements in the two-phase program area were concerned with the thermal decomposition of the fuel and heterogeneous NO/char reactions. The fate of the volatiles depends upon the chemistry of nitrogenous species during combustion of the gas phase pyrolysate composed primarily of hydrocarbons. This whole area was treated in the gas phase chemistry program area. The primary goal of the gas phase chemistry program was to produce a kinetic mechanism which described the fate of fuel nitrogen in gaseous mixtures which were likely to be found in pulverized coal and residual fuel oil flames. Thus, the gas phase chemistry area was divided into two program elements: one experimental and one aimed at mechanism development using computer simulations. A considerable effort was expended in the development of two-phase reactor experiments. These experiments coupled gas phase chemistry with fuel decomposition.

All of the above neglected the physics of turbulent transport. In flames the particles must be mixed with high-temperature gases before they can decompose, and oxidant must be mixed with the volatile fuel fractions before they can react. These fuel/air contacting processes were treated in the program area defined as transport processes in reacting systems. Three projects were carried out in this major program area. Theses were concerned with coupling of kinetics to turbulence, fuel injection systems and turbulent diffusion flames.

Although each of the projects in the various program areas were planned to

provide information which was of value in itself and was of direct use for data interpretation, the overall program flow was directed towards the development and verification of engineering tools. These tools could be used in the attainment of the two major goals concerning fuel NO formation in turbulent diffusion flames. It is not possible to show the overall interaction of the various program areas and program elements because of the additional complexity that would be added to Figure 2. However, the overall program placed great importance upon the use of analytical tools to help synthesize the program. Indeed, all the program elements can be considered to provide input to allow analytical tools to be developed. The application of these tools then provides the output of the FCR program.

It was recognized from the outset that within the time frame of FCR the development of a unified mathematical model for NO_x production in pulverized coal flames was unattainable. The major modeling effort in FCR concentrated upon the development of a framework of semi-empirical modular models. Thus, a complex system could be modeled using a collection of limit-case elements linked together by means of empirical knowledge of the exchange of heat and mass transfer between these elements. In its simplest application, modular elements could be used to analyze data generated in several of the program elements involving reactor experiments. The modules describing fuel decomposition could be applied to both reactors and turbulent diffusion flames. Recognizing how complex a pulverized-coal system is, the limit-case approach was deemed to be the most appropriate in analyzing fundamental data for application to real systems. In limit-case studies certain phenomena are assumed to dominate the process while other phenomena become suppressed, thus allowing the implications of specific phenomenological behavior to be examined. For example, limit-case studies could be used to define the times and temperatures needed to reach a certain total fixed-nitrogen content in a fuel-rich combustion system, or to define the extent of heterogeneous NO reduction in pulverized coal flames.

Although FCR placed considerable emphasis on the provision of information which was necessary to provide short-term solutions, long-term research was not entirely neglected. FCR pioneered the use of holography and two-color pyrometry as tools to study the thermal decomposition and combustion of fuels. Activities in coupling of kinetics to turbulence are beginning to show considerable promise

for the future. Effort was initiated to evaluate numerical techniques which could be used in the ultimate models of furnace performance. Projects such as these ensured that the CRB had a balanced fundamental combustion research program.

Having established an overall program structure it was necessary to formulate individual research efforts directed towards meeting the overall program goals. The following section describes the research efforts that lead to Volume 4.

This volume is concerned with Engineering Analysis and Transport Phenomena. The research efforts pursued under this Major Program Area focused on the development of mathematical models, with development efforts closely coupled to numerous experimental studies. The majority of the modeling work was performed at EER and directed towards development of the overall modular model discussed earlier. Models include a description of the following phenomena:

- Particle thermal history.
- Finite rate thermal decomposition.
- Heterogeneous chemical behavior.
- Finite-rate gas-phase chemistry.
- Fluid mechanics and ballistics of turbulent transport in two-phase systems.
- Complex flow fields associated with the near-field of highly swirl-stabilized combustors.
- The interaction between turbulent unmixedness and chemistry.

These modeling efforts have resulted in a hierarchy of analysis codes. Treatment of the fully-coupled finite-rate processes associated with particle heatup, thermal decomposition, heterogeneous reactions and gas phase chemistry was emphasized. The codes can handle with ease and efficiency as many as 200 coupled processes.

In the course of developing an understanding of the dominant mechanisms governing complex and poorly understood behavior, it is often necessary to start with a large coupled system and, through sensitivity analysis, reduce it so it contains first-order phenomena only. A good example of a situation requiring such an approach is NO_x generation in p.c. flames. The complexities of HCN, NH_i and C_2 chemistry, in conjunction with finite-rate devolitilization, defies a simple

intuitive understanding and requires complex analysis in order to generate such intuition.

This volume describes the FCR effort to develop engineering analysis tools.

PART 1

A COMPUTER PROGRAM FOR GENERAL FLAME ANALYSIS

Prepared by:
C. J. Kau
and
T. J. Tyson

TABLE OF CONTENTS

LIST OF FIGURES

LIST OF TABLES

1.0 INTRODUCTION

A computer model which is capable of predicting or analyzing various types of premixed or diffusion flames is reported. Detailed mathematical description of the problems involved and the numerical technique employed in the solution scheme are described.

The generality of the model allows computation for systems of various configurations; e.g., one-dimensional time-dependent planar/spherical, steady two-dimensional planar and steady axisymmetric nonrecirculating reacting flow systems.

Physical processes such as laminar unequal species diffusion, radiation, flame holder recombination effects and heat loss are treated extensively. Several phenomenological turbulent eddy viscosity models based on mixing length theory are also incorporated into the code. Kinetically, the code is capable of treating up to 200 two- or three-body basic reactions and up to 52 species.

A linearized implicit finite difference network is employed. Thus, except for cross-stream velocity, all dependent variables of all grid points at the same coordinate line (or at the same integration step) are solved simultaneously in coupled fashion. Thus, the inversion of a block tridiagonal matrix is required at each integration step. This numerical scheme is so efficient that the computational time required for a typical run is only about one-tenth to one-fifth of the time required for other popular methods such as the implicit/explicit method (Ref. 12) or the operator splitting method (Ref. 13).

For illustrative purposes, detailed analyses of four fundamental types of laminar flames are presented: flat flame, opposed-jet diffusion flame, co-flow diffusion flame, and nonrecirculating confined flame.

2.0 GOVERNING EQUATION IN PHYSICAL COORDINATES

The set of partial differential equations presented in this section is capable of describing two-dimensional (or axisymmetric) laminar (or time averaged turbulent) boundary layer flow with chemical reaction. These equations are evolved from full Navier-Stokes equations by incorporating boundary layer assumption, i.e.:

1. Momentum transfer in the main-stream direction is negligible compared to momentum transfer in cross-stream direction.

2. The momentum equation in the cross-stream direction is negligible compared to the momentum equation in the main-stream direction.

3. Energy and mass diffusion in the main-stream direction are negligible compared to diffusion in the cross-stream direction.

The resulting equations are:

Continuity Equation

$$\frac{\partial}{\partial x}(\rho u r^{\alpha}) + \frac{\partial}{\partial r}(\rho v r^{\alpha}) = 0 \tag{2-1}$$

Momentum Equation

$$\rho u \frac{\partial u}{\partial x} + \rho v \frac{\partial u}{\partial r} = - \frac{dp}{dx} + \frac{1}{r^{\alpha}} \frac{\partial}{\partial r}\left(\mu r^{\alpha} \frac{\partial u}{\partial r}\right) + \rho g_x \tag{2-2}$$

Species Equation

$$\rho u \frac{\partial \alpha_i}{\partial x} + \rho v \frac{\partial \alpha_i}{\partial r} = \frac{1}{r^{\alpha}} \frac{\partial}{\partial r}\left(\rho D_i r^{\alpha} \frac{\partial \alpha_i}{\partial r}\right) + \dot{w}_i \tag{2-3}$$

Energy Equation

$$\rho c_p \left[u\frac{\partial T}{\partial x} + v\frac{\partial T}{\partial r}\right] = u \frac{\partial P}{\partial x} + \mu\left(\frac{\partial u}{\partial r}\right)^2 + \dot{q}_r + \frac{1}{r^{\alpha}} \frac{\partial}{\partial r}\left(\lambda r^{\alpha} \frac{\partial T}{\partial r}\right) + \frac{\partial T}{\partial r}\sum \rho D_i C_{pi} \frac{\partial \alpha_i}{\partial r} - \sum_{i=1}^{k} h_i \dot{\omega}_i \tag{2-4}$$

Equation of State

$$\rho = \frac{P}{82.06\ T \sum_i \alpha_i} \tag{2-5}$$

where α is a geometric index. By setting α=0, 1 and 2, the equations can be obtained in terms of two-dimensional cartesian, polar cylindrical, and spherical coordinates, respectively. By setting μ=1 and ignoring the momentum equation (Eq. 2-2), the equations become time-dependent and one-dimensional, with the x-coordinate representing transient time. The nomenclature used in the above equation is defined at the end of Part 1.

The conservation law which the species equation (Eq. 2-3) must satisfy is:

$$\sum_i M_i \alpha_i = 1.0 \tag{2-6}$$

which states, by definition, that "sum of mass fractions equals one." For consistency, one of the species equations in Eq. (2-3) shall be replaced by Eq. (2-6).

Another conservation law to be satisfied is that "the chemical reactions neither create nor destroy mass." Mathematically:

$$\sum_i M_i \dot{w}_i = 0 \tag{2-7}$$

Summing Eq. (2-3) over all species and noting Eq. (2-6) and Eq. (2-7), we obtain the condition:

$$\sum M_i \rho D_i \frac{\partial \alpha_i}{\partial r} = 0 \tag{2-8}$$

Eq. (2-8) implies that not all diffusion coefficients are independent; therefore, in actual calculation the diffusivity of the dominant species is not specified and Eq. (2-6) is used to replace the species equation of the dominant species. The fifth term at the right hand side of the energy equation, Eq. (2-4)

can be rewritten as:

$$\frac{\partial T}{\partial r} \sum_i \left[\left(C_{pi} - \frac{M_j}{M_R} C_{p_R} \right) \rho D_i \frac{\partial \alpha_i}{\partial r} \right] \qquad (2\text{-}9)$$

which is the consequence of Eq. (2-8). Subscript "R" refers to the dominant species (usually N_2).

3.0 GOVERNING EQUATIONS IN STREAM FUNCTION COORDINATES

In some practical situations it is more convenient to write the governing equations in stream function coordinates via Von Mises Transformation. The stream function in Von Mises Transformation is defined by the following relations

$$\psi^{\alpha}\left(\frac{\partial\psi}{\partial r}\right)_x = \rho u r^{\alpha} \tag{3-1}$$

$$\psi^{\alpha}\left(\frac{\partial\psi}{\partial x}\right)_r = -\rho v r^{\alpha} \tag{3-2}$$

which automatically satisfy the continuity equation (Eq. 2-1). The transformation of differential equations from the physical coordinates (x,r) plane to the stream function (x', ψ) plane requires evaluation of partial derivatives in terms of (x', ψ); i.e.,

$$\left(\frac{\partial}{\partial x}\right)_r = \left(\frac{\partial}{\partial x'}\right)_{\psi} - \rho v f\left(\frac{\partial}{\partial\psi}\right)_{x'} \tag{3-3}$$

$$\left(\frac{\partial}{\partial r}\right)_x = \rho u f\left(\frac{\partial}{\partial\psi}\right)_{x'} \tag{3-4}$$

where $f \equiv \left(\frac{r}{\psi}\right)^{\alpha}$ and the streamline angle $\frac{\partial x'}{\partial r}$ is assumed to be small.

Introducing Eqs. (3-1) and (3-2) into Eqs. (2-2), (2-3) and (2-4) and dropping "'" from x', we have:

Momentum Equation

$$\rho u\frac{\partial u}{\partial x} = -\frac{dp}{dx} + \rho u\left\{\frac{1}{\psi^{\alpha}}\frac{\partial}{\partial\psi}\left[Ar^{\alpha}\mu\frac{\partial u}{\partial\psi}\right]\right\} + \rho g_x \tag{3-5}$$

Energy Equation

$$\rho u c_p\frac{\partial T}{\partial x} = u\frac{dp}{dx} + \dot{q}_r + \frac{\rho u}{\psi^{\alpha}}\frac{\partial}{\partial\psi}\left(\lambda r^{\alpha}A\frac{\partial T}{\partial\psi}\right) + \frac{\rho u r^{\alpha}A}{\psi^{\alpha}}\mu\left(\frac{\partial u}{\partial\psi}\right)^2 + \frac{\rho u r^{\alpha}A}{\psi^{\alpha}}\frac{\partial T}{\partial\psi}\sum\left[\left(C_{pi} - \frac{M_i}{M_R}C_{pR}\right)\rho D_i\frac{\partial\alpha_i}{\partial\psi}\right] - \sum_i h_i\dot{w}_i \tag{3-6}$$

Species Equation

$$\rho u \frac{\partial \alpha_i}{\partial x} = \rho u \left\{ \frac{1}{\psi^{\alpha}} \frac{\partial}{\partial \psi} \left[\rho D_i r^{\alpha} A \frac{\partial \alpha_i}{\partial \psi} \right] \right\} + \dot{w}_i \qquad (3\text{-}7)$$

where $A \equiv \left(\frac{\rho u r^{\alpha}}{\psi^{\alpha}} \right)$.

The Von Mises Transformation eliminates the continuity equation and the cross-stream convective terms in momentum, energy and species equations. These terms usually cause difficulties in numerical integration processes.

The equation of state in stream function coordinate remains the same as that in physical coordinate systems.

For a fixed value of x, the r-coordinate can be related to ψ by numerically integrating Eq. (3-1), giving

$$\int_0^{\psi} \frac{\psi'^{\alpha}}{\rho u} d\psi' = \int_0^{r} r'^{\alpha} dr'$$

4.0 GENERAL FORM OF GOVERNING EQUATIONS AND BOUNDARY CONDITIONS

4.1 General Form

The governing equations in two different coordinates can be combined and written in one general form:

$$C \frac{\partial F}{\partial x} = C_0 \frac{\partial F}{\partial y} + C_1 \frac{\partial}{\partial y}\left(C_2 \frac{\partial F}{\partial y}\right) + \dot{Q} + R \qquad (4\text{-}1)$$

where $F = \alpha_i$ or T or U. When $y \equiv r$, the system is in physical coordinates, while when $y \equiv \psi$ the system is in stream function coordinates. The coefficients C, C_0, C_1 and C_2, and functions $\dot{Q}$ and R for each coordinate system are listed in Table 1. Equation (4-1) is solved along with the equation of state (in differential form) to give

$$d\rho = \rho \left[- M \sum_i d\alpha_i - \frac{dT}{T} + \frac{dp}{p} \right] \qquad (4\text{-}2)$$

and the species equation of reference species R is replaced by Eq. (2-6) (in differential form):

$$d\alpha_R = \frac{1}{M_R} \sum_{i \neq R} M_i \, d\alpha_i \qquad (4\text{-}3)$$

When the system is in physical coordinates, the continuity equation (2-1) has to be integrated for cross-stream velocity v. It is noted that Eqs. (4-2) and (4-3) can also be written in general form (i.e., Eq. 4-1). The coefficient functions for the general form of Eqs. (4-2) and (4-3) are also listed in Table 1. The system of equations to be solved is a parabolic system of partial differential equations which require prescription of initial (x = 0) and boundary conditions pertinent to the individual flow problem at hand. The simplest and the most common types of boundary conditions which have been provided in this computer program are:

1. Zero order boundary condition: The known value of the dependent variable is specified at the boundary.

Table 1. Definition of C, C_o, C_1 and C_2, and $\dot{Q}$ and R in Eq. (4-1)

(a) Physical Coordinate System

F	C	C_o	C_1	C_2	$\dot{Q}$	R
u	ρu	$-(\rho v)$	$1/y^{\alpha}$	μy^{α}	-	$\rho g_x - \frac{dp}{dx}$
T	$\rho u c_p$	$-(\rho v C_p) + \sum \rho D_i \left(C_{pi} - \frac{M_i}{M_R} C_{p_R}\right) \frac{\partial \alpha_i}{\partial y}$	$1/y^{\alpha}$	λy^{α}	$-\sum_i h_i \dot{w}_i$	$u\frac{dp}{dx} + \dot{q}_r + \mu\left(\frac{\partial u}{\partial y}\right)^2$
α_i	ρu	$-(\rho v)$	$1/y^{\alpha}$	$\rho D_i y^{\alpha}$	$\dot{w}_i$	-
α_R	1	-	-	-	$\frac{1}{M_R} \sum_{i \neq R} M_i \frac{d\alpha_i}{dx}$	-
ρ	1	-	-	-	$\rho\left[-M\sum_i \frac{d\alpha_i}{dx} - \frac{1}{T}\frac{dT}{dx} + \frac{1}{p}\frac{dp}{dx}\right]$	-

(b) Stream Function Coordinate Systems

F	C	C_o	C_1	C_2	$\dot{Q}$	R
u	ρu	-	$\rho u/y^{\alpha}$	$Ar^{\alpha}\mu$	-	$\rho g_x - \frac{dp}{dx}$
T	$\rho u c_p$	$A^2 \sum \rho D_i \left(C_{pi} - \frac{M_i}{M_R} C_{p_R}\right) \frac{\partial \alpha_i}{\partial y}$	$\rho u/y^{\alpha}$	$Ar^{\alpha}\lambda$	$-\sum h_i \dot{w}_i$	$u\frac{dp}{dx} + q_r + A^2 \mu \left(\frac{\partial u}{\partial y}\right)^2$
α_i	ρu	-	$\rho u/y^{\alpha}$	$Ar^{\alpha}\rho D_i$	$\dot{w}_i$	-
α_R	1	-	-	-	$\frac{1}{M_R} \sum_{i \neq R} M_i \frac{d\alpha_i}{dx}$	-
ρ	1	-	-	-	$\rho\left[-M\sum \frac{d\alpha_i}{dx} - \frac{1}{T}\frac{dT}{dx} + \frac{1}{P}\frac{dp}{dx}\right]$	-

2. First order boundary condition: The first derivative (with respect to y-coordinates) or the dependent variable is specified.

3. Second-order boundary conditions: The second-order derivative (with respect to y-coordinate) of the dependent variable is specified.

In addition to these types of boundary conditions, the program also provides the choice of the following two types of frequently encountered boundaries in flame problems:

1. Symmetric plane/axis.

2. Catalytic surface.

4.2 Boundary Conditions for Symmetric Plane/Axis

On the plane/axis of symmetry (generally, y=0) we have:

$$\frac{\partial F}{\partial y} = 0 \qquad (4\text{-}4)$$

Due to numerical difficulties one cannot apply this condition directly to the boundary. The symmetric conditions must be derived from governing equations. By noting that (L'Hopital's rule):

$$\lim_{y \to 0} \left.\frac{\partial F}{\partial y}\right/_{y} = \frac{\partial^2 F}{\partial y^2}$$

and exerting some mathematical efforts, the governing equation at symmetric plane/axis (y=0) can be derived and reduced to the following general form:

$$C \frac{\partial F}{\partial x} = B_1 + B_2 \frac{\partial^2 F}{\partial y^2} \qquad \text{for } y = 0 \qquad (4\text{-}5)$$

where coefficient function C is given in Table 1 and coefficient functions B_1 and B_2 are listed in Table 2.

Table 2. Coefficient Function B_1 and B_2 for Eq. (4-5)

F	for (x,r) all α		for (x,ψ) and $\alpha = 0$		for (x,ψ) and $\alpha \neq 0$	
	B_1	B_2	B_1	B_2	B_1	B_2
α_i	$\dot{w}_i$	$(1+\alpha)\rho D_i$	$-\dot{w}_i$	$(\rho u)^2 \rho D_i$	$\dot{w}_i$	$(1+\alpha)\rho D_i \rho u$
T	$u\frac{dp}{dx} + \dot{q}_r - \Sigma h_i \dot{w}_i$	$(1+\alpha)\lambda$	$u\frac{dp}{dx} + \dot{q}_r - \Sigma h_i \dot{w}_i$	$(\rho u)^2 \lambda$	$u\frac{dp}{dx} + \dot{q}_r - \Sigma h_i \dot{w}_i$	$(1+\alpha)\rho u \lambda$
u	$\rho g_x - \frac{dp}{dx}$	$(1+\alpha)\mu$	$\rho g_x - \frac{dp}{dx}$	$(\rho u)^2 \mu$	$\rho g_x - \frac{dp}{dx}$	$(1+\alpha)\mu\rho u$

To compute ρ and α_R at the boundary, Eqs. (2-5) and (2-6) are used.

4.3 Boundary Condition for Catalytic Surface

The surfaces involving chemical reaction and heat and mass transfer (such as flameholder, burner surface) are commonly encountered in analysis of laboratory or industrial flames. The boundary conditions on these surfaces can be derived from the principles of conservation of heat and mass on the surface.

For plane surfaces in physical coordinates, the boundary conditions for reacting surfaces (say r=0) are:

Species

$$\left(\rho D_i \frac{\partial \alpha_i}{\partial r}\right)_s = \dot{m}\left[(\alpha_i)_s - (\alpha_i)_o\right] - \dot{w}_{s,i}\left(\frac{\text{mole}}{\text{cm}^2\text{-sec}}\right) \tag{4-6}$$

Energy

$$\left(\lambda \frac{\partial T}{\partial r}\right)_s = \dot{m}\left[\sum (h_i)_s (\alpha_i)_o - h_o + h_{loss}\right] + \sum_i (h_i)_s \dot{w}_{s,i} - \dot{q}_s \qquad \left(\frac{\text{cal}}{\text{cm}^2\text{-sec}}\right) \tag{4-7}$$

In the above, the subscripts "s" and "o" refer to the properties on the surface and far upstream (where diffusive flux is zero), respectively. $\dot{w}_{s,i}$ is the production rate of the ith species per unit surface area. h_{loss} denotes enthalpy loss (such as cooling or heating of reactants before entering the surface) per unit surface area per unit mass flux $\dot{m}$. Energy exchange of any form (such as surface radiation) is represented by $\dot{q}_s$.

For a plane surface in stream function coordinates, the boundary conditions for a reacting surface (say ψ=0) are:

Species

$$\rho D_i \frac{\partial \alpha_i}{\partial \psi} = \left\{\dot{m}\left[(\alpha_i)_s - (\alpha_i)_o\right] - \dot{w}_{s,i}\right\} / (\rho u) \tag{4-8}$$

Energy

$$\lambda \frac{\partial T}{\partial \psi} = \left\{ \dot{m} \left[\sum (h_i)_s (\alpha_i)_o - h_o + h_{loss} \right] + \sum (h_i)_s \dot{w}_{s,i} - \dot{q}_s \right\} / (\rho u) \qquad (4\text{-}9)$$

5.0 TRANSPORT PROPERTIES

5.1 Laminar Transport Properties

For multicomponent laminar flow, the mixture viscosity and conductivity are evaluated from component viscosities μ_i and conductivities λ_i using empirical formulas of Wilke and Wassiljewa (Ref. 1), respectively. The Wilke formula gives mixture viscosity as

$$\mu = \sum_{i=1}^{N} \frac{\mu_i}{\left[1 + \sum_{j \neq i}^{N} \phi_{ij}\left(\frac{x_j}{x_i}\right)\right]} \qquad \frac{gm}{cm\text{-}sec} \qquad (5\text{-}1)$$

Wassiljewa's equation gives mixture conductivity as

$$\lambda = \sum_{i=1}^{N} \frac{\lambda_i}{\left[1 + \sum_{j \neq i}^{N} 1.065\ \phi_{ij}\left(\frac{x_j}{x_i}\right)\right]} \qquad \frac{cal}{cm\text{-}sec\text{-}^{o}K} \qquad (5\text{-}2)$$

where x_i is mole fraction and ϕ_{ij} is defined as

$$\phi_{ij} = \frac{\left[1 + \left(\frac{\mu_i}{\mu_j}\right)^{\frac{1}{2}} \left(\frac{M_j}{M_i}\right)^{\frac{1}{4}}\right]^2}{\left[\sqrt{8}\left(1 + \frac{M_i}{M_j}\right)^{\frac{1}{2}}\right]} \qquad (5\text{-}3)$$

The single-component viscosities are computed theoretically from kinetic theory:

$$\mu_i = 2.669 \times 10^{-5} \frac{\sqrt{M_i T}}{\sigma_i^{\,2}\ \Omega^{(2.2)}} \qquad (5\text{-}4)$$

and

$$\lambda_i = 1.9891 \times 10^{-4}\ (T/M_i)^{\frac{1}{2}} \Big/ \sigma_i^{\,2}\ \Omega^{(2.2)} \qquad (5\text{-}5)$$

where $\Omega^{(2.2)}$ is the collision integral. $\Omega^{(2.2)}$ is a function of parameters in the potential function assumed. The Stockmayer potential function is assumed

here. Tabulated values of $\Omega^{(2.2)}$, which is a function of $T^*=KT/\varepsilon_o$ and δ, are first evaluated by the method of Monchick and Mason (Ref. 2). ε_o/K is minimum energy of attraction between molecules in ^oK and σ_1 is intermolecular distance when potential energy of interaction is zero and is in angstroms. δ is the description of angular dependency of dipole-dipole interaction energy. K is Boltzmann's constant.

The binary diffusion coefficient between unlike molecules is evaluated from

$$D_{ij} = 1.858 \times 10^{-3} T^{1.5} \frac{\left[\frac{m_i + m_j}{m_i m_j}\right]^{0.5}}{p\sigma_{ij}^2 \Omega_{ij}^{(1,1)}} \qquad \left(\frac{cm^2}{sec}\right) \qquad (5\text{-}6)$$

where the binary collision integral $\Omega_{ij}^{(1.1)}$ is a function of potential parameters ε_{oij}/K and δ_{ij}. σ_{ij}, ε_{oij}, and b_{ij} are evaluated from single component parameters by following combining laws.

$$\sigma_{ij} = \tfrac{1}{2}(\sigma_i + \sigma_j) \qquad (5\text{-}7)$$

$$\varepsilon_{oij} = \sqrt{\varepsilon_{oi}\varepsilon_{oj}} \qquad (5\text{-}8)$$

For polar-nonpolar pair of molecules, the combining laws are modified as:

$$\sigma_{np} = \tfrac{1}{2}(\sigma_n + \sigma_p) f_c^{-\frac{1}{6}} \qquad (5\text{-}9)$$

$$\varepsilon_{onp} = \sqrt{\varepsilon_{on}\varepsilon_{op}}\, f_c^2 \qquad (5\text{-}10)$$

$$f_c = 1 + \tfrac{1}{2}\left(\frac{\alpha_n \delta_n}{\sigma_n^3}\right)\sqrt{\frac{\varepsilon_{op}}{\varepsilon_{on}}} \qquad (5\text{-}11)$$

The subscripts p and n refer to the polar and nonpolar constituents.

For pair of polar molecules, the combining laws for σ_{ij} and ε_{ij} remain the same as for nonpolar pair. The parameter δ_{ij} is evaluated from:

$$\delta_{ij} = (\delta_i \delta_j)^{\frac{1}{2}} \left[\frac{(\sigma_i \sigma_j)^{\frac{1}{2}}}{\sigma_{ij}}\right]^3 \qquad (5\text{-}12)$$

The empirical equations for collision integrals, which fit the Monchick and Mason (Ref. 2) calculation, provided by Neufeld (Ref. 3) et al. are:

$$\Omega_{ij}^{(1,1)} = \frac{1.06036}{T^{*0.15610}} + \frac{0.19300}{\exp(0.47635T^*)} + \frac{1.03587}{\exp(1.52996T^*)} + \frac{1.76474}{\exp(3.89411T^*)} + \frac{0.19\,\delta_{ij}^2}{T^*} \quad (5\text{-}13)$$

$$\Omega_{ij}^{(2,2)} = \frac{1.16145}{T^{*0.14874}} + \frac{0.52487}{\exp(0.77320T^*)} + \frac{2.16178}{\exp(2.43187T^*)} - 6.435 \times 10^{-4}\, T^{*0.14874} \sin(18.0323\, T^{*-0.7683} - 7.27371) + \frac{0.2\,\delta_{ij}^2}{T^*} \quad (5\text{-}14)$$

The diffusivity of a single component into a mixture of n components is approximated by (Ref. 1):

$$D_i = \frac{1-X_i}{\sum_{j\neq i}^{n} \left(\frac{X_i}{D_{ij}}\right)} \quad (5\text{-}15)$$

where x_i is mole fraction.

Estimation of the multicomponent diffusivity requires the calculation of entire matrix of D_{ij}, which is one of the most time-consuming computational steps in the model. Evaluation of diffusivities by the so-called bifurcation approximation (Ref. 4) provides a less time-consuming but less accurate solution.

The basic assumption of bifurcation method is that the binary diffusion coefficient can be represented by

$$D_{ij} \approx f_i f_j D_{rr} \quad (5\text{-}16)$$

where f_i and f_j are diffusion factors and D_{rr} is a reference self-diffusion coefficient. For general flame calculation, the reference species, r, is usually taken to be oxygen. By setting j=r in Eq. (5-16), we obtain:

$$f_i = \frac{D_{ir}}{D_{rr}} \quad (5\text{-}17)$$

where $f_r = 1.0$ by definition. Using Eq. (5-6), Eq. (5-17) becomes:

$$f_i = \left(\frac{\sigma_{rr}}{\sigma_{ir}}\right)^2 \frac{\Omega_{rr}^{(1.1)}}{\Omega_{ir}^{(1.1)}} \left(\frac{M_i + M_r}{2M_i}\right)^{1/2} \tag{5-18}$$

if we take first terms from Neufeld's empirical equation for $\Omega_{ij}^{(1.1)}$ (Eq. 5-13) and substitute into above equation, we have:

$$f_i = \left(\frac{\sigma_{rr}}{\sigma_{ir}}\right)^2 \left[\frac{(\varepsilon_o/K)_{rr}}{(\varepsilon_o/K)_{ir}}\right]^{0.1561} \left(\frac{M_i + M_r}{2M_i}\right)^{1/2} \tag{5-19}$$

Here, f_i is found to be independent of temperature and pressure and can be precalculated. σ_{ir} and $(\varepsilon_o/K)_{ir}$ can be obtained using combining laws given in Eqs. (5-7) and (5-8). D_i can then be evaluated by Eq. (5-15) when all D_{ij}'s are calculated by Eq. (5-16). The laminar viscosity and conductivity are obtained by assuming constant Lewis and Prandtl numbers.

The force potential parameters for species which usually appear in the combustion products of hydrocarbon fuel are listed in Table 3. The diffusion factors calculated using Eq. (5-19) are also listed in Table 3. The diffusion factors, for unstable species for which the potential parameters are not available, are approximated by:

$$f_i = \left(\frac{M_i + M_r}{2M_i}\right)^{1/2}$$

These values of f_i will be improved as soon as their potential parameters become available.

5.2 Turbulent Eddy Viscosity Models

The attempt to treat detailed chemistry of combustion and turbulence simultaneously is not only impractical but also currently unfruitful. For turbulent flow systems, the program provides two phenomenological eddy viscosity models: Ferri's model (Ref. 5) and Schetz's model (Ref. 6). Both models are

TABLE 3. FORCE POTENTIAL PARAMETERS AND DIFFUSION FACTORS

i	σ_i(A)	ϵ_o/K (k)	δ	$\alpha_n \times 10^{+25}$ cm^3	M_i**	f_i***
H_2	2.827	59.7	-	7.9	2.016	3.69
CO	3.69	91.7	-	19.5	28.011	0.983
CH_4	3.78	142.1	-	26.0	16.043	1.09
NH_3	3.15	358.0	0.7	22.6	17.032	1.20
N_2	3.798	71.4	-	17.6	28.016	0.973
H_2O	2.71	506.0	1.23	14.70	18.016	1.31
CO_2	3.941	195.2	-	26.5	44.011	0.777
O	2.529	218.9	-	-	16.0	1.55
H	2.192	36.8	-	4.0	1.008	6.60
OH	3.147	79.8	4.01	-	17.008	1.35
HO_2	4.196	289.3	0.75	20.0	33.008	0.752
CH_3	3.79	142.1	-	-	15.035	1.12
CH_2	-	-	-	-	14.027	1.28
CH	-	-	-	-	13.019	1.40
CH_2O	4.304	340.4	0.71	-	30.027	0.739
CHO	-	-	-	-	29.019	1.03
NH_2	-	-	-	-	16.024	1.22
NH	-	-	-	-	15.016	1.25
N	-	-	-	-	14.008	1.28
NO	3.489	117.2	0.15	-	30.008	1.00
NO_2	3.712	404.3	0.028	-	46.008	0.774
N_2O	3.776	248.8	0.01	30.0	44.016	0.797
CHN	3.63	569.1	-	25.9	27.027	0.875
CN	-	-	-	-	26.019	1.06
HNO	3.492	116.7	-	-	31.016	0.994
HNCO	-	-	-	-	43.027	0.934
CH_3O	-	-	-	-	31.035	1.01
H_2O_2	4.196	289.3	-	-	34.016	0.746
C_2H_2	4.033	231.8	-	33.3	26.038	0.849
C_2H_4	4.163	224.7	-	42.6	28.054	0.806
C_2H_6	4.443	215.7	-	44.7	30.070	0.739
O_2	3.467	106.7	-	16.0	32.0	1.0
NCO	-	-	-	-	42.019	0.938
C_2H	-	-	-	-	25.030	1.07
C_2H_3	-	-	-	-	27.046	1.04
C_2H_5	-	-	-	-	29.062	1.02

*Polarizability of molecules.

**Molecular weight.

***$$f_i = \left(\frac{\sigma}{\sigma_i}\right)^2 \left[\frac{(\epsilon_o/K)_{rr}}{(\epsilon_o/K)_{ir}}\right]^{0.1561} \left(\frac{M_i + Mo_2}{2M_i}\right)^{1/2}$$

$$f_i = \left(\frac{M_i + Mo_2}{2M_i}\right)^{1/2}$$ (for species with no potential parameters available).

locally dependent. Ferri's model is recommended for systems such as jet into still surroundings or axisymmetric wake. The form of the expression is

$$\mu = 0.025 b_{\frac{1}{2}} \left| \rho_o u_o - \rho_e u_e \right|$$

where b1/2 is the value of r at u = 0.5 ($\rho_o u_o + \rho_e u_e$). The subscripts "o" and "e" refer to the values at the axis of symmetry (r=0) and the edge of the mixing layer. Schetz's model has the form

$$\mu = \frac{0.018}{r_j} \int_0^\infty \left| \rho_e u_e - \rho u \right| 2\pi d\, r$$

where r_j is initial radius of jet. It is said that "the turbulent viscosity if proportional to the excess mass flow per unit width in the mixing region." Schetz's model is recommended for coaxial jets with large density gradients across the mixing zone (e.g., hydrogen jet into air). Constant turbulent Lewis number and constant turbulent Prandtl number are assumed for all turbulent flows. Thus, conductivity is calculated by

$$\lambda = \frac{\mu C_p}{Pr}$$

and turbulent diffusivities of all species are evaluated by:

$$\rho D_i = \mu \left(\frac{Le}{Pr} \right)$$

where Le and Pr are turbulent Lewis number and turbulent Prandtl number, respectively.

6.0 CHEMICAL REACTIONS AND THERMOCHEMICAL PROPERTIES

6.1 Chemical Reaction Rate Equations

In general form, the Kth chemical reaction can be written as:

$$\sum_i N_{i,K} Z_i \rightleftharpoons \sum_i N'_{i,K} Z_i \tag{6-1}$$

where $N_{i,K}$ and $N'_{i,K}$ are integers representing the stoichiometric coefficients of the ith species in the Kth reaction. Prime denotes products and no prime denotes reactants. Z_i is the chemical symbol (or species name) of the ith species. The net production rate (in forward direction) of the ith species in the Kth reaction is given by:

$$\dot{w}_{i,K} = (N'_{i,K} - N_{i,K}) \left[K_{f,K} \rho^{\sum_j N_{f,K}} \prod_i \alpha_j^{N_{i,j}} - \frac{K_{f,K}}{K_{e,K}} \rho^{\sum_j N'_{j,K}} \prod_i \alpha_j^{N_{i,j}} \right] E_K \tag{6-2}$$

where the forward reaction rate has Arrhenius form. The equilibrium constant, $K_{e,K}$, is calculated by:

$$K_{e,K} = \exp\left(\frac{-\Delta G_K}{RT}\right) (RT)^{-\sum_i \left(N'_{i,K} - N_{i,K}\right)} \tag{6-3}$$

where ΔG_K is net production of Gibbs free energy and is defined as:

$$\Delta G_K = \sum_i N'_{i,K} G'_i - \sum_i N_{i,K} G_i \quad . \tag{6-4}$$

The term E_K in Eq. (6-2) is the modification of reaction rate due to a third body and is defined as:

$$E_K = \sum E_{K,i} \alpha_i \quad \text{for three body reactions} \tag{6-5}$$

$$= 1 \quad \text{for all others}$$

where $E_{K,i}$ is the third body efficiency of the ith species in the Kth reaction.

The overall production rate of the ith species is the sum of $\dot{w}_{i,K}$ over all K; i.e.,

$$\dot{W}_i = \sum_K \dot{W}_{i,K} \qquad (6\text{-}6)$$

6.2 Thermochemical Data

The thermochemical properties (specific heat, enthalpy and Gibbs free energy) for each species are taken directly from JANAF Thermochemical Table (Ref. 10) in tabular form as a function of temperature. Linear interpolation is used to compute the properties at local temperature.

7.0 FLAME RADIATION

The major radiating species in a hydrogen flame is water vapor. For a hydrocarbon flame, carbon dioxide and carbon monoxide are also among the major radiating species. For the optically thin limit (photon mean free path is much greater than the characteristic dimension of the flame), the Planck mean absorptance coefficient of species i can be obtained from gas emittance data (Ref. 7):

$$K_{pi} = \tfrac{1}{2}\left(\frac{\varepsilon_{gi}}{L}\right)_{L\to 0}$$

where L is the characteristic dimension of the flame, and ε_{gi} is the emittance of the ith species. The values of K_{pi} for H_2O, CO_2, and CO calculated by Kelly and Kendall (Ref. 8) based on emittance data of Edwards and Balakrishnan (Ref. 9) are shown in Figure 1. The Planck mean absorptance for a mixture can be estimated by:

$$K_p = \sum_i P_i K_{pi}$$

where P_i is partial pressure of the ith radiating species.

The volumetric radiative heat transfer term, $\dot{q}_r$, in governing equation can be expressed as

$$\dot{q}_r = -4K_p\sigma(T^4 - T_w^4) \qquad \frac{cal}{cm^3\text{-}sec}$$

The second term represents the radiation back from the environment having temperature Tw.

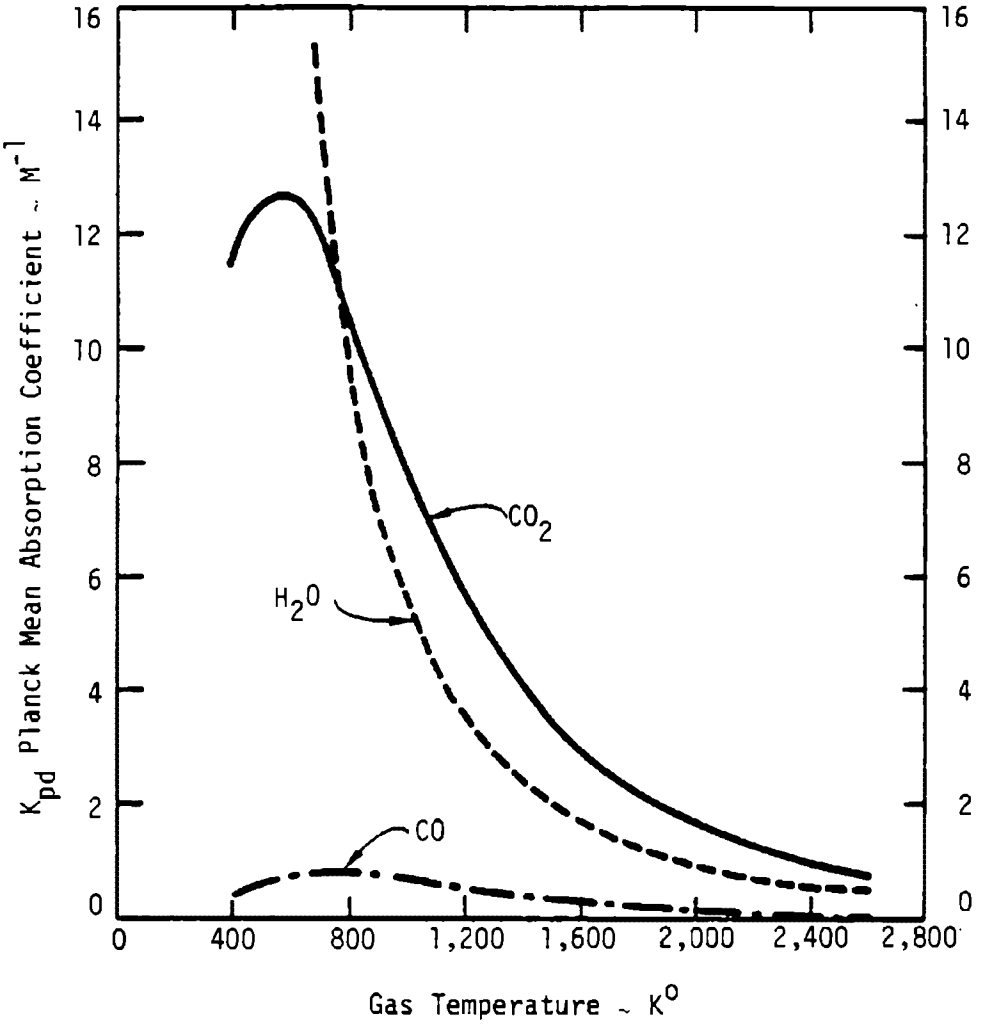

Figure 1. Planck Mean Absorption Coefficients at One Atmosphere Total Pressure

8.0 NUMERICAL METHOD OF SOLUTION

The governing set of parabolic partial differential equations [Eqs. (4-2), (4-2), and (4-3)] are first rewritten in backward finite difference form which gives implicit formulation. The implicit formulation is necessary due to stiffness of the partial differential equations which describe the flow system involving fast finite-rate chemistry.

Numerical marching is in the x-direction. That is, all equations at all grid points in the r-direction will be solved simultaneously at each x station. The following basic differencing formulations, based on nonuniform numerical grids, are used.

$$\left(\frac{\partial F}{\partial x}\right)_{n+1,m} = \frac{F_{n+1,m} - F_{n,m}}{\Delta x} \tag{8-1}$$

$$\left(\frac{\partial F}{\partial y}\right)_{n+1,m} = \frac{\Delta y_m}{(\Delta y_{m+1} + \Delta y_m)} \frac{F_{n+1,m+1} - F_{n+1,m}}{\Delta y_{m+1}} + \frac{\Delta y_{m+1}}{(\Delta y_{m+1} + \Delta y_m)} \frac{F_{n+1,m} - F_{n+1,m-1}}{\Delta y_m} \tag{8-2}$$

$$\left[\frac{\partial}{\partial y}\left(C \frac{\partial F}{\partial y}\right)\right]_{n+1,m} = \frac{1}{0.5\,(\Delta y_{m+1} + \Delta y_m)} \left[C_{n,m+\frac{1}{2}} \frac{F_{n+1,m+1} - F_{n+1,m}}{\Delta y_{m+1}} - C_{n,m-\frac{1}{2}} \frac{F_{n+1,m} - F_{n+1,m-1}}{\Delta y_m}\right] \tag{8-3}$$

where $\Delta y_m = y_m - y_{m-1}$ and $C_{n,m+1/2} = 0.5\,(C_{n,m+1} + C_{n,m})$. The subscript n denotes the nth grid point in the x-direction and m denotes the mth grid point in the y-direction.

Applying Eqs. (8-1), (8-2), and (8-3) to Eq. (4-1), and linearizing the nonlinear terms in $\dot{Q}$ function via Taylor series expansion (truncated after the first-order term) gives:

$$\frac{C}{\Delta x}\left(F^i_{n+1,m} - F^i_{n,m}\right) = \left\{a^i\left(F^i_{n+1,m+1} - F^i_{n+1,m}\right) + b^i\left(F^i_{n+1,m} - F^i_{n+1,m-1}\right)\right\} + \left\{c^i\left(F^i_{n+1,m+1} - F^i_{n+1,m}\right) + d^i\left(F^i_{n+1,m} - F^i_{n+1,m-1}\right)\right\} + \left\{\dot{Q}^i_{n,m} + \sum_j \beta_{ij}\left(F^j_{n+1,m} - F^j_{n,m}\right)\right\} + R^i_{n,m} \tag{8-4}$$

where

$$a^i = C^i_{o,m} \frac{\Delta y_m}{\left(\Delta y_{m+1} + \Delta y_m\right) \Delta y_{m+1}}$$

$$b^i = C^i_{o,m} \frac{\Delta y_{m+1}}{\left(\Delta y_{m+1} + \Delta y_m\right) \Delta y_m}$$

$$c^i = \frac{C^i_{1,m}\, C^i_{2,m+\frac{1}{2}}}{0.5 \left(\Delta y_{m+1} + \Delta y_m\right) \Delta y_{m+1}}$$

$$d^i = \frac{-C^i_{1,m}\, C_{2,m-\frac{1}{2}}}{0.5 \left(\Delta y_{m+1} + \Delta y_m\right) \Delta y_m}$$

$$\beta_{ij} = \left(\frac{\partial \dot{Q}^i}{\partial F^j}\right)_{n,m}$$

In the above, the superscript "i" was introduced as an equation index. Species, energy and density equations have to be solved in coupled fashion, while momentum and continuity equations can be solved subsequently in uncoupled fashion. After some algebra, Eq. (8-4) can be rearranged to form:

$$A^i_{n,m} F^i_{n+1,m-1} + \sum_j B_{ij} F^j_{n+1,m} + C^i_{n,m} F^i_{n+1,m+1} = (QR)^i_{n,m} \qquad (8\text{-}5)$$

where:

$$A^i_{n,m} = -\left(b^i + d^i\right)$$

$$B_{ij} = \beta_{ij} \qquad \text{if } i \neq j$$

$$= \left(\beta_{ii} - \frac{C}{\Delta x} - a^i - c^i + b^i + d^i\right) \quad \text{if } i = j$$

$$C^i_{n,m} = \left(a^i + c^i\right)$$

$$(QR)^i_{n,m} = -\left(\dot{Q}^i_{n,m} + R^i_{n,m} + \frac{C}{\Delta x} F^i_{n,m}\right) + \sum_j \beta_{ij} F^j_{n,m} \quad .$$

Incorporating proper boundary conditions into Eq. (8-5), the resulting equation can be rearranged to obtain the following block matrix equation:

$$\bar{M}\,\bar{F} = \bar{Q} \tag{8-6}$$

where $\bar{F}$ is a solution vector of elements $F^{i}_{n+1,m}$ and $\bar{Q}$ is a vector of elements $(QR)^{i}_{n,m}$. $\bar{M}$ is a tridiagonal block matrix:

$$\bar{M} = \begin{bmatrix} \bar{B}_1 & C_1 & & & \\ A_2 & \bar{B}_2 & C_2 & & \\ & & & & \\ & & \bar{A}_{m-1} & \bar{B}_{m-1} & \bar{C}_{m-1} \\ & & & \bar{A}_m & \bar{B}_m \end{bmatrix} \tag{8-7}$$

The matrix $\bar{B}_i$ is a full matrix of elements B_{ij} and the matrices $\bar{A}$ and $\bar{B}$ are diagonal matrices of elements $A^{i}_{n,m}$ and $B^{i}_{n,m}$.

Block matrix equation (Eq. 8-6) can be solved directly using the band-matrix factorization method (Appendix A). The solution vector $\bar{F}$ contains species distribution, temperature and density of all grid points at the fixed value of x. Momentum finite difference equation (Eq. 8-4, $F^{i} = U$) is solved individually via tridiagonal matrix method for mainstream velocity U at all grid points. Cross-stream velocity v is obtained via numerical integration of the continuity equation point-by-point from the boundary where v is known.

The method is basically noniterative. Therefore, the truncation error due to the linearization of nonlinear terms has to be carefully controlled. The error is controlled by varying the marching step size Δx, since the finite difference equations asymptotically approach the differential equations they represent when $\Delta x \to 0$. The general strategy used is to limit the step size Δx so that no component of solution can vary by more than the same small percentage of its value at the last step; i.e.,

$$\Delta_{max} \equiv \underset{i,m}{\text{Max}} \left| \frac{F^i_{n+1,m} - F^i_{n,m}}{F^i_{n,m}} \right| < \varepsilon_1 \qquad (8\text{-}8)$$

If Δ_{max} is greater than ε_1 the numerical integration is repeated, cutting the step size in half. The integration is repeated, continually halving the step size until criterion (8-8) is satisfied. A lower limit (say, ε_2) for Δ_{max} is also set. If Δ_{max} is less than $\varepsilon_2 (< \varepsilon_1)$, the step size is doubled for next integration step. Based on past experience in numerical experiments, ε_2 = 2% and ε_1 = 5% are good error limits for general steady-state or time-dependent problems. For the class of problems such as flat flame and strain flame in which only asymptotic solutions are of interest, the error limits ε_1 and ε_2 can be increased as long as solutions remained stable. Since the calculations seek only asymptotic solutions, the calculations will stop when the time-wise change of all variables becomes very small, i.e.

$$\Delta_{max} \left(\frac{u}{\Delta x} \right) < \varepsilon_3 \qquad (8\text{-}9)$$

where ε_3 is a small number to be input to the program. The value of ε_3 varies with the class of the problems. Generally, ε_3 = 0.001 gives sufficiently accurate solutions to problems such as flat flames or strain flames.

9.0 APPLICATIONS

9.1 Free Jet Diffusion Flame

As an example of a typical flame calculation, a hydrogen-jet is considered with maximum nozzle exit velocity of 1000 cm/sec. The jet issues into still air. The nozzle diameter is 0.635 cm. Both the air and hydrogen temperatures are 300^{o}K at atmospheric pressure. This case is the same as the sample case in Kee and Miller's work (Ref. 13). The initial velocity distribution at nozzle exit plane is assigned in the same way as with Kee and Miller (Ref. 13). The initial ignition source is somewhat arbitrary, has no physical significance and represents a very small percentage of total energy. Distributions of initial velocity and temperature are plotted in Figure 2. The calculation was done in a physical coordinate system with uniform good spacing in the r-direction. Radiative heat transfer is not considered in this calculation. Initial number of grid points is 25, which includes two free-stream points. The flame shows very rapid expansion in the radial direction near the nozzle exit plane. Therefore, the code allows the addition of a grid point (at free-stream condition) whenever the "next-to-last" radial grid point value of temperature or velocity or species differs from the corresponding free-stream value by more than a specified percentage of free-stream value (one percent has been selected in this calculation). The number of grid points is not allowed to grow unbounded, with the number of points being halved (eliminating every other point) when the maximum number of points (50) is reached.

The reaction mechanism used is the H_2-subset of the basic EER kinetic set (Appendix B). The H_2-subset involves 9 species (H_2, O_2, N_2, O, H, OH, H_2O_2 and HO_2) and 18 reactions.

The numerical results of this calculation are shown in Figures 3 - 6. Figure 3 shows the isothermal contours of the flame. The flame length, which is defined as the peak temperature at the center line, is 5.8 cm. Figure 4 shows the distributions of downstream velocity and cross-stream velocity at a distance of 5 nozzle radii from exit plane. The distributions of major stable species and temperature (at X/R=5.0) are plotted in Figure 5. It is noted that the peak temperature is on the rich side of the flame, which is consistent with the result of the equilibrium

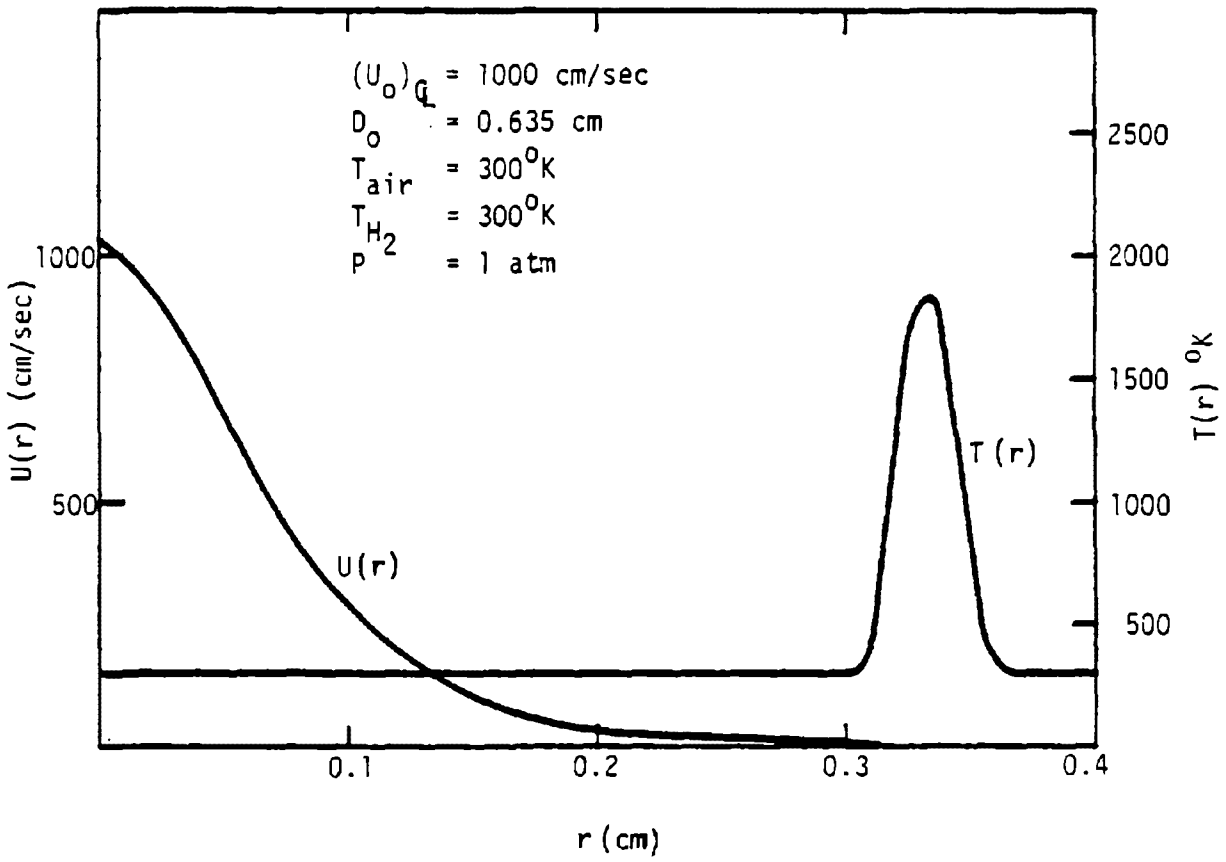

Figure 2. Initial Velocity and Initial Temperature Distribution.

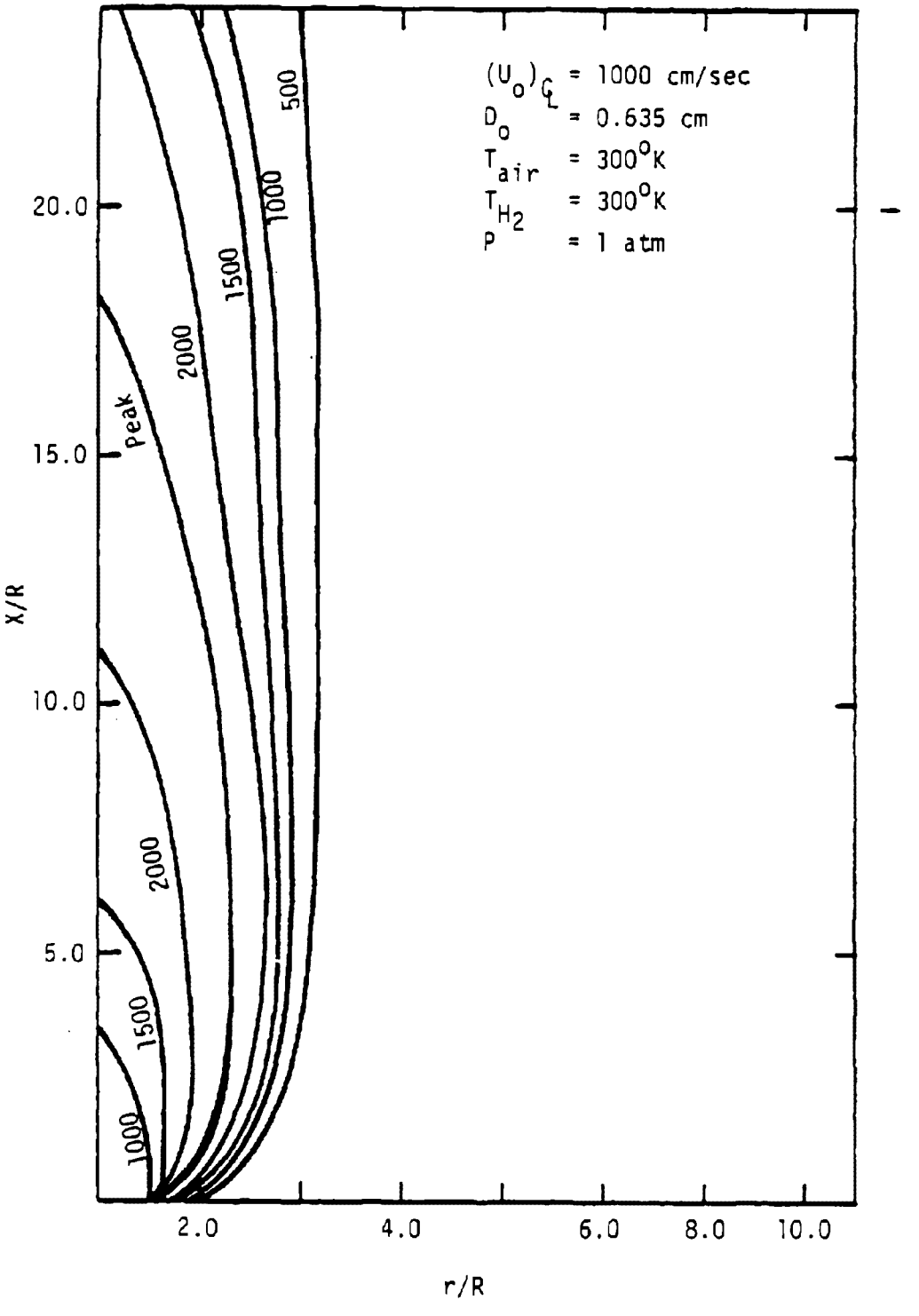

Figure 3. Isothermal Contours for Laminar H_2/Air Diffusion Flame.

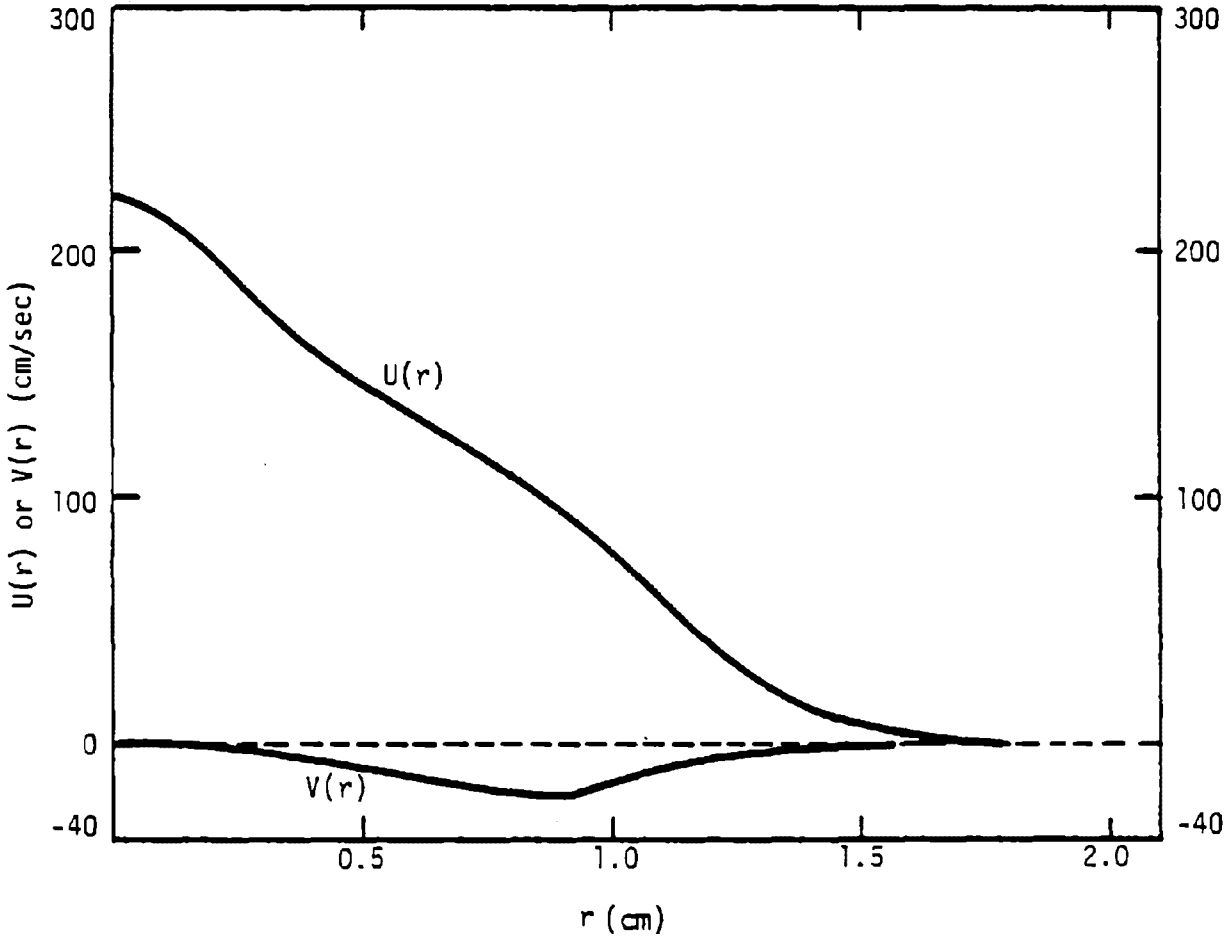

Figure 4. Velocity Components U(r) and V(r) at X/R = 5.0.

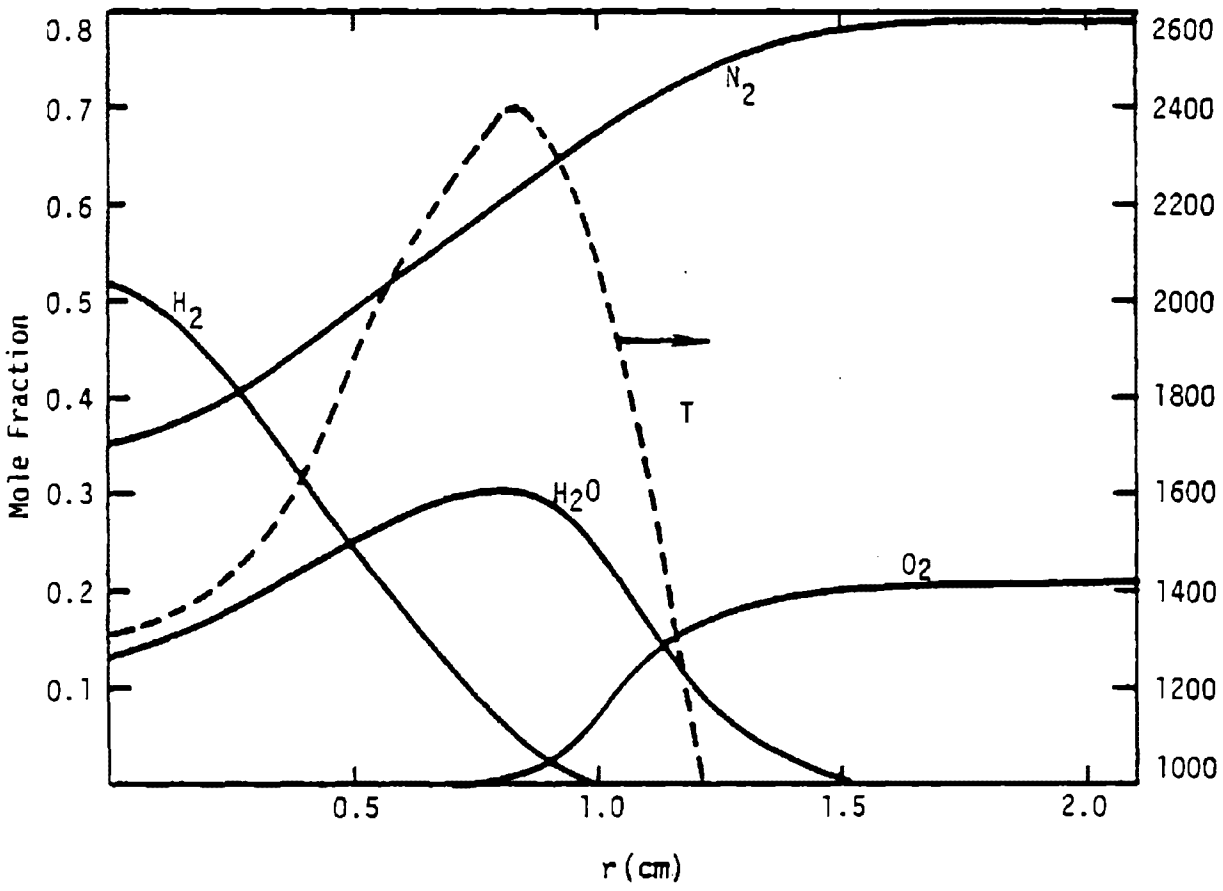

Figure 5. Distribution of Stable Species and Temperature at X/R = 5.0.

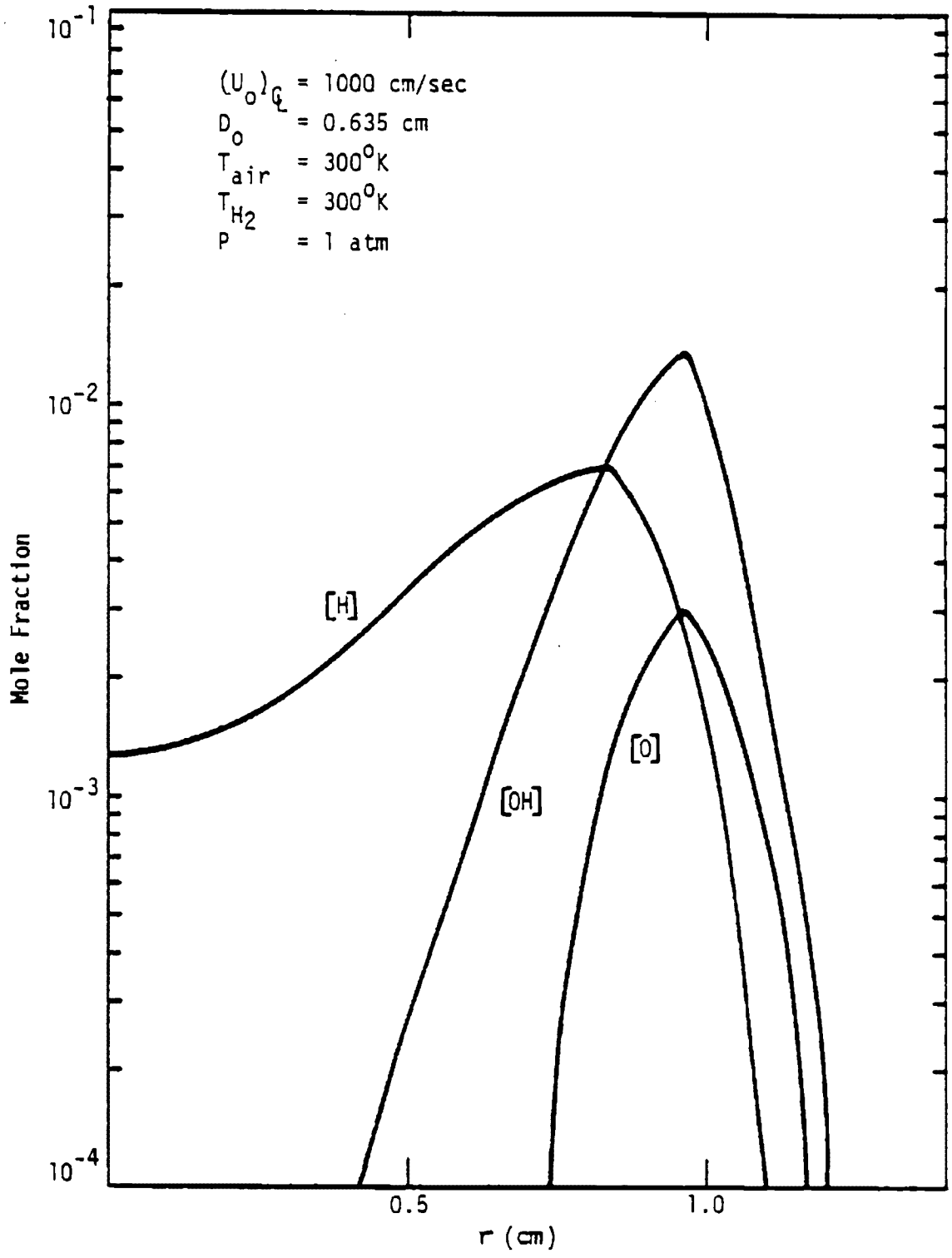

Figure 6. Distributions of Radical Species in an H_2/Air Diffusion Flame at X/R = 5.0.

calculation. The peak temperature is very close to the actual adiabatic flame temperature. The distributions of radical species (at X/R = 5.0) are plotted in Figure 6.

The entire calculation for the process, which occurs 13 cm from exit plane, takes 930 noniterative integration steps in the x-direction. The computer time is about 200 sec CPU time (in a CDC 7600 computer) which is equivalent to about one twentieth of the computational time needed by Kee and Miller (Ref. 13) for the same calculation (using a split-operator method).

The numerical results of the present calculations are not expected to be identical with those of Kee and Miller, since the formulation of diffusion coefficients and the reaction mechanism used in present calculations are different from those used by Kee and Miller.

9.2 Confined, Co-flowing LBG Diffusion Flame and Fuel Nitrogen Conversion

In order to study the effect of methane level in low Btu gas diffusion flames on fuel nitrogen conversion, a series of laboratory scale laminar diffusion flame experiments has been conducted in EER's laboratory (Ref. 14). Some of these results have also been simulated using GFAP's confined diffusion flame model.

Flame burner parameters are (see Figure 7):

Fuel tube ID = 0.236 cm
Air tube ID = 5.08 cm

The low Btu gas used in the EER experiment is basically composed of $CO/H_2/N_2$. Normally, the CO/H_2 ratio is 1.0 and N_2 is 55 percent in the fuel; however, CO/H_2 in the fuel can be replaced by CH_4. The fuel was doped with 3059 ppm of either NH_3 or NO, with air as the oxidant. The basic flame parameters are:

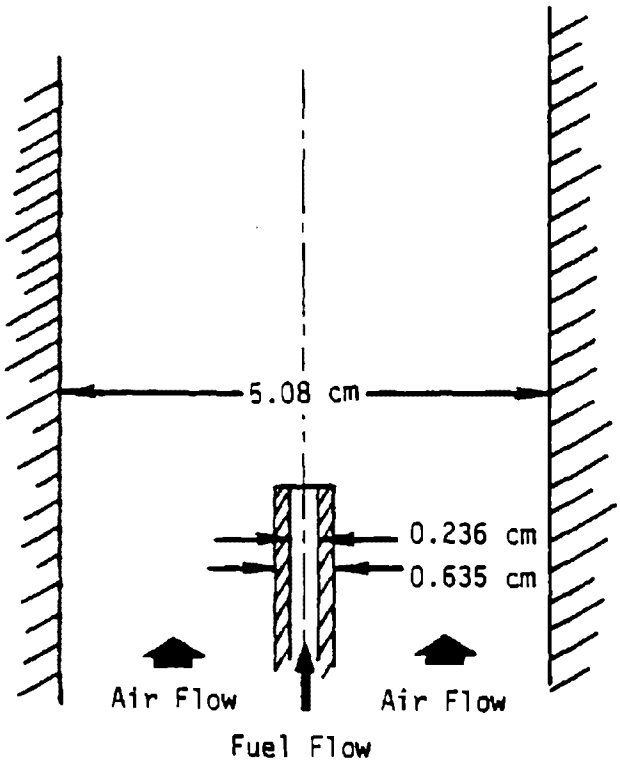

Figure 7. EER Diffusion Flame Burner.

Case No.	1	2	3
Percent CH_4 in Fuel	0	5	10
Fuel Mean Velocity (cm/sec)	685	685	685
Air Mean Velocity (cm/sec)	13.15	17.53	21.92
Air Temperature (^{o}K)	367	367	367
Fuel Temperature (^{o}K)	367	367	367
Visual Flame Length (cm)	35.5	40.6	50.8

This gives a constant overall stoichiometry equal to 150 percent T.A. when the effects of dopants on stoichiometry are neglected.

In comparison with EER's experimental data, the predicted exhaust NO levels are shown in Figures 8 and 9 for NH_3 doping and NO doping, respectively. EER's latest kinetic set was used in these calculations, quantitatively predicting the exhaust NO level for the flame with various types of LBG fuel and dopant.

The exhaust NO levels without dopant, i.e. thermal NO, are also shown in Figures 8 and 9 in comparison with experimental data. The discrepancy is due to the sensitivity of thermal NO level to the flame sheet temperature. The predicted flame temperature for the flame sheet of the flame with 10 percent CH_4 (in fuel) ranges from 1960^{o}K to 1720^{o}K and is, of course, sensitive to the accuracy of the heat transfer model.

Calculations were made for the NO doping case with 10 percent methane to establish the effect of flame temperature on fuel nitrogen conversion. Figure 10 shows the peak flame sheet temperature, total NO, and NO with a thermal level subtracted out, all as a function of increasing heat transfer; i.e., decreasing flame sheet temperature. Heat transfer increases linearly with the heat transfer index shown in Figure 10. The index has a value of zero for the adiabatic case and a value of one for the heat transfer associated with a simple radiation model. Although the peak flame sheet temperature varies by over 200^{o}K, the total NO level remains approximately constant. However, due to the change in production of thermal NO, the uncoupled "fuel nitrogen conversion" is predicted to increase substantially as flame temperature is depressed.

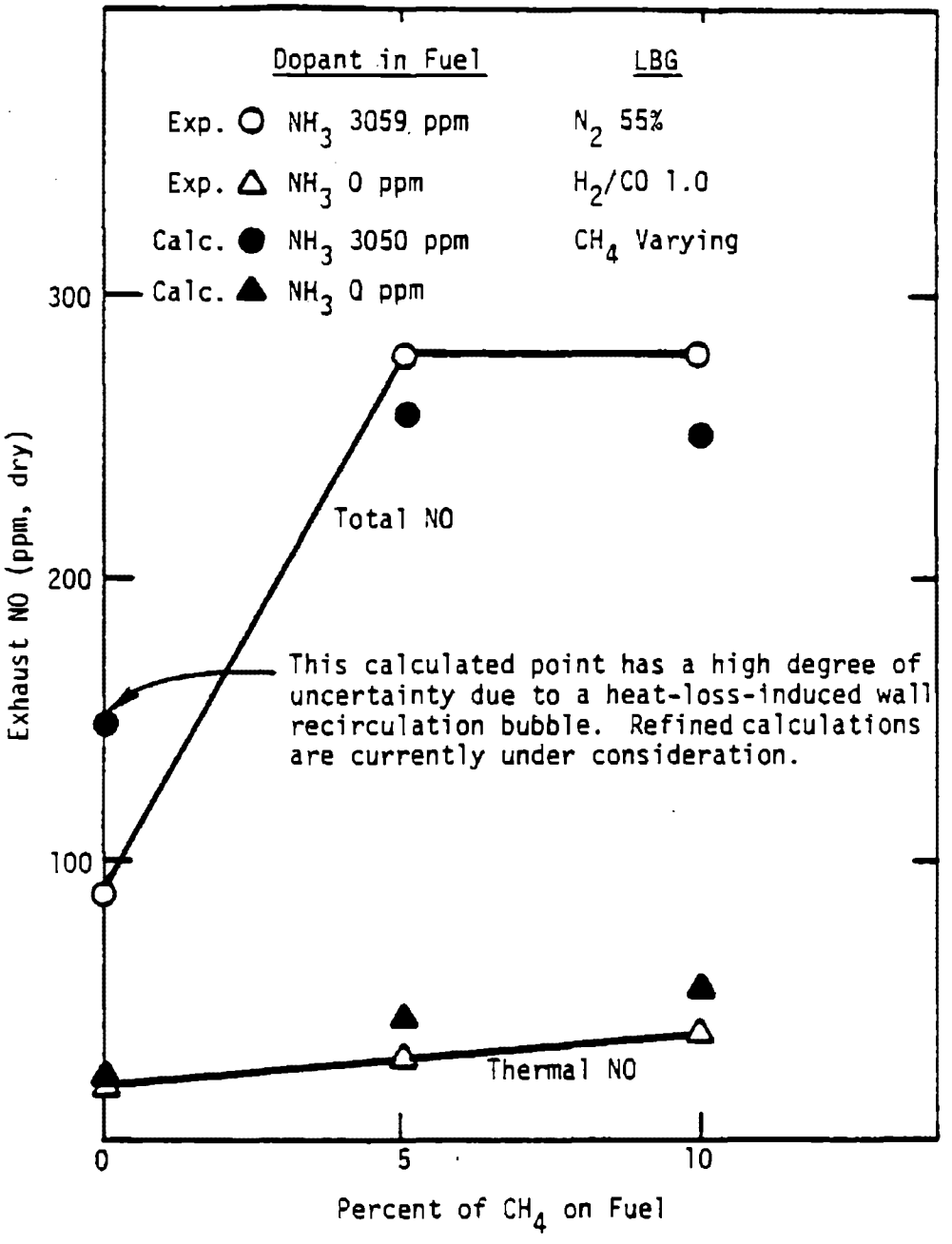

Figure 8. Influence of CH_4 Content on NH_3 Conversion in LBG Diffusion Flames.

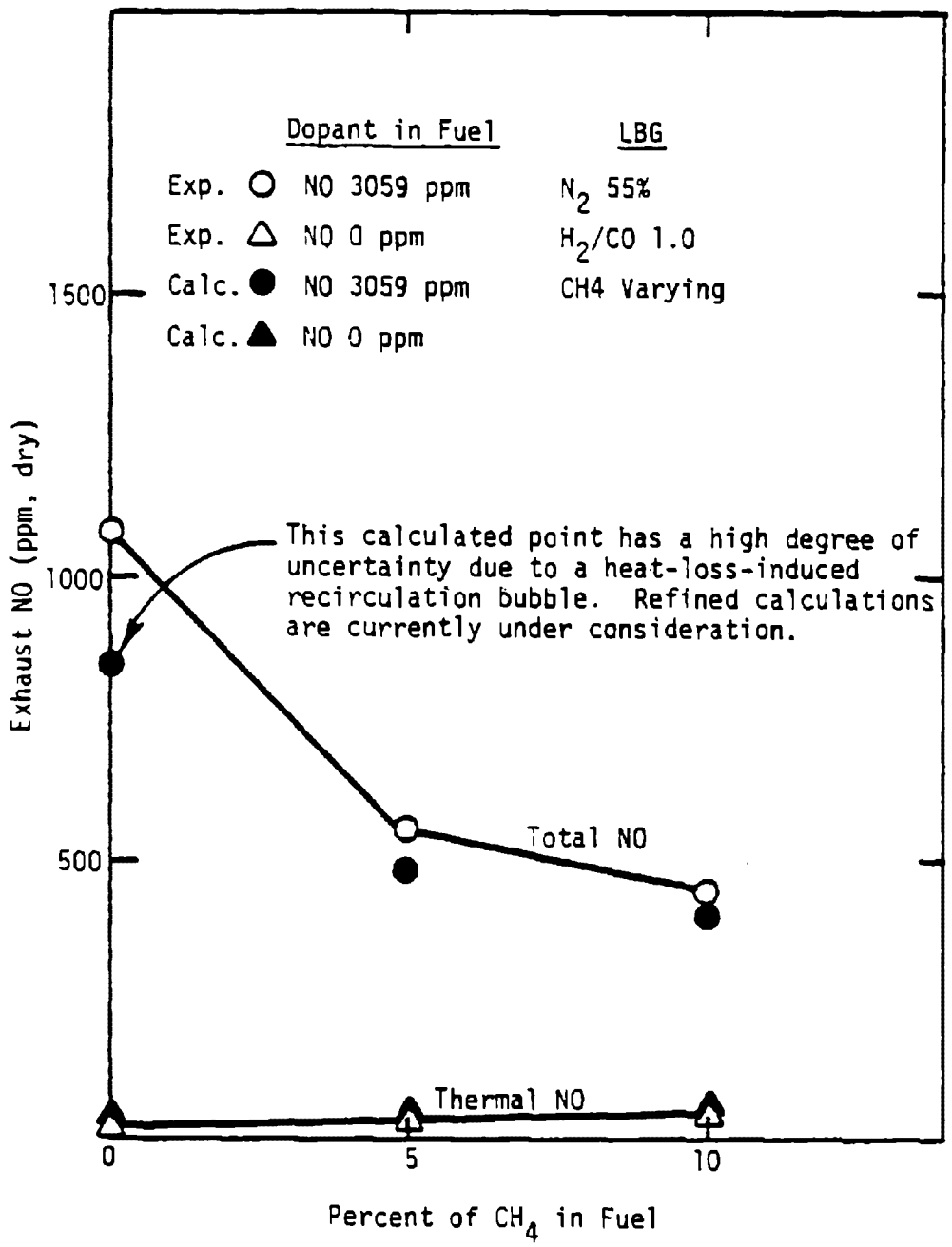

Figure 9. Influence of CH_4 Content on NO Conversion in LBG Diffusion Flames.

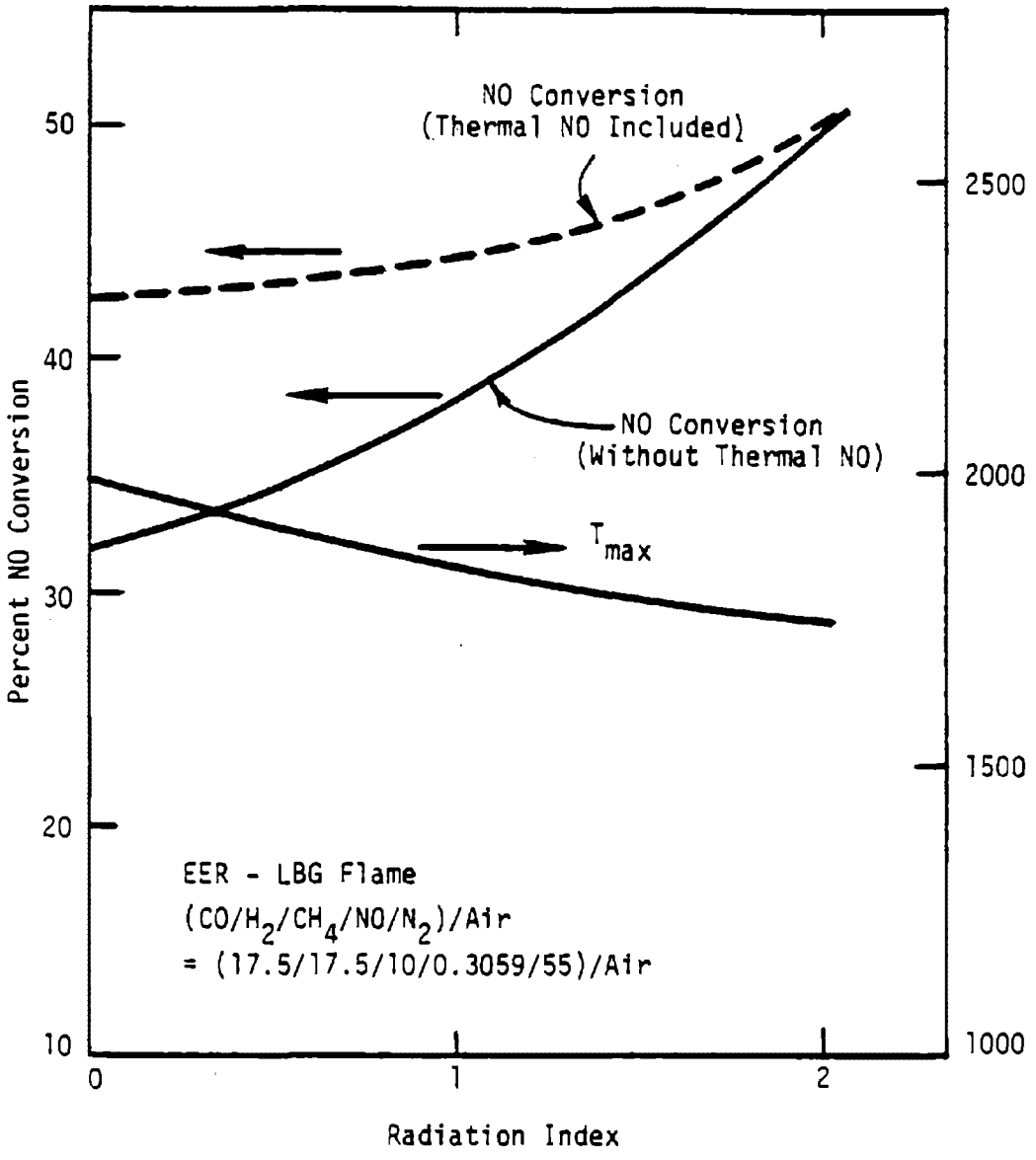

Figure 10. Influence of Temperature on NO Conversion in Diffusion Flames--10 Percent CH_4.

9.3 Flat Flame Simulation

Flat flame calculation is a typical time-dependent problems with an asymptotic solution. Here the methane flame of Biordi et al. (Ref. 15) has been chosen as an example for comparison to GFAP's prediction. Biordi's study used a low-pressure (32 torr) premixed methane flame (10.3 percent CH_4, 21.6 percent O_2, 68.1 percent AR). Flow velocity at 300°K was 80 cm/sec from a flat-flame burner. Molecular beam mass spectroscopy was used to determine stable and radical species concentrations. The flame was simulated as a free (unattached to the flat flame burner surface) flat flame. The free flame velocity calculated is 76.2 cm/sec, which agrees very well with the experimental value. The stable species profiles calculated are plotted in Figure 11 in comparison with Biordi et al.'s measurements. The major deviation appears to be underprediction of CO oxidation rate by the current EER kinetic set. Figure 12 illustrates the comparison between experimental data and GFAP predictions for a number of radical species. In general, the agreements are less than satisfactory. The predicted OH shows fair agreement with data, while both O and H radicals are about 50 percent below the experimental values. The predicted temperature profile is higher than the measured value, which is probably partially due to gas radiation which was not taken into consideration. The only intention here is to illustrate the application of GFAP; further discussion of kinetic aspect of this calculation is beyond the scope of this report.

9.4 Constant Strain-Rate Laminar Diffusion Flame

The constant strain-rate laminar diffusion flame is a planar nonpremixed diffusion flame with external fuel and oxidizer flow undergoing uniform accelerations (e.g. u=ax) such that the strain rate, du/dx, is independent of position along the flame. This situation exists, for example, near the stagnation point in opposed-jet combustion. More importantly, a constant strain-rate laminar diffusion flame characterizes the flamelet behavior of the fuel/oxidizer "eddy" interface in nonpremixed turbulent flame. In these regions, the strain rate is slowly varying.

It can be shown that the solution to the Navier-Stokes equation describing the behavior of constant strain-rate laminar diffusion flames is self-similar in

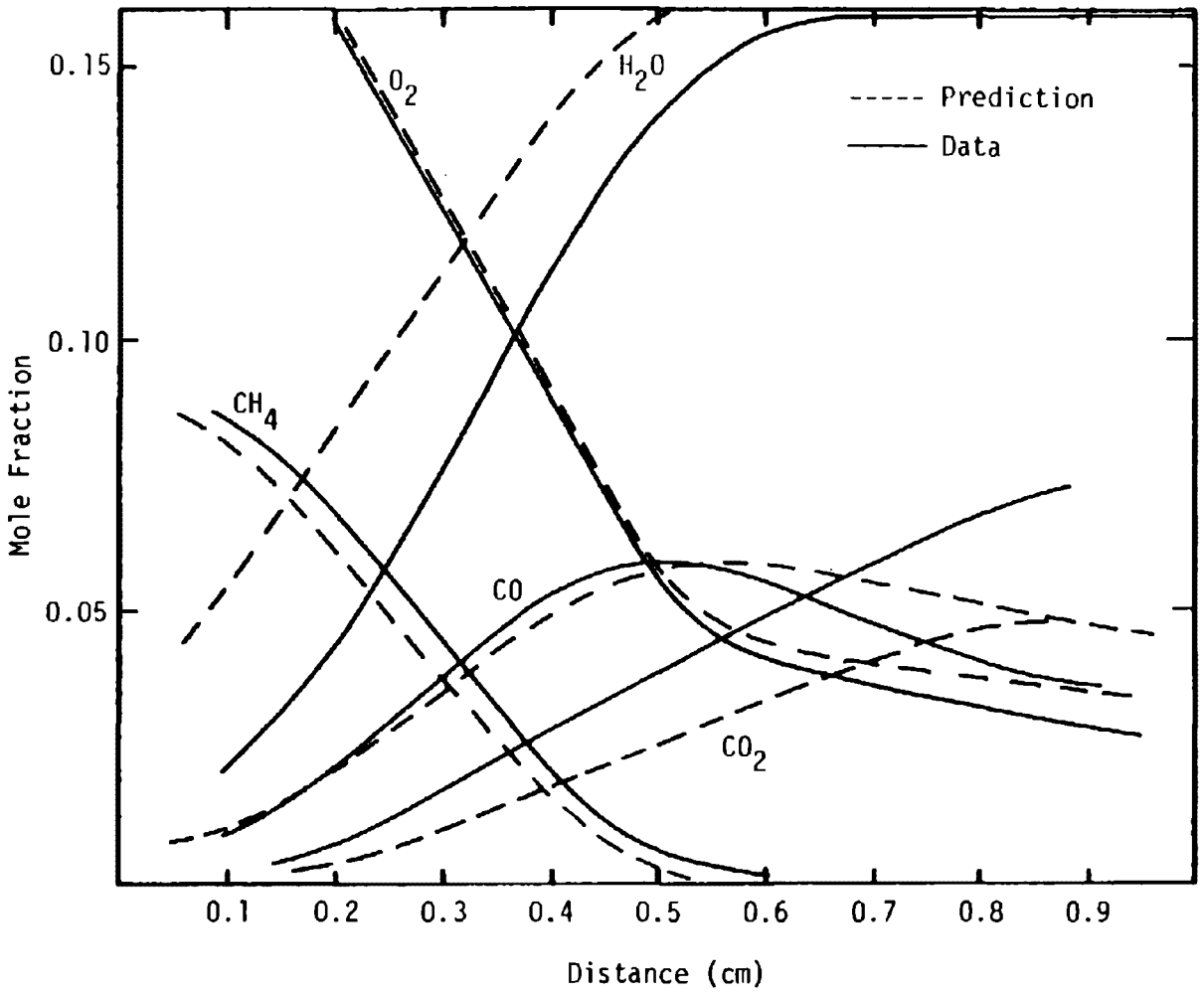

Figure 11. Flame Profiles of Biordi et al. (1975). Solid Lines are Data; Dashed Are Model.

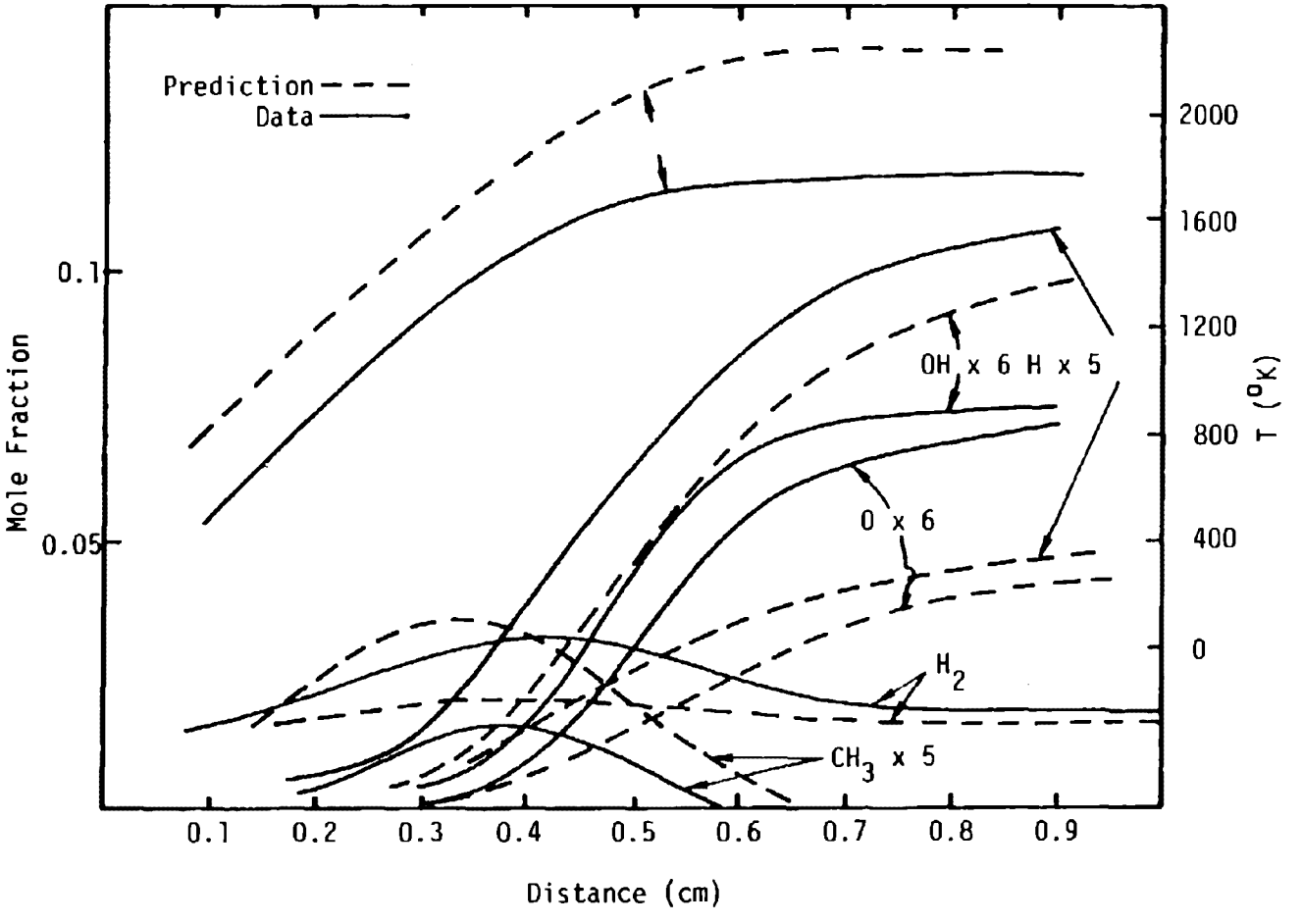

Figure 12. Profiles Through the Flame of Biordi et al. (1975).

the streamwise (x) direction and can be represented by the boundary layer equation under uniformly accelerating flows.

The GFAP model properly analyzes a constant strain-rate laminar diffusion flame. The computation can start with an arbitrary distribution and march forward in the streamwise direction until a steady solution is achieved. The pressure gradient in the momentum equation is obtained from Bernoulli's equation in differential form:

$$\rho u \frac{du}{dx} = - \frac{dp}{dx}$$

Noting that the fuel side acceleration u equals ax, it can be shown that

$$\frac{dp}{dx} = - \rho a^2 x \quad .$$

The sample calculation here is for a CH_4/air opposed jet diffusion flame (see Figure 13). The fuel side strain rate is set to 250 (1/sec). Both fuel and air are at 300°K and one atm. The velocity (v) profile for the steady solution is plotted in Figure 14. The displacement δ is the distance between imaginary (nonreacting and inviscid solution) stagnation point of the fuel jet and that of the air jet. For this case δ is 0.15 cm. The CH_4 and O_2 profiles are shown in Figure 15. The temperature profile is also shown in Figure 15. The peak flame temperature is about 1950°K. Peak temperature decreases with increasing strain rate since increase in strain rate means a thinner flame zone and shorter effective residence time of reactants in reaction zone. Figure 16 shows the flame temperature as a function of strain rate. The critical value of strain rate is shown to be 650 (1/sec), beyond which a flame cannot exist (i.e. the extinction limit). The critical value is a function of reaction chemistry alone and is independent of molecular transport coefficients (i.e. independent of Reynolds number). This is due to the fact that the molecular transport coefficients (e.g. viscosity) influence the solution only through an affine transformation of the r-coordinate; i.e.

$$\eta = r\sqrt{\frac{a}{\nu}}$$

The self-similar solution of temperature and species concentration is found as a

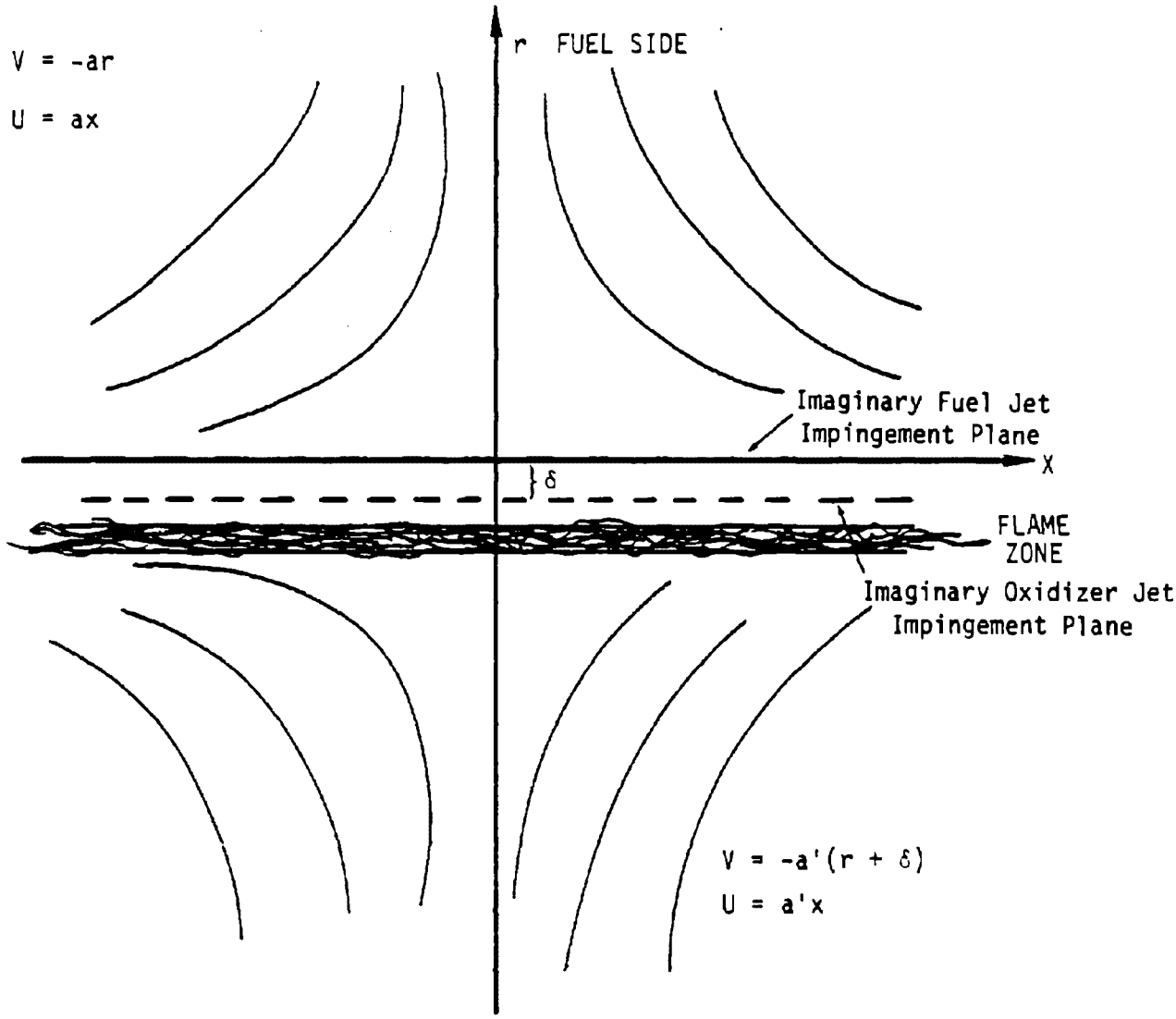

Figure 13. Schematic of Opposed-Jet Diffusion Flame.

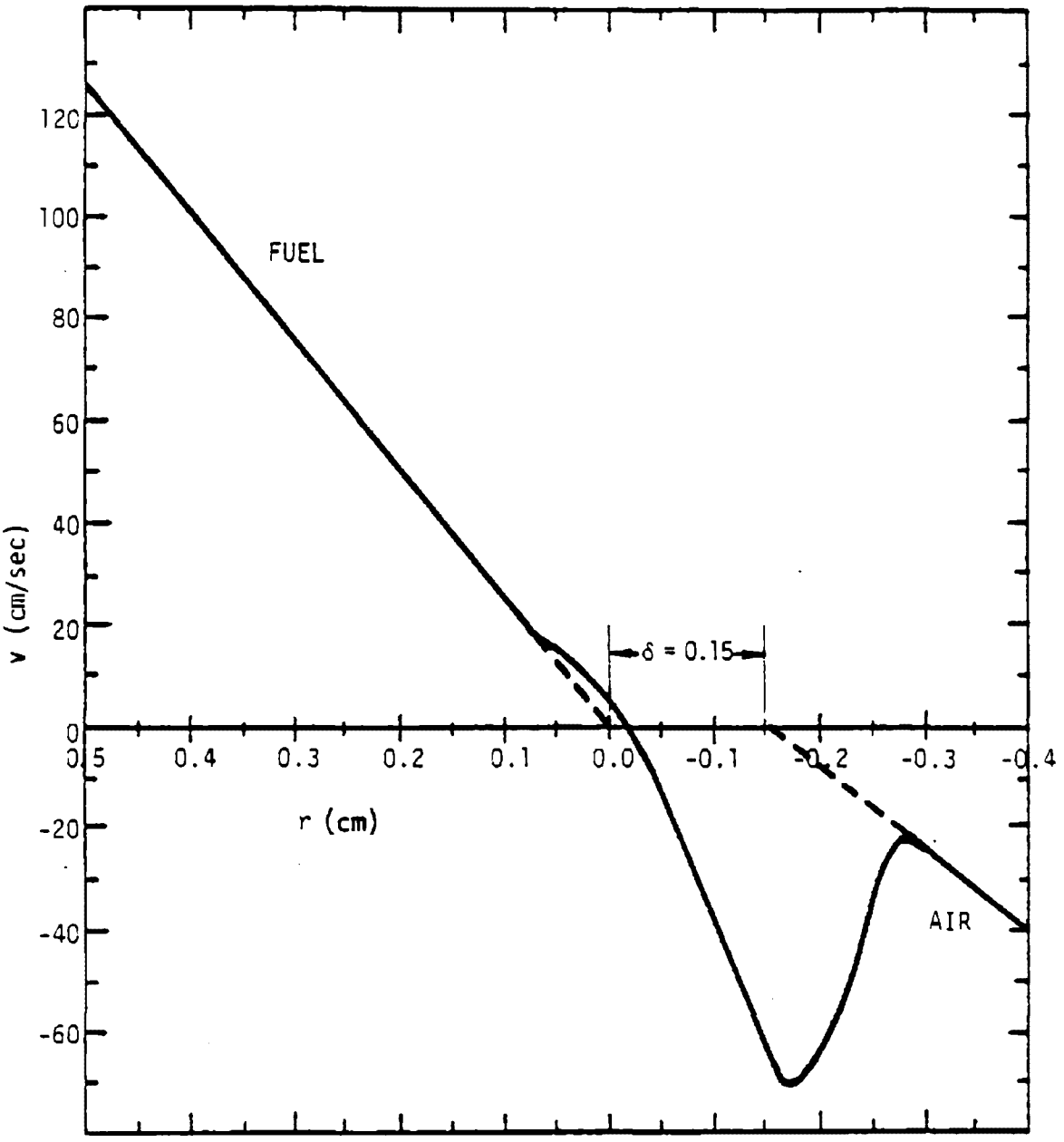

Figure 14. Velocity Profile of CH_4/Air Opposed-Jet Diffusion Flame (a=250 1/sec).

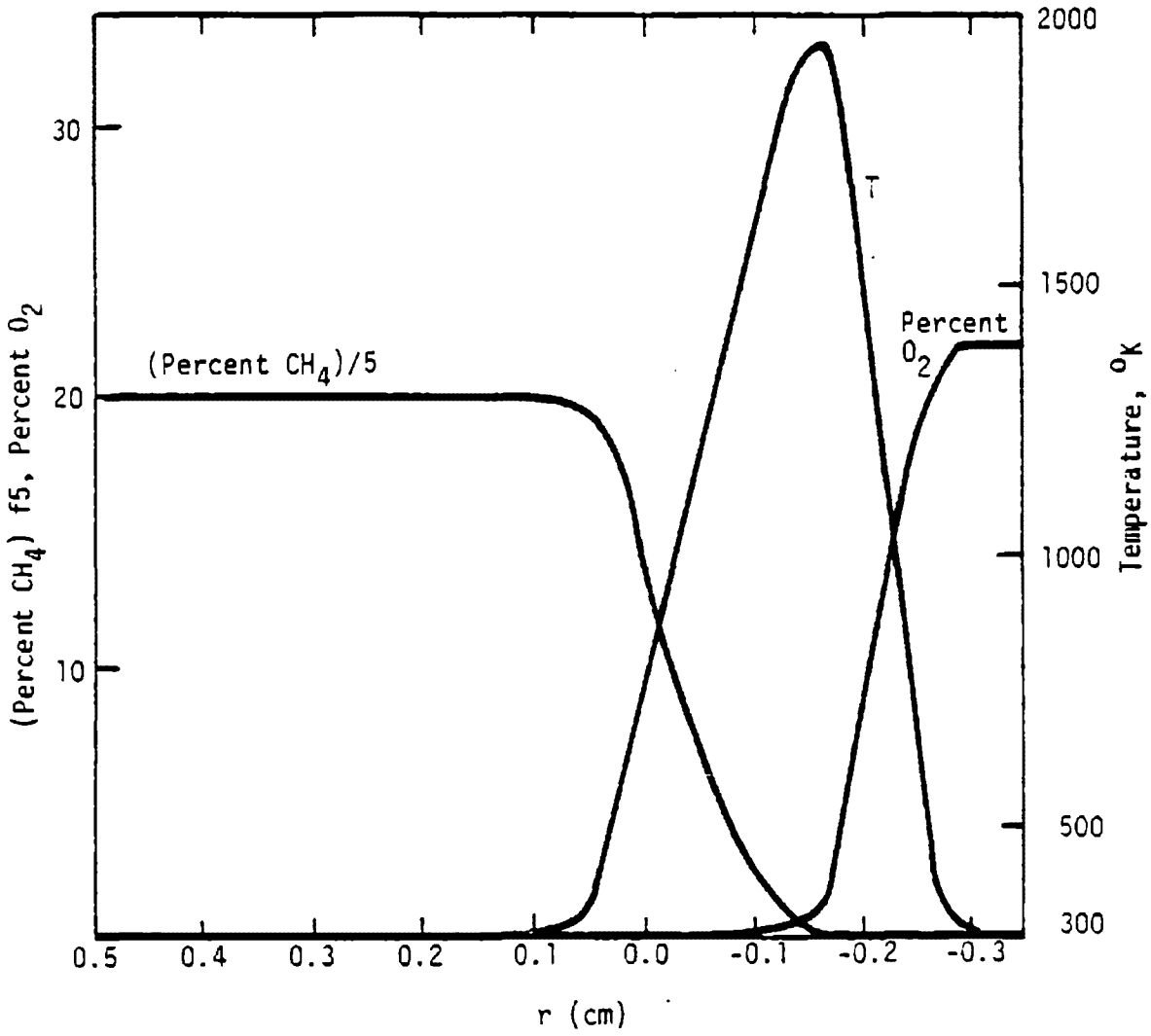

Figure 15. CH_4 and O_2 Profiles of CH_4/Air Opposed-Jet Diffusion Flame (a=250 1/sec).

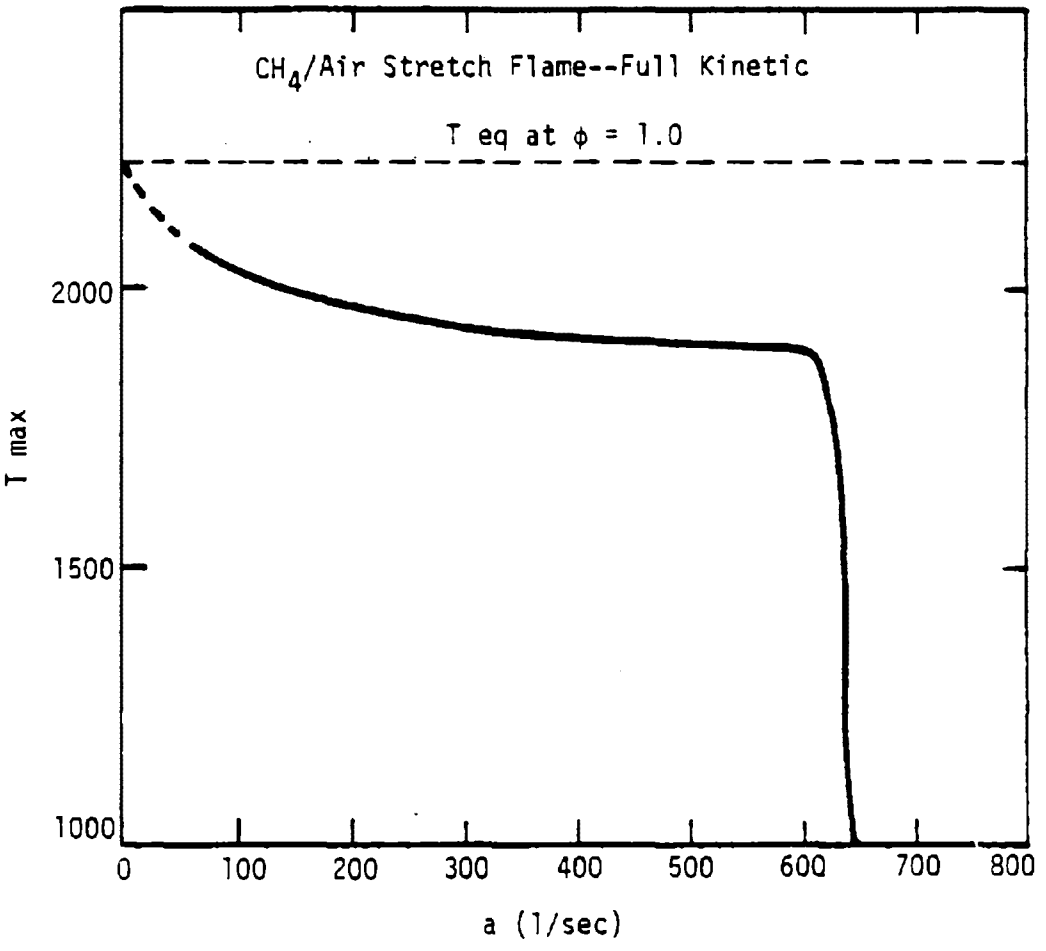

Figure 16. Flame Temperature vs. Strain Rate for CH_4/Air Opposed Jet Diffusion Flame.

function of η only. Viscosity has an influence on flame thickness and therefore on total burning rate.

Figure 17 shows the flame thickness, which is defined as the distance between the intersections of maximum slope of temperature curve and the T = 300°K coordinate line, as a function of strain rate. Figure 18 shows the stagnation point displacement as a function of strain rate. The computations are carried out using the basic EER kinetic subset including 71 reactions and 28 species. The computational time per case is approximately 4 minutes CPU time in CDC 7600.

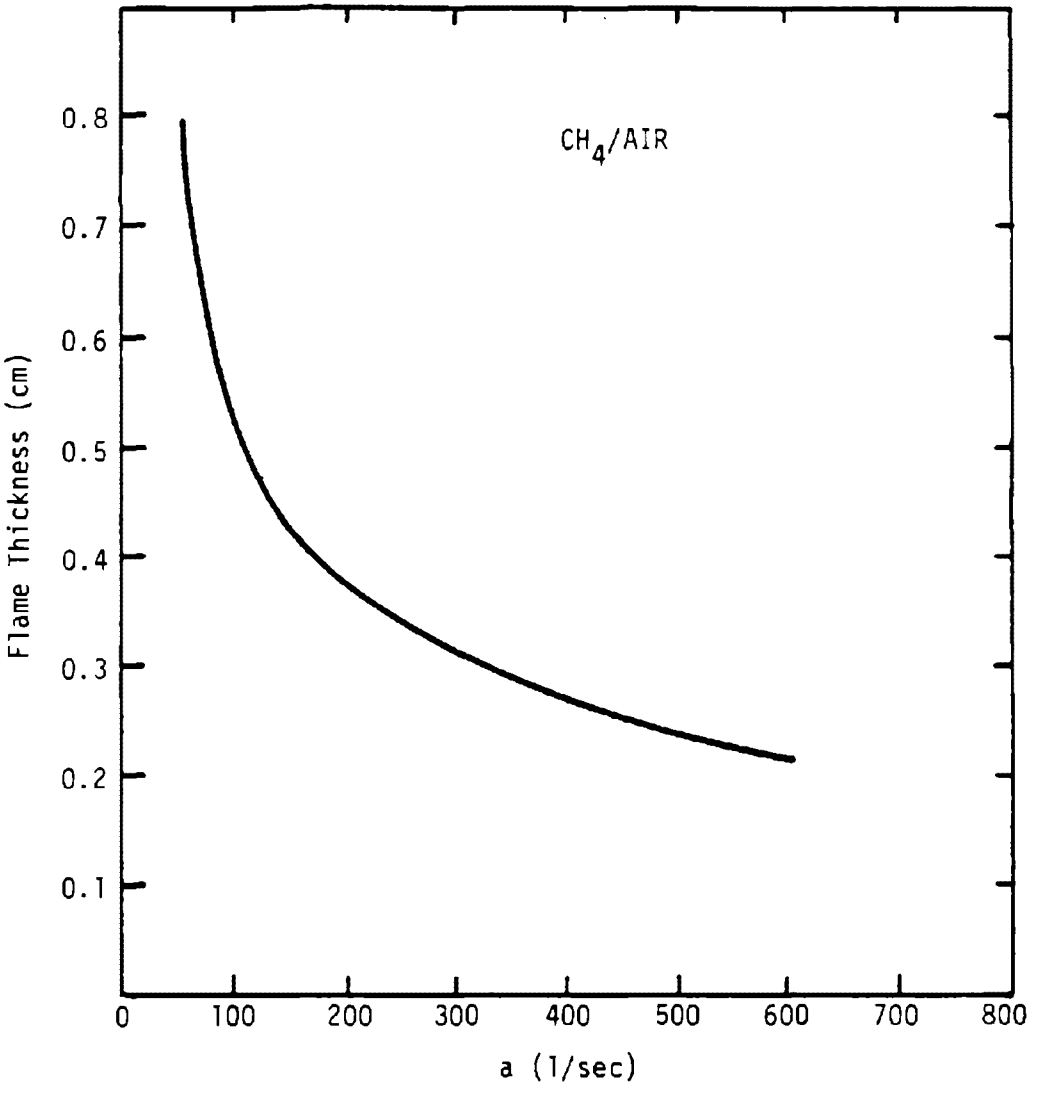

Figure 17. Flame Thickness vs. Strain Rate for CH_4/Air Opposed-Jet Diffusion Flame.

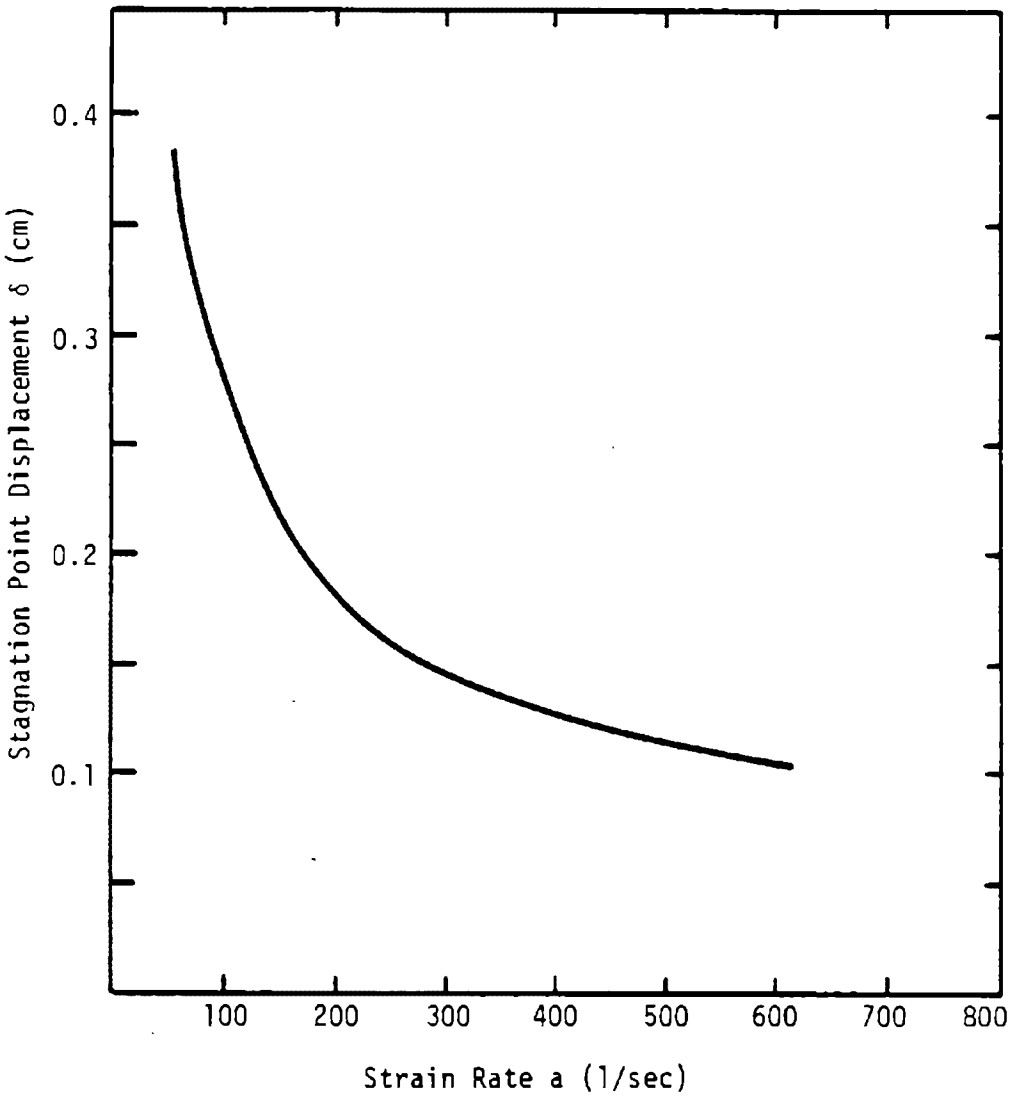

Figure 18. Stagnation Point Displacement vs. Strain Rate for CH_4/Air Opposed-Jet Diffusion Flame.

10.0 REFERENCES

1. Reid, R. C., Prensnitz, J. M., and Sherwood, T. K., The Properties of Gases and Liquids, 3rd edition (1977).

2. Monchick, L. and Mason, E. A., "Transport Properties of Polar Gases," J. of Chemical Physics, Vol. 35, No. 5, p. 1676 (1961).

3. Neufeld, P. D., Janzen, A. R., and Aziz, R. A., "Empirical Equations to Calculate 16 of the Transport Collision Integrals $\Omega^{(1,S)*}$ for Lennard-Jones (12-6) Potential," J. of Chemical Physics, Vol. 57, No. 3, p. 1100 (1972).

4. Bartlett, E. P., Kendall, R. M., and Rindal, R. A., "A unified Approximation for Mixture Transport Properties for Multicomponent Boundary Layer Applications," NASA CR-1063 (1967).

5. Ferri, A. J., "Review of Problems in Application of Supersonic Combustion," J. Roy. Aeron. Soc. 68 p. 575 (1964).

6. Schetz, J. A., "Turbulent Mixing of a Jet in Co-flowing Stream," AIAA, Vol. 6, No. 10 (1968).

7. Sparrow, E. M. and Cess, R. D., Radiation Heat Transfer, Brook/Cole Publishing Company, Belmont, California (1970).

8. Kelly, J. T. and Kendall, R. M., "Further Development of the Premixed One-dimensional Flame (PROF) Code," EPA-600/7-78-172a (NTIS PB286243) (1978).

9. Edwards, D. K. and Balakrishnan, A., "Thermal Radiation by Combustion Gases," Int. J. Heat and Mass Transfer, Vol. 16, p. 221 (1973).

10. Stull, D. R. and Prophet, H., "JANAF Thermochemical Tables--Second Edition," Dow Chemical Company, (1970).

11. Peaceman, D. W., "Fundamentals of Numerical Reservoir Simulation," Elsevier Scientific Publishing Co., New York (1977).

12. Kau, C. J., Pergament, H. S., and Mikatarian, R. R., "A New Computational Technique for Chemically Reacting Free-Shear Layer Flows," Symposium on Application of Computers to Fluid Dynamic Analysis and Design, Polytechnic Institute of Brooklyn, N.Y., Paper 4A(4), (1973).

13. Kee, R. J. and Miller, J. A., "A Split-Operator, Finite Difference Solution for Axisymmetric Laminar Jet Diffusion Flames," Sandia Laboratories, Livermore, CA, Rept. No. SAND 77-8502, (1977).

14. Folsom, B. A., Courtney, C. W., Corley, T. L., and Clark, W. D., "Advanced Combustion Concepts for Low Btu Gas Combustion," Proceedings of the Third Stationary Source Combustion Symposium; Volume II, EPA-600/7-79-050b (NTIS PB292540) (1979), p. 163.

15. Biordi, J. C., Lazzara, C. P., and Papp, J. F., "Flame Structure Studies of CF_3Br-Inhibited Methane Flames, II. Kinetics and Mechanisms," Proceedings of the Fifteenth Symposium (International) on Combustion, The Combustion Institute (1975), p. 917.

11.0 LIST OF NOMENCLATURE

A : defined as $\left(\frac{\rho u r^{\alpha}}{\psi^{\alpha}}\right)$

$B_1 B_2$: defined in Table 2

C, C_o, C_1, C_2 : defined in Table 1

C_{pi} : specific heat of species i

D_i : diffusion coefficients (cm^3/sec)

E_k : third body efficiency defined in Eq. (6-5)

f : defined as $\left(\frac{r}{\psi}\right)^{\alpha}$

f_i : diffusion factor of species i

G_i : Gibbs free energy

h_i : enthalpy of species i (cal/mole)

Ke : equilibrium constant

K_f : forward reaction constant

K_p : gas emittance

L : characteristic dimension of flame

Le : Lewis number

M_i : molecular weight of species i

P : pressure

P_i : partial pressure of species i

Pr : Prandtl number

$\dot{Q}$: defined in Table 1

$\dot{q}_r$: radiative heat transfer rate (cal/cm^3-sec)

R : defined in Table 1, or gas constant

r : cross-stream coordinate (cm)

T	:	Temperature (^{o}K)
u	:	downstream velocity (cm/sec)
v	:	cross-stream velocity (cm/sec)
$\dot{W}_i$	:	chemical production rate (mole/cm^3-sec)
x	:	downstream coordinate (cm)
X_i	:	species mole fraction
y	:	cross-stream coordinate = r for physical coordinate = ψ for stream function coordinate

Superscripts

i	:	equation index

Subscripts

ℓ	:	center line
e	:	edge of mixing layer
i	:	species index
m	:	grid index in r or ψ direction
n	:	grid index in x-direction
R,r	:	reference species

Greek Symbols

α	:	geometric index = 0 for 2-D cartesian coordinate system = 1 for polar cylindrical coordinate system = 2 for spherical coordinates
α_1	:	ith species concentration (mole/gm)
ρ	:	density (gm/cm^3)
λ	:	heat conductivity ($cal/cm\text{-}sec\text{-}^oK$)
ψ	:	stream function coordinate
μ	:	molecular/turbulent viscosity
φ_{ij}	:	defined in Eq. (5-3)
$\Omega^{(1.1)}$ $\Omega^{(2.2)}$	:	collision integrals
ε_o	:	minimum energy of attraction between molecules
$\varepsilon_1, \varepsilon_2, \varepsilon_3$	:	numerical error controls

APPENDIX A. Block Tridiagonal Matrix Equation Solver

To solve a matrix, the equation used is

$$\bar{M}\,\bar{F} = \bar{Q} \tag{A-1}$$

where $\bar{Q}$ and $\bar{F}$ are column reactors. $\bar{Q}$ is given, $\bar{F}$ is the solution matrix, and $\bar{M}$ is a block tridiagonal matrix of the form:

$$\bar{M} = \begin{bmatrix} B_1 C_1 & & & & \\ A_2 & B_2 & C_2 & & \\ & A_3 & B_3 & C_3 & \\ & & \ddots & \ddots & \ddots \\ & & & A_{m-1} B_{m-1} & C_{m-1} \\ & & & & A_m B_m \end{bmatrix} \tag{A-2}$$

here B_i are full matrices, A_i and C_i are diagonal matrices.

This matrix equation can be solved by band matrix factorization method (Ref. 11). The method will be described briefly in the following section.

The block tridiagonal matrix $\bar{M}$ can be factorized into lower and upper band matrices:

$$\bar{M} = \bar{L}\,\bar{U} \tag{A-3}$$

where $\bar{L}$ is the lower band matrix and $\bar{U}$ is the upper band matrix:

$$\bar{L} = \begin{bmatrix} L_1 & & & & \\ A_2 & L_2 & & & \\ & A_3 & L_3 & & \\ & & \ddots & \ddots & \\ & & & A_{m-1} L_{m-1} & \\ & & & & A_m L_m \end{bmatrix}$$

and

$$\bar{U} = \begin{bmatrix} I & U_1 & & & \\ & I & U_2 & & \\ & & I & U_3 & \\ & & & \ddots & \\ & & & I & U_{m-1} \\ & & & & I \end{bmatrix}$$

I is an identity matrix and A_i remains the same as A_i in matrix $\bar{M}$. L_i and U_i are full matrices and are defined by:

$$L_1 = B_1$$

$$L_i = B_i - A_i L^{-1}_{i-1} C_{i-1} \text{ for } i = 2,3, \ldots, m \qquad \text{(A-4)}$$

and

$$U_i = L_i^{-1} C_i \text{ for } i = 1,2, \ldots, m-1 \qquad \text{(A-5)}$$

where L_i^{-1} is the inverse of matrix L_i.

Now the matrix equation (A-1) becomes:

$$\bar{L}\,\bar{U}\,\bar{F} = \bar{Q} \qquad \text{(A-6)}$$

The equation can be solved by the following matrix algorithm:

Let $\bar{U}\,\bar{F} = \bar{G}$, equation (A-6) becomes

$\bar{L}\,\bar{G} = \bar{Q}$

or

$$\begin{bmatrix} L_1 & & & & \\ A_2 & L_2 & & & \\ & A_3 & L_3 & & \\ & & \ddots & \ddots & \\ & & & A_{m-1} & L_{m-1} \\ & & & & A_m \; L_m \end{bmatrix} \begin{bmatrix} G_1 \\ G_2 \\ \vdots \\ G_m \end{bmatrix} = \begin{bmatrix} Q_1 \\ Q_2 \\ \vdots \\ Q_m \end{bmatrix}$$

Now we can solve for G_i by following relations (forward pass):

$$G_1 = L_1^{-1} Q_1$$

$$G_i = L_i^{-1} (Q_i - A_i G_{i-1}) \text{ for } i = 2, 3, \ldots, m$$

After $\bar{G}$ is obtained, we can solve matrix equation

$$\bar{U} \bar{F} = \bar{G}$$

for solution vector $\bar{F}$ by following relations (backward pass):

$$F_m = G_m$$

and

$$F_i = G_i - U_i F_{i+1} \text{ for } i = m-1, m-2, \ldots, 1$$

Appendix. Basic EER CH_4/Air Reaction Mechanism and Rate Constants

REACTIONS BEING CONSIDERED

															KF=A*T**(-N)*EXP(-B/RT) A	N	B
1	1	H2	+	1	O	+	0	=	1	HO	+	1	H	+ 0	1.800E+10	-1.00	8900.0
2	1	H2	+	1	HO	+	0	=	1	H2O	+	1	H	+ 0	1.100E+09	-1.30	3640.0
3	1	H2	+	1	O2	+	0	=	1	HO	+	1	HO	+ 0	2.510E+12	0.	39000.0
4	1	H	+	1	M	+	1 M	=	1	H2	+	1	M	+ 0	9.000E+17	1.00	0.
	3RD BODY EFF. 5.000/H2O																
5	1	H	+	1	HO	+	1 M	=	1	H2O	+	1	M	+ 0	2.200E+22	2.00	0.
	3RD BODY EFF. 5.000/H2O																
6	1	H	+	1	O2	+	1 M	=	1	HO2	+	1	M	+ 0	1.040E+15	0.	-1000.0
	3RD BODY EFF. 2.500/H2 3.800/CH4 15.000/H2O 3.750/CO2																
7	1	O	+	1	O	+	1 M	=	1	O2	+	1	M	+ 0	1.000E+18	1.00	0.
8	1	H	+	1	O2	+	0	=	1	HO	+	1	O	+ 0	4.500E+10	-1.00	14805.0
9	1	HO	+	1	HO	+	0	=	1	H2O	+	1	O	+ 0	2.140E+09	-1.10	0.
10	1	H	+	1	HO2	+	0	=	1	HO	+	1	HO	+ 0	2.500E+14	0.	1900.0
11	1	HO	+	1	HO2	+	0	=	1	H2O	+	1	O2	+ 0	5.000E+13	0.	1000.0
12	1	O	+	1	HO2	+	0	=	1	HO	+	1	O2	+ 0	5.000E+13	0.	1000.0
13	1	H	+	1	HO2	+	0	=	1	O2	+	1	H2	+ 0	2.500E+13	0.	700.0
14	1	H2O2	+	1	M	+	0	=	1	HO	+	1	HO	+ 1 M	1.200E+17	0.	45500.0
15	1	H2O2	+	1	H	+	0	=	1	H2O	+	1	HO	+ 0	3.000E+14	0.	9000.0
16	1	H2O2	+	1	HO	+	0	=	1	H2O	+	1	HO2	+ 0	1.000E+13	0.	1000.0
17	1	HO2	+	1	H2	+	0	=	1	H2O2	+	1	H	+ 0	3.000E+11	0.	18680.0
18	1	HO2	+	1	HO2	+	0	=	1	H2O2	+	1	O2	+ 0	2.000E+12	0.	0.
19	1	CO	+	1	O	+	1 M	=	1	CO2	+	1	M	+ 0	3.800E+24	3.00	6170.0
20	1	CO	+	1	O2	+	0	=	1	CO2	+	1	O	+ 0	6.910E+07	-1.00	34810.0
21	1	CO	+	1	HO	+	0	=	1	CO2	+	1	H	+ 0	1.510E+07	-1.30	-765.0
22	1	CO	+	1	HO2	+	0	=	1	CO2	+	1	HO	+ 0	1.000E+11	0.	10000.0
23	1	CH4	+	1	M	+	0	=	1	CH3	+	1	H	+ 1 M	1.260E+17	0.	88400.0
24	1	CH4	+	1	O	+	0	=	1	CH3	+	1	HO	+ 0	1.170E+07	-2.10	7630.0
25	1	CH4	+	1	H	+	0	=	1	CH3	+	1	H2	+ 0	1.410E+07	-2.00	8840.0
26	1	CH4	+	1	HO	+	0	=	1	CH3	+	1	H2O	+ 0	1.550E+06	-2.10	2452.0
27	1	CH4	+	1	O2	+	0	=	1	CH3	+	1	HO2	+ 0	8.510E+06	-2.00	51970.0
28	1	CH4	+	1	HO2	+	0	=	1	CH3	+	1	H2O2	+ 0	2.000E+13	0.	18000.0
29	1	CH4	+	1	CH	+	0	=	1	CH3	+	1	CH2	+ 0	2.500E+11	-.70	6000.0
30	1	CH4	+	1	CH2	+	0	=	1	CH3	+	1	CH3	+ 0	1.260E+10	-.70	20000.0
31	1	CH3	+	1	O	+	0	=	1	CH2O	+	1	H	+ 0	9.000E+13	0.	2000.0
32	1	CH3	+	1	HO	+	0	=	1	CH2	+	1	H2O	+ 0	6.300E+10	-.70	2000.0
33	1	CH3	+	1	O2	+	0	=	1	CH3O	+	1	O	+ 0	6.000E+09	-1.00	28000.0

34	1	CH3O	+	1	M	+	0	=	1	CH2O	+	1	H	+	1	M	5.000E+13	0.	21000.0
35	1	CH3O	+	1	O	+	0	=	1	CH2O	+	1	HO	+	0		1.000E+14	0.	0.
36	1	CH3O	+	1	H	+	0	=	1	CH2O	+	1	H2	+	0		1.000E+14	0.	0.
37	1	CH3O	+	1	HO	+	0	=	1	CH2O	+	1	H2O	+	0		3.000E+13	0.	0.
38	1	CH2	+	1	O	+	0	=	1	CHO	+	1	H	+	0		6.500E+13	0.	0.
39	1	CH2	+	1	HO	+	0	=	1	CH	+	1	H2O	+	0		5.000E+11	-.50	6000.0
40	1	CH2	+	1	HO	+	0	=	1	CH3	+	1	O	+	0		5.000E+11	-.50	6000.0
41	1	CH2	+	1	HO	+	0	=	1	CH2O	+	1	H	+	0		1.000E+13	0.	5000.0
42	1	CH2	+	1	O2	+	0	=	1	CH2O	+	1	O	+	0		7.700E+09	-1.00	540.0
43	1	CH2	+	1	H2	+	0	=	1	CH3	+	1	H	+	0		1.000E+11	-.50	5730.0
44	1	CH2	+	1	CH2	+	0	=	1	CH3	+	1	CH	+	0		5.000E+11	-.50	6000.0
45	1	CH2O	+	1	M	+	0	=	1	CHO	+	1	H	+	1	M	3.310E+16	0.	81020.0
46	1	CH2O	+	1	O	+	0	=	1	CHO	+	1	HO	+	0		1.300E+10	-1.00	2050.0
47	1	CH2O	+	1	H	+	0	=	1	CHO	+	1	H2	+	0		2.500E+10	-1.00	3200.0
48	1	CH2O	+	1	HO	+	0	=	1	CHO	+	1	H2O	+	0		5.000E+09	-1.00	1650.0
49	1	CH2O	+	1	HO2	+	0	=	1	CHO	+	1	H2O2	+	0		1.000E+12	0.	8000.0
50	1	CH	+	1	O	+	0	=	1	CO	+	1	H	+	0		5.000E+11	-.50	0.
51	1	CH	+	1	HO	+	0	=	1	CHO	+	1	H	+	0		5.000E+11	-.50	5620.0
52	1	CH	+	1	O2	+	0	=	1	CHO	+	1	O	+	0		2.000E+13	0.	0.
53	1	CH	+	1	H2	+	0	=	1	CH2	+	1	H	+	0		1.200E+13	0.	0.
54	1	CH	+	1	CO2	+	0	=	1	CHO	+	1	CO	+	0		1.000E+10	-.50	6000.0
55	1	CHO	+	1	M	+	0	=	1	CO	+	1	H	+	1	M	1.550E+14	0.	14675.0
56	1	CHO	+	1	O	+	0	=	1	CO	+	1	HO	+	0		5.500E+12	-.50	0.
57	1	CHO	+	1	O	+	0	=	1	CO2	+	1	H	+	0		5.500E+12	-.50	0.
58	1	CHO	+	1	H	+	0	=	1	CO	+	1	H2	+	0		2.000E+14	0.	0.
59	1	CHO	+	1	HO	+	0	=	1	CO	+	1	H2O	+	0		3.000E+10	-1.00	0.
60	1	CHO	+	1	O2	+	0	=	1	CO	+	1	HO2	+	0		5.000E+11	-.50	834.0
61	1	CHO	+	1	CHO	+	0	=	1	CH2O	+	1	CO	+	0		4.000E+13	0.	0.
62	1	NH3	+	1	M	+	0	=	1	NH2	+	1	H	+	1	M	2.520E+16	0.	93800.0
63	1	NH3	+	1	M	+	0	=	1	NH	+	1	H2	+	1	M	2.520E+14	0.	93800.0
64	1	NH3	+	1	O	+	0	=	1	NH2	+	1	HO	+	0		5.500E+09	-.75	5030.0
65	1	NH3	+	1	H	+	0	=	1	NH2	+	1	H2	+	0		3.630E+10	-.75	13790.0
66	1	NH3	+	1	HO	+	0	=	1	NH2	+	1	H2O	+	0		8.500E+09	-.75	1100.0
67	1	NH3	+	1	HO2	+	0	=	1	H2O2	+	1	NH2	+	0		1.000E+12	0.	24300.0
68	1	NH2	+	1	O	+	0	=	1	NH	+	1	HO	+	0		1.000E+11	-.50	1000.0
69	1	NH2	+	1	O	+	0	=	1	HNO	+	1	H	+	0		1.000E+11	-.50	0.
70	1	NH2	+	1	H	+	0	=	1	NH	+	1	H2	+	0		5.000E+11	-.50	7570.0
71	1	NH2	+	1	HO	+	0	=	1	NH	+	1	H2O	+	0		6.300E+11	-.50	0.
72	1	NH2	+	1	O2	+	0	=	1	HNO	+	1	HO	+	0		5.000E+06	-.75	6080.0

73	1	NH2	+	1	HO2	+	0		=	1	NH	+	1	H2O2	+	0			1.000E+14	0.	1200.0
74	1	NH2	+	1	HO2	+	0		=	1	NH3	+	1	O2	+	0			2.000E+10	-.50	2590.0
75	1	NH2	+	1	HNO	+	0		=	1	NH3	+	1	NO	+	0			5.000E+11	-.50	2740.0
76	1	NH2	+	1	NH2	+	0		=	1	NH3	+	1	NH	+	0			1.200E+11	-.50	5640.0
77	1	NH2	+	1	NH2	+	0		=	1	N2	+	1	H2	+	1	H2		3.980E+13	0.	12000.0
78	1	NH	+	1	O	+	0		=	1	NO	+	1	H	+	0			6.310E+11	-.50	0.
79	1	NH	+	1	O	+	0		=	1	N	+	1	HO	+	0			6.310E+11	-.50	8000.0
80	1	NH	+	1	H	+	1	M	=	1	NH2	+	1	M	+	0			2.000E+16	.50	0.
81	1	NH	+	1	H	+	0		=	1	N	+	1	H2	+	0			6.310E+11	-.50	8000.0
82	1	NH	+	1	HO	+	0		=	1	HNO	+	1	H	+	0			5.000E+11	-.50	5620.0
83	1	NH	+	1	HO	+	0		=	1	N	+	1	H2O	+	0			5.000E+11	-.50	4450.0
84	1	NH	+	1	O2	+	0		=	1	HNO	+	1	O	+	0			5.000E+11	-.50	4370.0
85	1	NH	+	1	HO2	+	0		=	1	HNO	+	1	HO	+	0			6.300E+11	-.50	0.
86	1	NH	+	1	NH	+	0		=	1	N2	+	1	H2	+	0			3.600E+11	-.55	1900.0
87	1	HNO	+	1	O	+	0		=	1	HO	+	1	NO	+	0			5.000E+11	-.50	2740.0
88	1	HNO	+	1	H	+	0		=	1	H2	+	1	NO	+	0			1.000E+13	0.	2500.0
89	1	HNO	+	1	HO	+	0		=	1	H2O	+	1	NO	+	0			1.000E+12	-.50	2740.0
90	1	N	+	1	H	+	1	M	=	1	NH	+	1	M	+	0			3.000E+16	.50	0.
91	1	N	+	1	O2	+	0		=	1	NO	+	1	O	+	0			6.400E+09	-1.00	6260.0
92	1	N	+	1	HO	+	0		=	1	NO	+	1	H	+	0			6.310E+11	-.50	0.
93	1	N	+	1	NH3	+	0		=	1	NH	+	1	NH2	+	0			1.000E+11	-.50	31640.0
94	1	N	+	1	NH2	+	0		=	1	NH	+	1	NH	+	0			2.000E+11	-.50	22160.0
95	1	N	+	1	NH	+	0		=	1	N2	+	1	H	+	0			6.310E+11	-.50	0.
96	1	N	+	1	NO	+	0		=	1	N2	+	1	O	+	0			3.100E+13	0.	334.0
97	1	N	+	1	NO2	+	0		=	1	N2O	+	1	O	+	0			3.000E+11	-.50	0.
98	1	NO	+	1	O	+	1	M	=	1	NO2	+	1	M	+	0			1.000E+21	1.86	0.
99	1	NO	+	1	H	+	1	M	=	1	HNO	+	1	M	+	0			2.200E+17	.50	0.
100	1	NO	+	1	HO2	+	0		=	1	NO2	+	1	HO	+	0			3.000E+11	-.50	0.
101	1	NO	+	1	NH2	+	0		=	1	N2O	+	1	H2	+	0			5.000E+08	-.50	0.
102	1	NO	+	1	NH2	+	0		=	1	N2	+	1	H	+	1	HO		1.380E+17	1.85	0.
103	1	NO	+	1	NH2	+	0		=	1	N2	+	1	H2O	+	0			2.370E+17	1.85	0.
104	1	NO	+	1	NH	+	0		=	1	N2O	+	1	H	+	0			5.400E+16	1.40	0.
105	1	N2O	+	1	M	+	0		=	1	N2	+	1	O	+	1	M		1.420E+14	0.	51280.0
106	1	N2O	+	1	O	+	0		=	1	N2	+	1	O2	+	0			6.230E+13	0.	24540.0
107	1	N2O	+	1	O	+	0		=	1	NO	+	1	NO	+	0			3.060E+13	0.	21800.0
108	1	N2O	+	1	H	+	0		=	1	N2	+	1	HO	+	0			7.600E+13	0.	15100.0
109	1	N2O	+	1	NO	+	0		=	1	N2	+	1	NO2	+	0			2.000E+14	0.	50000.0
110	1	N2O	+	1	NH	+	0		=	1	N2	+	1	HNO	+	0			2.000E+10	-1.00	12000.0
111	1	NO2	+	1	O	+	0		=	1	NO	+	1	O2	+	0			1.000E+13	0.	600.0
112	1	NO2	+	1	H	+	0		=	1	HO	+	1	NO	+	0			2.900E+14	0.	800.0
113	1	N2	+	1	M	+	0		=	1	N	+	1	N	+	1	M		3.700E+21	1.60	225000.0

114	1	C2H6	+	1	H	+	0		=	1	C2H5	+	1	H2	+	0										5.370E+02	-3.50	5200.0
115	1	C2H6	+	1	HO	+	0		=	1	C2H5	+	1	H2O	+	0										6.310E+11	0.	2450.0
116	1	C2H6	+	1	CH2	+	0		=	1	CH3	+	1	C2H5	+	0										1.220E+13	0.	15700.0
117	1	C2H6	+	1	CH3	+	0		=	1	C2H5	+	1	CH4	+	0										5.500E-01	4.00	8280.0
118	1	CH2	+	1	CH2	+	0		=	1	C2H2	+	1	H2	+	0										3.200E+13	0.	0.
119	1	CH	+	1	CH4	+	0		=	1	C2H4	+	1	H	+	0										1.500E+12	0.	0.
120	1	CH2	+	1	CH3	+	0		=	1	C2H4	+	1	H	+	0										6.000E+13	0.	0.
121	1	CH3	+	1	CH4	+	0		=	1	C2H5	+	1	H2	+	0										1.000E+13	0.	25000.0
122	1	CH3	+	1	CH3	+	1	M	=	1	C2H6	+	1	M	+	0										2.400E+13	0.	0.
123	1	CH4	+	1	CH3	+	0		=	1	C2H6	+	1	H	+	0										8.000E+13	0.	40000.0
124	1	CHN	+	1	M	+	0		=	1	CN	+	1	H	+	1	M									5.700E+16	0.	117000.0
125	1	CHN	+	1	O	+	0		=	1	H	+	1	NCO	+	0										1.300E+11	-.50	6810.0
126	1	CHN	+	1	HO	+	0		=	1	CN	+	1	H2O	+	0										2.000E+11	-.50	5000.0
127	1	CHN	+	1	HO	+	0		=	1	HNCO	+	1	H	+	0										2.000E+10	-.50	5620.0
128	1	CN	+	1	O	+	0		=	1	CO	+	1	N	+	0										6.310E+11	-.50	0.
129	1	CN	+	1	HO	+	0		=	1	NCO	+	1	H	+	0										6.200E+13	0.	0.
130	1	CN	+	1	HO	+	0		=	1	CHN	+	1	O	+	0										3.160E+12	0.	3000.0
131	1	CN	+	1	O2	+	0		=	1	NCO	+	1	O	+	0										3.200E+13	0.	1000.0
132	1	CN	+	1	H2	+	0		=	1	CHN	+	1	H	+	0										6.200E+12	0.	5300.0
133	1	CN	+	1	CO2	+	0		=	1	NCO	+	1	CO	+	0										4.000E+11	-.50	7000.0
134	1	CN	+	1	NH2	+	0		=	1	CHN	+	1	NH	+	0										5.000E+10	-.70	2000.0
135	1	CN	+	1	NH3	+	0		=	1	CHN	+	1	NH2	+	0										7.000E+10	-.70	2000.0
136	1	NCO	+	1	O	+	0		=	1	NO	+	1	CO	+	0										5.000E+11	-.50	6875.0
137	1	NCO	+	1	H	+	0		=	1	NH	+	1	CO	+	0										5.000E+11	-.50	6870.0
138	1	NCO	+	1	H2	+	0		=	1	HNCO	+	1	H	+	0										3.000E+10	-.50	5700.0
139	1	NCO	+	1	NH2	+	0		=	1	NH	+	1	HNCO	+	0										1.000E+11	-.50	5000.0
140	1	HNCO	+	1	HO	+	0		=	1	NCO	+	1	H2O	+	0										1.000E+11	-.50	6290.0
141	1	HNCO	+	1	H	+	0		=	1	NH2	+	1	CO	+	0										5.000E+11	-.50	4830.0
142	1	CHO	+	1	N	+	0		=	1	CHN	+	1	O	+	0										1.000E+14	0.	0.
143	1	CHN	+	1	N	+	0		=	1	CH	+	1	N2	+	0										2.500E+11	0.	16000.0
144	1	CHN	+	1	O	+	0		=	1	CH	+	1	NO	+	0										1.000E+14	0.	72000.0
145	1	CH4	+	1	CN	+	0		=	1	CH3	+	1	CHN	+	0										3.160E+11	-.70	5000.0
146	1	CH3	+	1	CN	+	0		=	1	CH2	+	1	CHN	+	0										1.000E+11	-.70	3000.0
147	1	CH2	+	1	NO	+	0		=	1	CH2O	+	1	N	+	0										1.600E+12	0.	7000.0
148	1	CH2	+	1	N2	+	0		=	1	CHN	+	1	NH	+	0										1.000E+14	0.	60000.0
149	1	CH	+	1	N	+	0		=	1	CN	+	1	H	+	0										6.300E+11	-.50	0.
150	1	CHO	+	1	N	+	0		=	1	CH	+	1	NO	+	0										1.000E+14	0.	48600.0
151	1	C2H	+	1	O	+	0		=	1	CH	+	1	CO	+	0										5.000E+13	0.	0.
152	1	C2H	+	1	HO	+	0		=	1	CH2	+	1	CO	+	0										6.000E+12	0.	0.
153	1	C2H	+	1	O2	+	0		=	1	CHO	+	1	CO	+	0										1.000E+13	0.	0.
154	1	C2H2	+	1	M	+	0		=	1	C2H	+	1	M	+	1	M									4.170E+16	0.	107000.0
155	1	C2H2	+	1	O	+	0		=	1	CH2	+	1	CO	+	0										6.750E+13	0.	4000.0

156	1	C2H2	+	1	H	+	0		=	1	C2H	+	1	H2	+	0		7.760E+00	-3.20	500.0
157	1	C2H2	+	1	O	+	0		=	1	C2H	+	1	HO	+	0		3.200E+15	.60	17000.0
158	1	C2H2	+	1	HO	+	0		=	1	C2H	+	1	H2O	+	0		1.400E+13	0.	7000.0
159	1	C2H2	+	1	HO	+	0		=	1	CH3	+	1	CO	+	0		5.500E+13	0.	13700.0
160	1	C2H2	+	1	O2	+	0		=	1	CHO	+	1	CHO	+	0		4.000E+12	0.	28000.0
161	1	C2H2	+	1	CH	+	0		=	1	CH2	+	1	C2H	+	0		7.100E+13	0.	11920.0
162	1	C2H2	+	1	CH2	+	0		=	1	CH3	+	1	C2H	+	0		1.000E+12	0.	0.
163	1	C2H3	+	1	M	+	0		=	1	C2H2	+	1	H	+	1	M	7.940E+14	0.	31500.0
164	1	C2H3	+	1	H	+	0		=	1	C2H2	+	1	H2	+	0		1.000E+13	0.	0.
165	1	C2H4	+	1	M	+	0		=	1	C2H2	+	1	H2	+	1	M	2.600E+17	0.	79290.0
166	1	C2H4	+	1	M	+	0		=	1	C2H3	+	1	H	+	1	M	3.800E+17	0.	98170.0
167	1	C2H4	+	1	O	+	0		=	1	CH2	+	1	CH2O	+	0		8.060E+06	-2.00	307.0
168	1	C2H4	+	1	O	+	0		=	1	CH3	+	1	CHO	+	0		5.930E+10	-.74	560.0
169	1	C2H4	+	1	H	+	0		=	1	C2H3	+	1	H2	+	0		1.100E+14	0.	8500.0
170	1	C2H4	+	1	H	+	1	M	=	1	C2H5	+	1	M	+	0		1.000E+13	0.	1500.0
171	1	C2H4	+	1	HO	+	0		=	1	CH3	+	1	CH2O	+	0		4.500E+12	0.	220.0
172	1	C2H4	+	1	HO	+	0		=	1	C2H3	+	1	H2O	+	0		1.000E+14	0.	3500.0
173	1	C2H4	+	1	CH2	+	0		=	1	CH3	+	1	C2H3	+	0		1.090E+13	0.	12400.0
174	1	C2H4	+	1	CH3	+	0		=	1	CH4	+	1	C2H3	+	0		5.000E+12	0.	13000.0
175	1	C2H5	+	1	H	+	0		=	1	CH3	+	1	CH3	+	0		3.720E+13	0.	0.
176	1	C2H5	+	1	H	+	0		=	1	C2H4	+	1	H2	+	0		1.860E+12	0.	0.
177	1	C2H5	+	1	O2	+	0		=	1	C2H4	+	1	HO2	+	0		1.000E+12	0.	5000.0
178	1	C2H5	+	1	CH3	+	0		=	1	CH4	+	1	C2H4	+	0		2.500E+11	0.	0.
179	1	C2H5	+	1	C2H3	+	0		=	1	C2H4	+	1	C2H4	+	0		3.100E+17	0.	35600.0
180	1	C2H5	+	1	C2H5	+	0		=	1	C2H6	+	1	C2H4	+	0		5.000E+10	0.	0.
181	1	C2H6	+	1	O	+	0		=	1	C2H5	+	1	HO	+	0		2.500E+13	0.	6360.0

PART 2

MATHEMATICAL MODELING
OF
MICROSCALE COMBUSTION OF A COAL PARTICLE

Prepared by:

C. J. Kau

and

T. J. Tyson

TABLE OF CONTENTS

LIST OF FIGURES

LIST OF TABLES

1.0 DEVOLATILIZATION MODELING

For the purpose of mathematical modeling of coal decomposition, the constituents of raw coal are catalogued into five categories. They are:

1. Light volatiles: including H_2, CO, CO_2, H_2O, moisture and aliphatics
2. Volatile nitrogens
3. Tar: having chemical structure similar to parent coal
4. Char: basically carbon plus some residual nitrogen
5. Ash: including sulfur, sulfur compounds, and all other mineral matters which are not treated chemically in this model.

Since the devolatilization (thermal pyrolysis) of coal is a purely chemical decomposition process, the evolution of light volatiles, volatile nitrogen and tar can be viewed as a first-order chemical reaction, having rate equation

$$\frac{dY_i}{dt} = K_i Y_i$$

where Y_i is the mass fraction of ith solid species (or functional group, in Solomon's terminology). K_i is a rate constant of Arrhenius form:

$$K_i = A_i \exp(-E_i/RT) \ (1/sec)$$

Currently, the devolatilization model in EER computer codes (OFAP and GFAP) can handle two types of coals: Montana lignite and Pittsburgh bituminous. The rate constants, K_i, were derived from the following experimental works:

1. Suuberg's (1979) measurements: providing the rate data and information on functional group partition of light volatiles.
2. Kobayashi (1977) measurements: providing data on total weight loss and rate constant, which can be used to estimate tar yield and evolution rate.
3. Pohl (1977) measurements: providing nitrogen retention data and data on the rate of devolatilization of fuel nitrogen.

The aliphatic group, which is the collection of all measurable light

hydrocarbons such as CH_4, C_2H_2, C_2H_4 and other higher HC, is treated as one single component that is evolved at a single rate. The instantaneous secondary pyrolysis which follows the initial pyrolysis decomposes aliphatics into kinetically more manageable gas species such as CH_4, C_2H_2, C_2H_4 and H_2 or soot. The in-use fractions of CH_4, C_2H_2 and C_2H_4 are determined from MIT's asymptotic yield data shown in columns 1 and 2 of Table 2. Whether H_2 or soot is yielded is determined by the conservation of H and C atoms in aliphatics.

The difference between total weight loss and light volatiles yield is considered to be heavy volatile (or "tar") yield. The resemblance of Infrared Spectra of Tar and Coal (Solomon, 1979) suggests that the tar consists of "monmers" released from parent coal. Therefore, it is logical to assume that tar has a similar structure to parent coal. However, due to difficulties in balancing O-atoms in MIT data, basic contents of tar are modified to be similar to those of the parent coal, except the solid CO group is assumed to be the only oxygen-containing group in tar. There is only one "tar" group in the EER rate set. The instantaneous secondary pyrolysis of tar decomposes "tar" into its basic contents (in gas form).

Volatile nitrogen is treated as a separate category since it is of major interest. The asymptotic yield of volatile nitrogen is expressed as a function of temperature by a cubic polynomial

$$N\% \text{ (as volatile nitrogen)} = A + BT + CT^3$$

The values of A,B, and C used are listed in Table 2. The polynomial agrees reasonably well with most of the experimental data (Blair, 1977; Pohl, 1977). Experiments also revealed that the nominal pyrolysis product of volatile nitrogen is HCN. The small amount of NH_3 observed (Axworthy, et al., 1978) is neglected in the current model. The balance of coal nitrogen, which stays with char, is eventually oxidized along with the char.

Functional group partitions, coefficients for Arrhenius rate constants and asymptotic yields currently used in EER flame codes are listed in Tables 1 and 2. MIT (Suuberg et al.) and UTRC (Solomon et al.) rate constants are also listed in Table 1. EER rate constants are practically the same as those of MIT, except for

TABLE 1. RATE COEFFICIENTS

Functional Group	MIT (Lignite)	MIT (Bituminous)	UTRC (General)	EER (Lignite)	EER (Bituminous)
CO_2 (1)	2.138(11)/36.2*	1.0(13)/40	75/11.6	2.138(11)/36.2	1.0(13)/40
CO_2 (2)	5.128(13)/64.3	1.0(13)/65		3.65(13)/64.3	1.0(13)/65
CO_2 (3)	5.495(6)/42.0				
H_2O (1)+	-	-	-	-	-
H_2O (2)	7.95(13)/51.4	1.0(13)/35	370/13.6	7.95(13)/51.4	1.0(13)/35.0
CO (1)	1.82(12)/44.4	1.0(13)/55	8.7(5)/24.0	1.82(12)/44.4	1.0(13)/55.0
CO (2)	2.63(12)/59.5	1.0(13)/65	4.0(9)/70.0	1.85(12)59.5	1.0(13)/65.0
CO (3)	5.89(9)/58.4				
HCN	-	-	200/15.2	9.3(3)/22.7	9.3(3)/22.7
N (S)	-	-	290/25.4	Same as Char Rate	Same as Char Rate
H_2	1.588(18)/88.8	1.0(17)/90	3600/25.4	1.585(18)/88.8	1.0(17)/90.0
CH_4 (1)	1.62(14)51.6	1.0(13)/55			
CH_4 (2)	4.677(4)/69.4	1.0(13)/65			
CH_2H_4 (1)	1.78(20)/74.8	1.0(13)/55	3.3(5)/24.0	6.48(13)/51.6	5.56(12)/55.0
C_2H_4 (2)	7.08(12)/60.4	1.0(13)/65			
C_2H_6	-	1.0(13)/55			
HC	1.7(16)/70.1				
Tar (1)	7.58(11)/37.4	8.7(2)/13.2	9.3(4)/19.6	1.3(7)/40.0	1.3(7)/40.0
Tar (2)	2.0(17)/75.3				

*A/E: for A exp (-E/RT), A is in (1/sec), E is in (Kcal/mole)
+Moisture

Table 2. Asymptotic Yields (% Mass)

	MIT Lignite	MIT Bituminous	UTRC Lignite	UTRC Bituminous	EER Lignite	EER Bituminous
CO_2 (1)	5.7	0.4	5.0	1.2	5.7	0.4
CO_2 (2)	2.70	0.9	-	-	3.79	0.9
CO_2 (3)	1.09	-	-	-	-	-
H_2O (1)+	6.8	1.4	-	-	-	-
H_2O (2)	9.7	5.4	6.0	2.4	13.0	6.8
CO (1)	1.77	0.4	9.0	1.3	1.77	0.4
CO (2)	5.35	2.1	19.9	9.8	7.61	2.1
CO (3)	2.26	-	-	-		
HCN	f(T)*	f(T)	0.38	0.38	f(T)	f(T)
N (S)	f(T)	f(T)	0.8	1.2	f(T)	f(T)
H_2	0.5	1.0	1.3	1.7	0.5	1.0
CH_4 (1)	0.34	0.7				
CH_4 (2)	0.92	1.8				
C_2H_4(1)	0.15	0.2	17.0	24.1	2.77	8.6
C_2H_4(2)	0.41	0.6				
C_2H_6	0.95	0.5				
HC	-	4.8				
Tar (1)	2.45	-				
Tar (2)	2.93	-	16.0		f(T)	f(T)
A					-92.08	-92.08
B					0.129245	0.129245
C					-9.0290522(-9)	-9.0290522 (-9)

*As a function of particle temperature.

+Moisture

minor variations in speciation and asymptotic yields. The variation is partly due to atomic imbalance in data and partly due to the consideration of mathematical convenience for further improvement of the model. Therefore, EER's model should agree with MIT data if experimental coal temperature history is known.

Due to the lack of thermochemical information on pyrolysis reactions, the devolatilization processes are assumed to be neutral thermal. Thus, the thermochemical properties of functional groups are set equal to those of their gas-phase counterparts. The heat of formation of char is treated as a variable to accommodate the uncertainty and is calculated by

$$h_{fchar} = \frac{H_{fcoal} - \sum_{i \neq char} \left(h_{fi} Y_{i,\infty} / M_i \right)}{\left(Y_{char,\infty} / M_{char} \right)} \quad \left(\frac{cal}{mole} \right)$$

where h_{fi} is heat of formation at 298.15°K, M_i is molecular weight and $Y_{i,\infty}$ is asymptotic yield of group "i."

Heat of formation of coal, H_{vcoal}, can be derived from the heating value (LHV) of coal by

$$H_{fcoal} = \frac{h_{fCO_2} + 0.5\, h_{fH_2O} - LHV}{M_C + XM_H + YM_O + ZM_N + SM_{ash}}$$

The apparent molecular formula is $CH_XO_YN_ZA_S$, where A stands for ash.

It is understood that error in calculation of energy release might be incurred locally due to the uncertainty as to thermochemical properties. However, the model predictions are consistent with conservation of overall thermal-chemical energy.

2.0 CHAR COMBUSTION MODEL

Mass rate of oxidation of char is taken from the work of Smith (1971):

$$\left(\frac{dC}{dt}\right)_{O_2} = 20.4 \exp(-1900/RT) \qquad \frac{\text{gm of carbon}}{\text{cm}^2 - \text{sec} - \text{atm of } O_2}$$

Rate is calculated per unit external surface area of char particle.

At 1000°K the oxidation and gasification rates of char can be found from the following relationships (Walker, 1959):

$$\left(\frac{dC}{dt}\right)_{CO_2} / \left(\frac{dC}{dt}\right)_{O_2} = 3.16(-3)$$

$$\left(\frac{dC}{dt}\right)_{H_2O} / \left(\frac{dC}{dt}\right)_{CO_2} = 1.732$$

Thus, the gasification rate of char by CO_2 is

$$\left(\frac{dC}{dt}\right)_{CO_2} = 192.0 \exp(-35000/RT)$$

and the gasification rate of char by H_2O is

$$\left(\frac{dC}{dt}\right)_{H_2O} = 27.3 \exp(-30000/RT) \ .$$

The elementary rate constants are related to mass rate constants by

$$K_i = \left(\frac{6\ \tilde{R} T_p}{\rho_s\ d_p}\right) \left(\frac{dC}{dt}\right)_i \ .$$

where gas constant $\tilde{R} = 82.06$ (cm^3-atm/mole-°K). T_p is particle temperature in °K and d_p is particle diameter in cm. ρ_s is particle material density in gm/cm^3.

For macroscale calculation, the elementary char oxidation and gasification reactions are expressed as

1. $C + 1/2\ O_2 \rightarrow CO$ $\qquad \Delta H_c = -21.6$ Kcal/gmole

2. $C + CO_2 \rightarrow 2CO$ $\qquad \Delta H_c = +41.2$ Kcal/gmole

3. $C + H_2O \rightarrow CO + H_2$ $\Delta H_c = +31.4$ Kcal/gmole

In the computer programs, these reactions are built-in and are not listed in Appendix A of Part 1.

Additional heterogeneous reactions listed in Appendix A of Part 1 are:

(i) Soot combustions (Reactions 181 and 182)

(ii) Soot NO reduction (Reaction 184)

(iii) Char nitrogen combustion (Reactions 187 and 188).

3.0 MICROSCALE COMBUSTION OF A SINGLE COAL PARTICLE

Detailed mathematical formulation of the system of partial differential equations which describe the physical and chemical processes around a burning coal particle will not be presented here. Instead, only highlights of physical and mathematical assumptions are listed:

1. Coal particles are assumed to be nonswelling and spherically symmetrical.
2. Time-dependent one-dimensional (in spherical coordinates) boundary layer equations and equations-of-state are employed.
3. Unequal binary diffusion coefficients, based on the bifurcation approximation, are utilized with Fick's law of species diffusion.
4. Constant mean Lewis number is employed along with Fourier's law for thermal conduction.
5. Detailed coal devolatilization and the char combustion model are described in a previous section.
6. Gas-phase chemistry is fully detailed (188 reactions and 41 species, listed in Appendix A of Part 1).
7. Thermochemical properties are taken from JANAF Tables.
8. Impermeable and expandable boundary finite particle environment is continuously vitiated by the combustion products.
9. Pressure is constant.
10. Particle-ambient and gas-ambient radiation are considered.
11. Internal particle temperature distribution is uniform (infinite solid-phase conductivity).

A schematic of the system of the microscale coal particle combustion is shown in Figure 1.

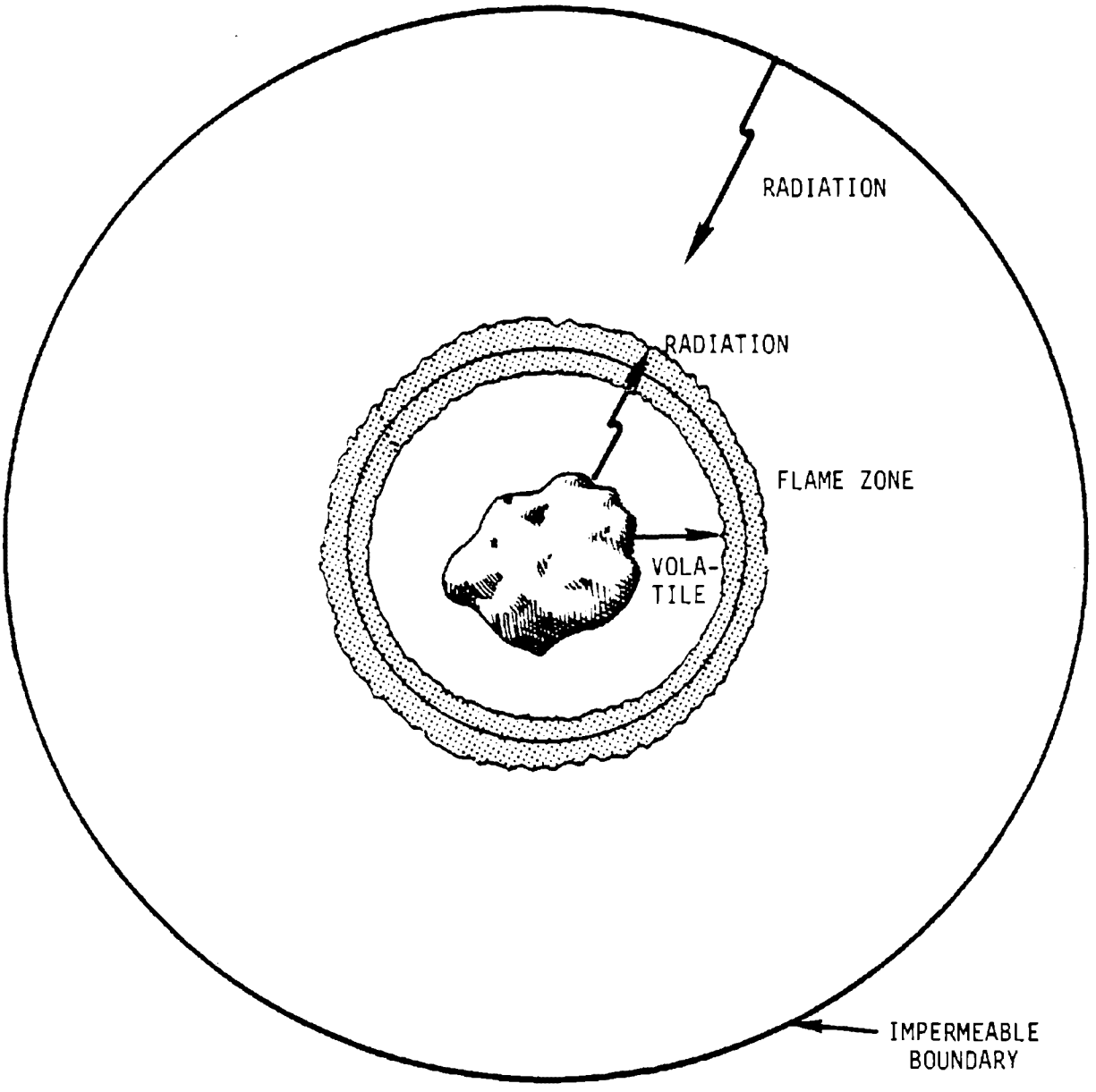

Figure 1. Schematic of Microscale Combustion of a Coal Particle in a Confined Space.

4.0 SUDDEN IMMERSION OF COAL PARTICLE INTO HOT COMBUSTION PRODUCTS

In order to look into the microphysical and chemical processes of coal particles during their lifetimes in typical coal-fired furnaces, in this section numerical simulation of a single coal particle suddenly immersed into a puff of lean combustion products will be examined.

Particle sizes are chosen to be 50 μm and 100 μm , which covers the range of average particle sizes in coal combustors. Combustor wall temperatures are chosen to be 1500°K and 1900°K. The particle is assumed to be initially surrounded by equilibrium combustion products of CH_4 at an equivalence ratio of 1.67. The initial ambient gas is assumed to be at its equilibrium temperature (i.e. T_{go} = 1662°K). The thermodynamic state of the gas and the ratio of interparticle distance to particle size are chosen independent of wall temperature and are functions of particle size alone. If we choose the interparticle distance to be 57 times the particle diameter, the final combustion products of the system will maintain approximately two percent oxygen. The initial particle temperature is 300°K.

Figure 2 shows the rate of devolatilization of volatiles and the rate of combustion of char for a 50 μm bituminous particle at T_{wall} = 1500°K. The first rate peak at 2 ms was determined to be from water contents in the coal. The second peak is the contribution from evolution of CO_2. CO and aliphatic "tar" evolved mainly between tightly bounded light volatiles (e.g. CO, CO_2, and H_2) and combustion of char. The lifetime of a 50 μm coal particle is about 95 msec while the lifetime of a 100 μm particle is about 350 msec. Doubling the particle size approximately quadruples the burn-out time.

Figure 3 shows the temperature histories of particle and gas (far field) under a higher heat loss environment (T_{wall} = 1500°K). Increasing particle size reduces heating rate which in turn reduces peak devolatilization rate. The ignition time in gas phase is increased from approximately 5 msec to 15 msec when particle size is increased from 50 μm to 100 μm .

Similar results for particles in lower heat loss environment (T_{wall} = 1800°K) are shown in Figure 4 and Figure 5.

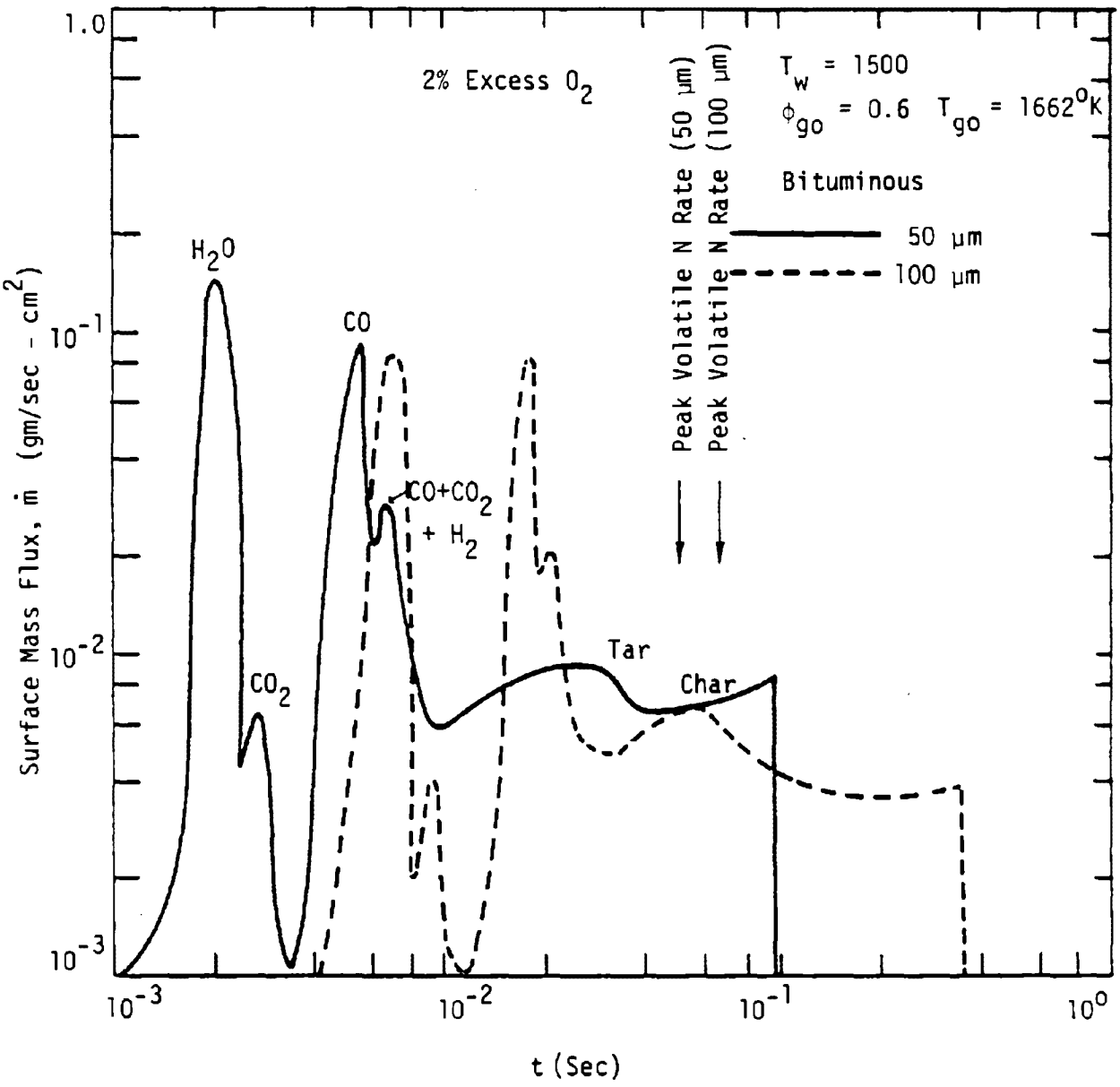

Figure 2. Mass flux rate of 50 μm and 100 μm, bituminous particle in higher heat loss environment (T_{wall} = 1500°K).

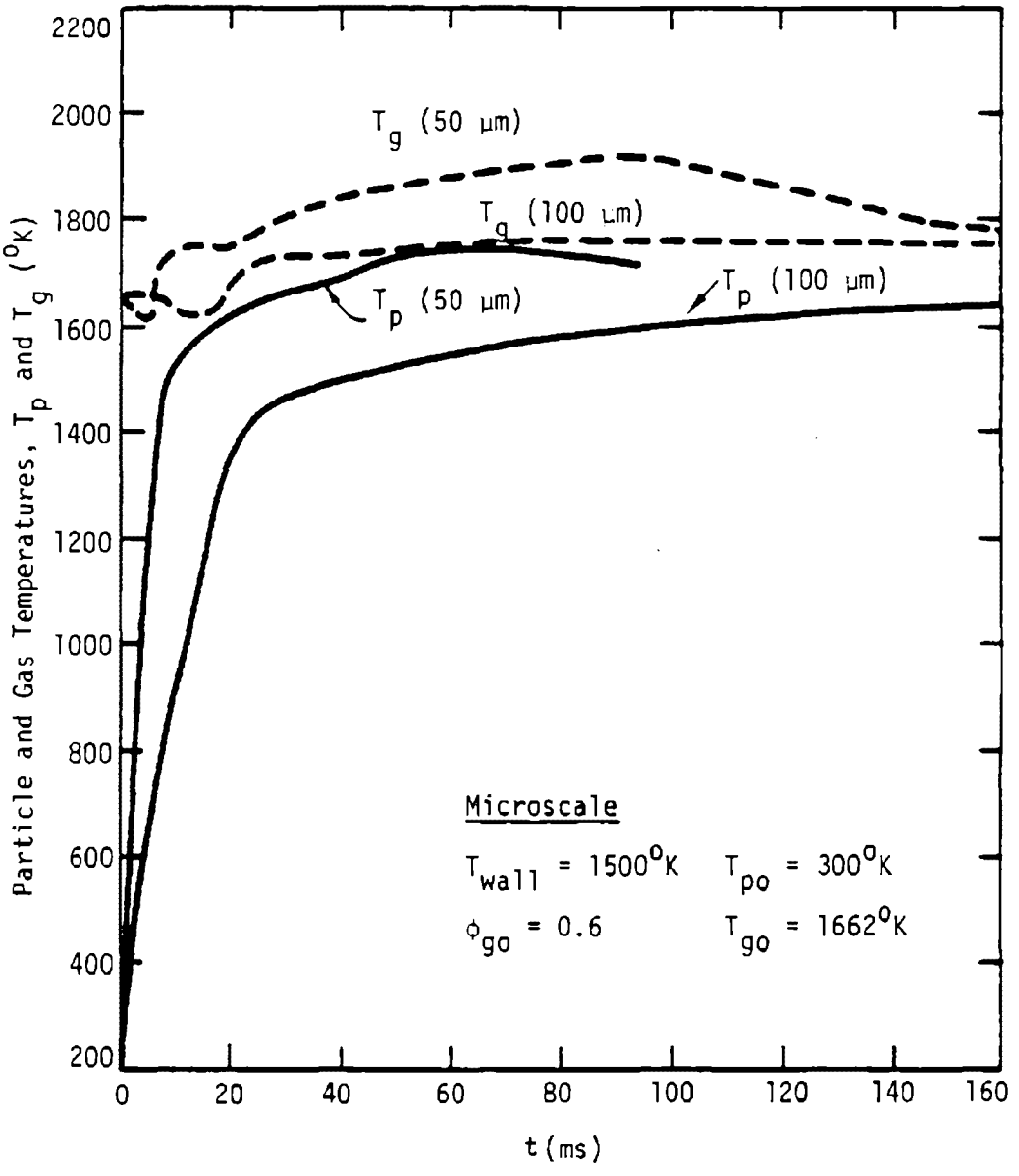

Figure 3. Particle and Gas Phase Temperature Histories for T_{wall} = 1500^{o}K.

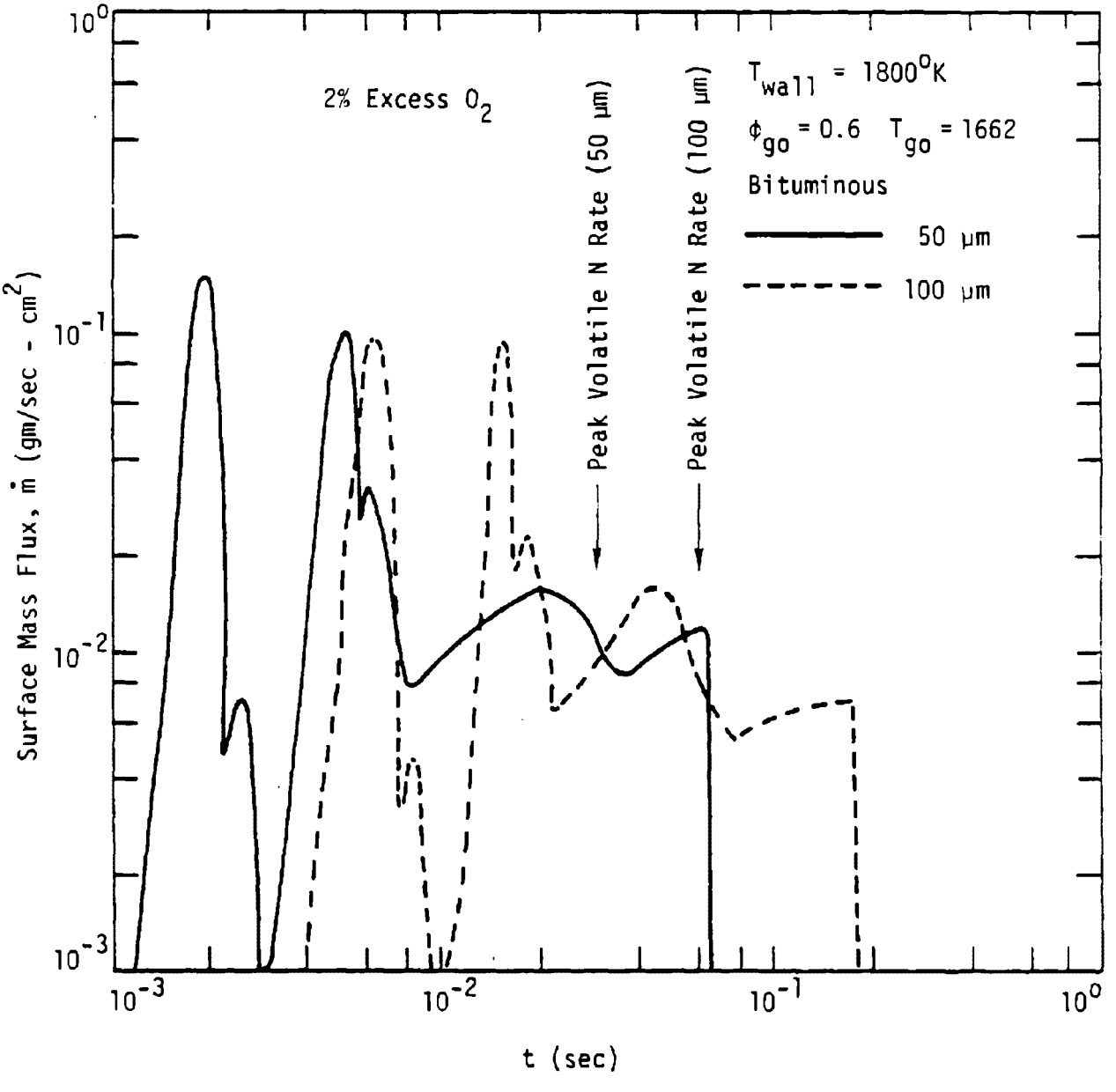

Figure 4. Mass flux rate of 50 μm and 100 μm bituminous particle lower heat loss environment (T_{wall} = 1800°K).

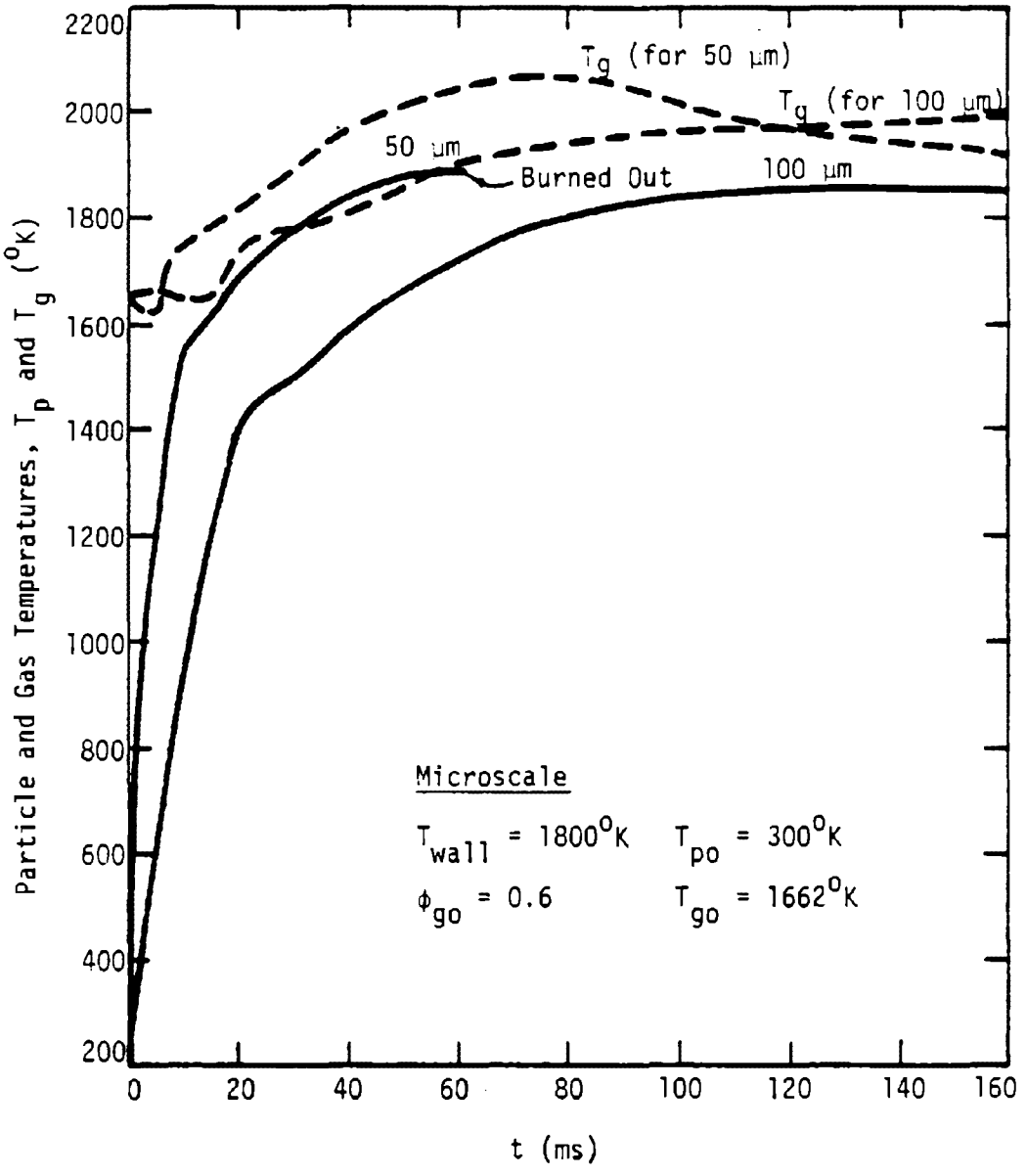

Figure 5. Particle and Gas Phase Temperature Histories for T_{wall} = 1800^{o}K.

Temperature distributions for three different stages (for T_{wall} = 1800°K) of combustion of a 100μm particle are plotted in Figure 6. At t = 30 ms (final stage of energetic light volatile evolution) the temperature peak is very close to the particle surface. The temperature over-shoot is about 130°K. At t = 50 ms (during the state of "tar" evolution) the temperature peak has moved away from the particle surface. However, the temperature over-shoot increases to 370°K. At t = 75 ms (during char combustion stage) the temperature peak is not obvious since the char combustion rate is slower than the devolatilization rate, and thus the reaction time becomes comparable to the diffusion time. The diffusion flame is not established. The system is controlled by char combustion rate. Oxygen distributions are also shown in Figure 7.

One of the main objectives of microscale simulation of the particle is to investigate effects of the microscale process of fuel bounded nitrogen conversion to fixed nitrogen species (NO_x, NH_3, and CHN). Figure 8 shows the production rate of NO around a 100μm particle (T_{wall} = 1800°K) at three different stages. In general, gas-phase NO reactions occur within 10 particle radii of the particle surface. Kinetic information can be calculated using equations found in the computer code. The percentage contribution to the production of each species by each reaction can be readily obtained.

The reactions which contribute significantly to the direct production of NO at t = 50 ms are as follows (The overall contribution refers to the spatial integration of the local NO production rate):

		% Contribution (Vol. Rate)	
Reaction No.		Overall	At Tmax
(99)	$HNO \rightarrow H + NO$	27.0	44.0
(89)	$HNO + OH \rightarrow H_2O + NO$	20.3	11.3
(112)	$N_2O + H \rightarrow OH + NO$	20.2	<0.5
(92)	$N_2 + OH \rightarrow H + NO$	6.8	17.5
(128)	$NCO + O \rightarrow CO + NO$	6.8	<0.5

HNO and NCO are the important intermediates in CHN and NH_3 oxidation processes. In these processes, NO from the overall thermal process [reaction (92)] contributes less than 7 percent; however, the local (peak temperature zone)

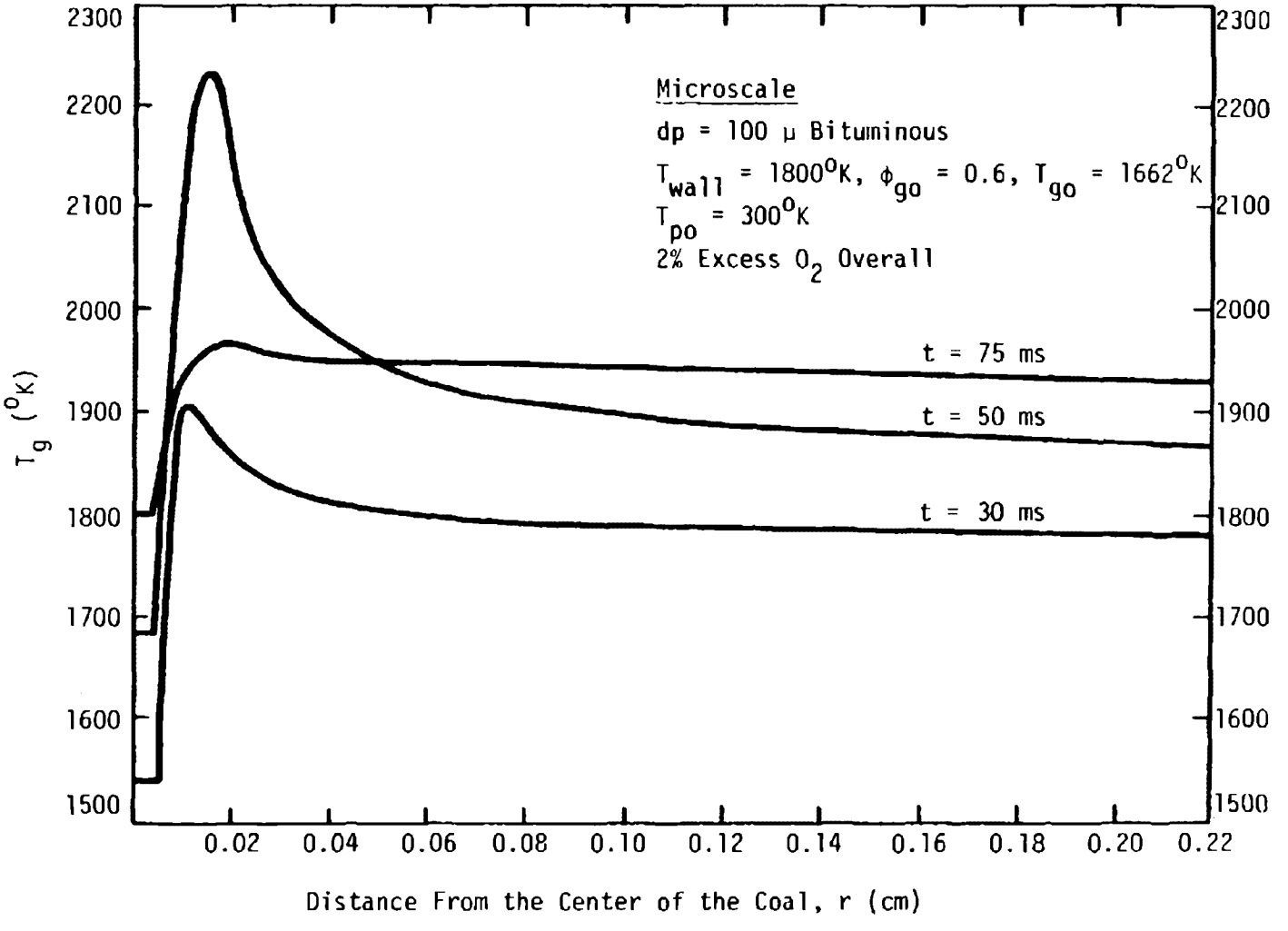

Figure 6. Temperature Distribution Around a Coal Particle.

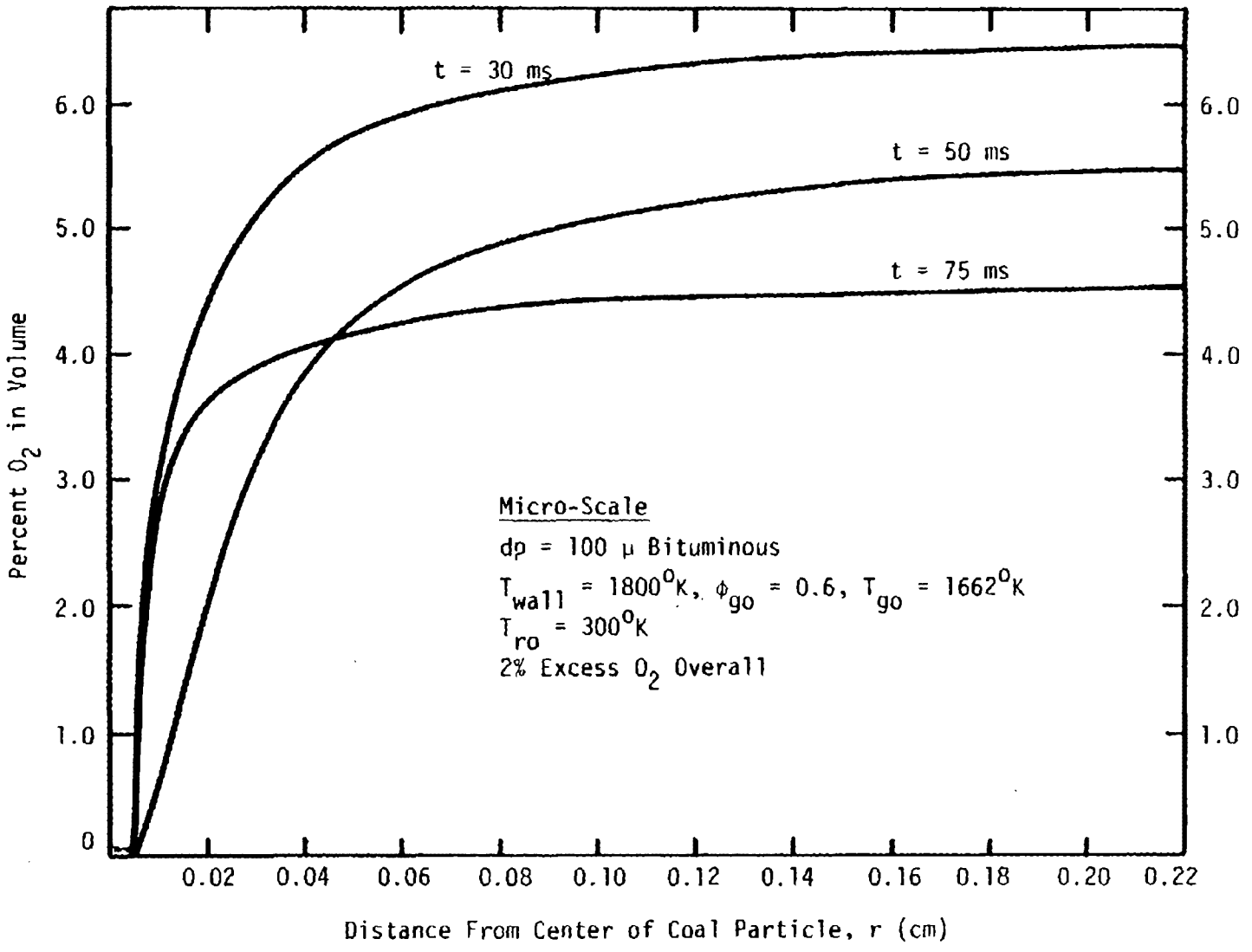

Figure 7. Oxygen Distribution Around a Coal Particle.

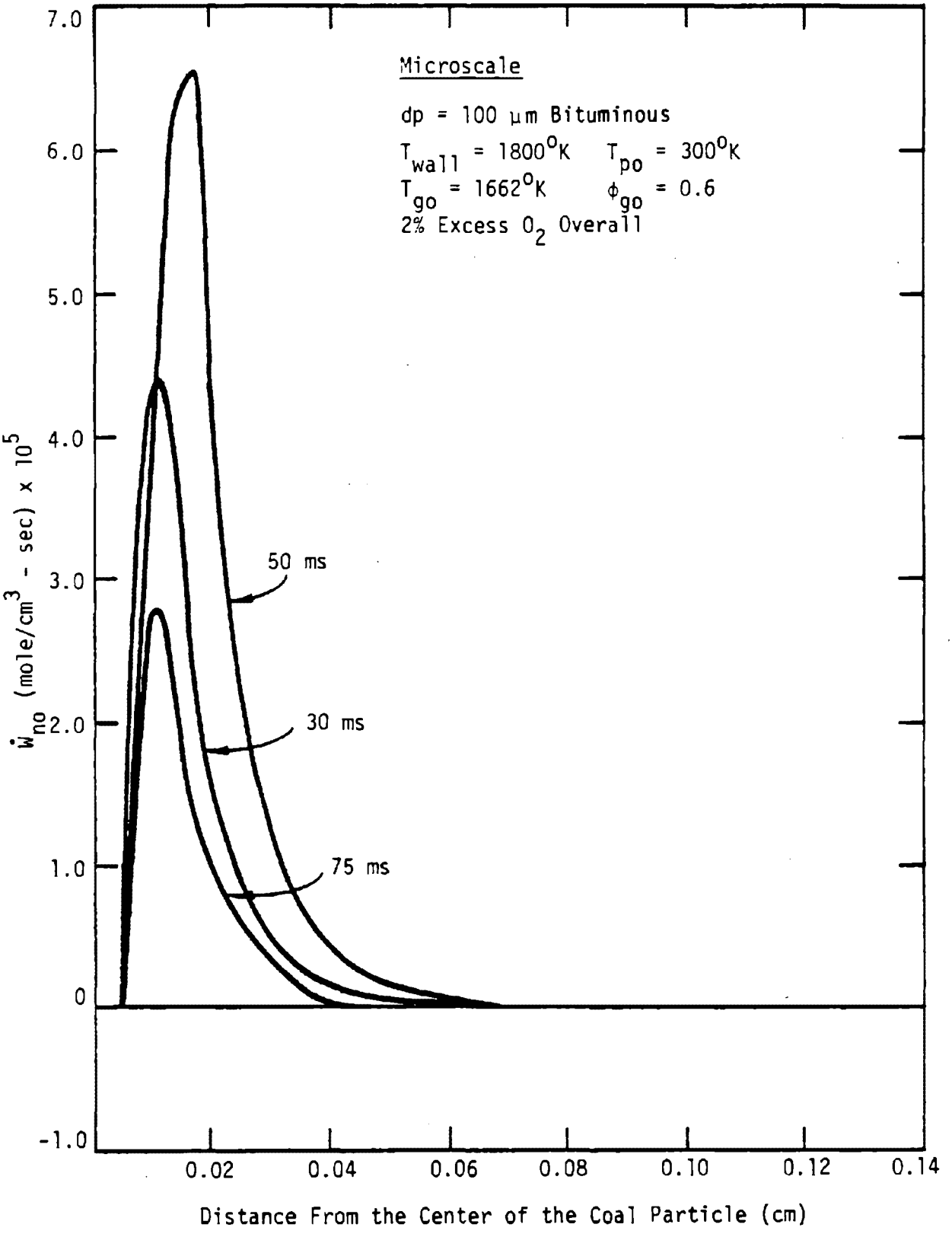

Figure 8. Distribution of NO Production Rate Around a Coal Particle.

thermal NO contribution is as high as 17.5 percent.

The production rates of N_2 at the three stages are shown in Figure 9. The key reactions which contribute to the direct production of N_2 at t = 50 ms are as follows:

		% Contribution (Vol. Rate)	
Reaction No.	Reactions	Overall	At Tmax
(183)	(N) + (N) → N_2	72.6	53.1
(96)	NO + N → O + N_2	12.0	41.5
(108)	N_2O + H → OH + H_2	9.3	1.9

Reaction (183) represents the path by which 90 percent of char nitrogen converts to N_2. The reaction is an ad hoc simulation of char nitrogen conversion and should be improved later. The key reaction for N_2 production is reaction (96), which is the well known reverse Zeldovich mechanism. This reaction is responsible for 12 percent of the overall N_2 production and contributes 41.5 percent at its peak temperature.

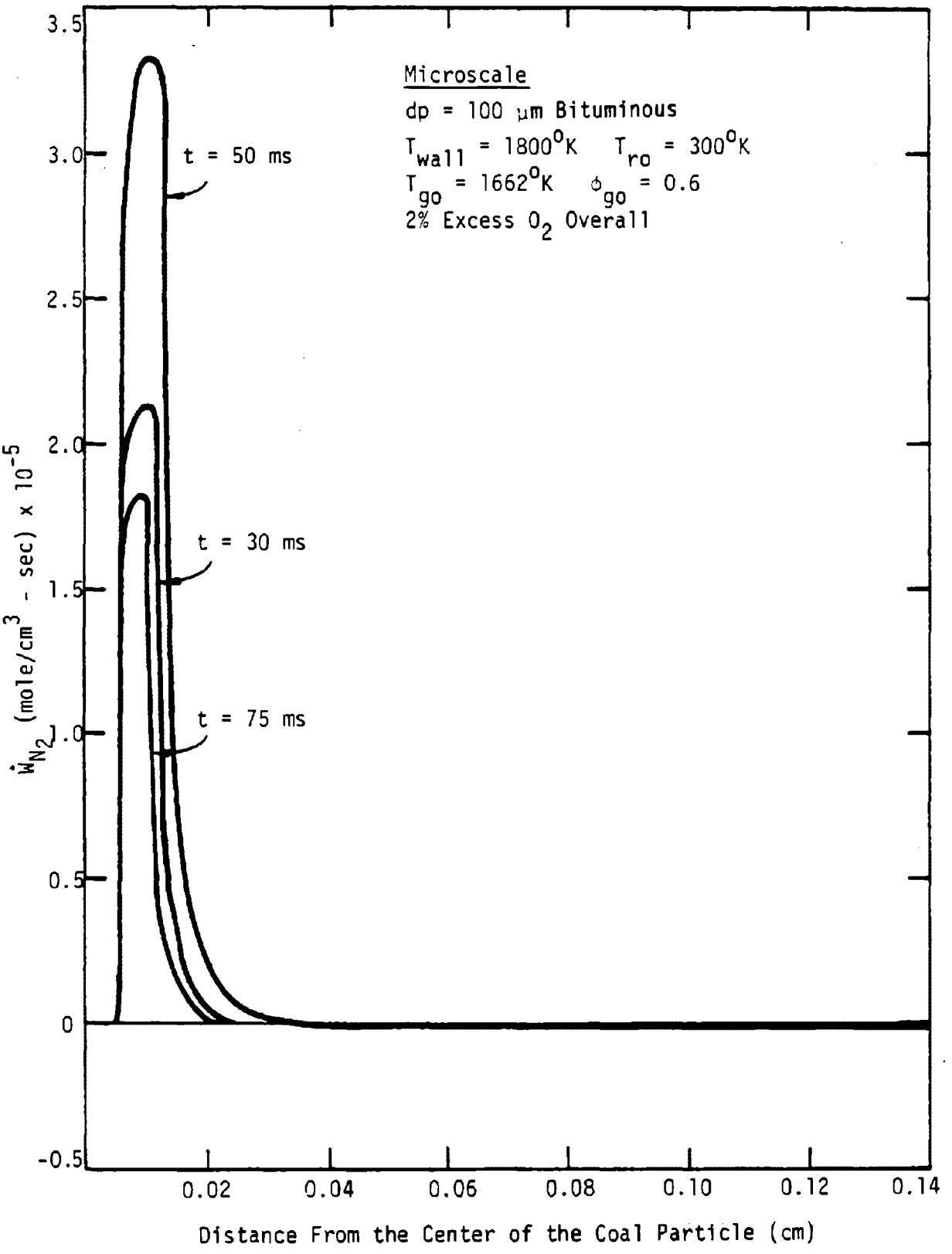

Figure 9. Distribution of N_2 Production Rate Around a Coal Particle.

5.0 MACROSCALE VS. MICROSCALE

Data from Pershing's (1981) experimental work suggests that the presence of char significantly reduces the yield of NO from fuel nitrogen species (NH_3 was used in the experiments).

It was speculated that microscale phenomena surrounding the coal particle might have a significant impact upon fuel nitrogen species conversion to NO. In order to examine the impact of microscale phenomena on fuel nitrogen conversion, numerical experiments were conducted using the microscale model described in previous sections. The computed results are compared to the macroscale results obtained from OFAP (One-Dimensional Flame Analysis Program). OFAP codes operate in plug flow mode where the coal particle has identical chemical characteristics to those used in microscale calculations. However, the volatiles evolved are assumed to mix instantaneously with the surroundings. Therefore, no microscale structures around particles are considered.

Table 3 shows the NO concentration and percent conversion of fuel nitrogen to NO from microscale and macroscale calculations. For smaller particles (50 μm), the results from microscale and macroscale calculations are almost the same for the lower heating case (T_{wall} = 1500°K). There is about 2 percent deviation due to the microscale structure at the higher heating case (T_{wall} = 1800°K). For larger coal particles (100 μm) the microscale effects are somewhat more significant. The deviations are 1.8 percent and 11 percent for T_{wall} = 1500°K and T_{wall} = 1800°K, respectively.

For heterogeneous NO reduction reaction by char, i.e.,

$$NO + CO \rightarrow 1/2N_2 + CO_2$$

the microscale simulation calculations are also listed in Table 3. The results show that heterogeneous NO reduction reaction has only a modest effect on overall NO concentration. For 100 μm particles, the effect is about 5 percent. The rate constant used in these calculations is derived from DeSoete's work (1977):

$$\dot{W}_{NO\ s} = 1.75 \times 10^7 \ Exp\ (-29{,}600/RT)\ \frac{M}{\rho}^{0.7}\ C_{NO}\ C_{CO}^{0.7} \quad \frac{mole}{cm^2\text{-}sec}$$

This reaction is built into the computer code and is not listed in Appendix A. C_{NO} and C_{CO} are in (mole/cc), W is the mixture molecular weight, and ρ is the

Table 3. PPM levels of NO and Percentage Conversion of Fuel-N* Calculated by Microscale and Macroscale Models.

dp = 50 μm

T_{wall}	Macroscale	Microscale	Microscale (With Heterogeneous NO Reduction**)
1500	625 ppm/77.5%	621 ppm/77.0%	-
1800	886 ppm/109%	871 ppm/107%	-

dp = 100 μm

T_{wall}	Macroscale	Microscale	Microscale (With Heterogeneous NO Reduction**)
1500	592 ppm/73.4%	578 ppm/71.6%	540 ppm/66.8%
1800	909 ppm/111%	826 ppm/100%	752 ppm/94.6%

*Pittsburgh Bituminous

**$NO + CO \rightarrow \frac{1}{2}N_2 + CO_2$

mixture density. Thus, the microscale processes simulated here do not explain the degree of impact of char on NO conversion which was observed in Pershing's work. Pershing's work shows only 25-30 percent conversion of fuel nitrogen to NO for most of the coal in various ranges of excess oxygen. Our microscale model predicts 70-100 percent conversion, which is far off. Possible areas of improvement in the microscale model are:

1. Fuel nitrogen pyrolysis chemistry. The current model assumes instant conversion of fuel nitrogen to CHN upon devolatilization, which might partially be responsible for overprediction of NO conversion. Some intermediates of fuel-n furing pyrolysis might have an effect on final conversion.
2. Gas-phase CHN/NH_3 chemistry. The validity of the current CHN/NH_3 chemistry may have to be reexamined, particularly in rich mixtures; Exxon data suggest that our chemistry set seriously overpredicts NH_3 conversion to NO.
3. Heterogeneous NO reduction by soot. Although the mechanism of NO reduction by soot is included in these computations (Reaction 184), the soot formation mechanism in our model is an ad hoc mechanism (based only on an atom balance of the aliphatic group). The impact of soot concentration on fuel-N conversion will be reexamined when the mechanism of soot formation is better understood.

6.0 CHARACTERISTIC TIME SCALES ON SINGLE PARTICLE COMBUSTION

Several physical and chemical characteristic time scales, which may help to better understand the processes occurring around a single burning coal particle, are listed in Table 4. The definitions of those characteristic times are described as follows.

1. Heat-up time: the time interval required for the coal particle to be heated by the amount which is equal to 95 percent of the difference between T_{wall} and initial particle temperature.
2. Diffusion time: the time interval required for a gas molecule to diffuse from the particle surface to the outer boundary of the gas puff. This is estimated by $L_g^2/\bar{D}_g$ where L_g is the dimension of the gas puff. $\bar{D}_g$ is the mean diffusivity of the gas molecule.
3. Devolatilization time for light volatiles/tar/volatile nitrogen: the time at which peak evolution rate occurs. Values listed in Table 4 are taken directly from Figure 2 and Figure 4. For light volatiles, the last peak (for the tightest bounded species) was taken.
4. Particle life time: the period during which char is completely burned.
5. CO combustion time: an estimate of the time required for CO to be burned. The values (order of magnitude only) are taken to be the reciprocal of the multiplication of $K_{21}(T_{wall})$ by the mean HO concentration within the zone of influence.
6. NO formation time: an approximate estimation of the time required for NO to be formed from fuel nitrogen (i.e., CHN) destruction. The values (order of magnitude only) are taken to be the reciprocal of the multiplication of $K_{89}(T_{wall})$ by the mean OH concentration within the zone of influence.
7. N_2 formation time: a rough estimate of the time required for N_2 to be formed from NO which is presumably coming from fuel nitrogen. The values (order of magnitude only) are taken to be the reciprocal of the multiplication of $K_{96}(T_{wall})$ by the mean N atom concentration within the zone of influence.

Table 4. Physical and Chemical Time Scale

Time Scale (ms)	dp = 50 μm		dp = 100 μm	
	T_{wall}=1500°K	T_{wall}=1800°K	T_{wall}=1500°K	T_{wall}=1800°K
Heat-up Time, τ_{hu}	7.0	25.0	25.0	60.0
Diffusion Time, t_{df}	7.2	7.2	28.8	28.8
Devolatilization Time, τ_{dv}				
Light Volatile	7.0	6.0	20.0	18.0
Tar	25.0	20.0	55.0	42.0
Volatile N	50.0	30.0	75.0	60.0
Particle Life Time, τ_p	95	62	350	180
CO Combustion Time, τ_{co}	<1.0	<1.0	<1.0	<1.0
NO Formation Time, τ	<0.01	<0.01	<0.01	<0.01
N_2 Formation Time, τ_{N_2}	~10	~10	~10	~10
CHN Destruction Time, τ_{CHN}	<0.1	<0.1	<0.1	<0.1
Ignition Time, τ_{Tg}	4.7	4.2	15.5	13.5
Heterogeneous NO Reduction $(\tau_{NO})_{Heter}$	10^4	10^4	10^4	10^4

8. CHN destruction time: an estimate of the time required for CHN to be destroyed. Values are taken to be the reciprocal of the multiplication of $K_{117}(T_{wall})$ by the mean OH concentration within the zone of influence.
9. Ignition time: the time at which gas temperature suddenly increases. The values are taken directly from Figure 3 and Figure 5.
10. Heterogeneous NO reduction time is defined as

$$(\tau_{NO})\,\text{Heter} = \frac{\text{overall NO in the puff (mole)}}{(\text{particle surface area, cm}^2)\left[(\dot{w}_{NO})_s,\ \text{mole/cm}^2\text{-sec}\right]}$$

It is noted that for all cases the particle heat-up time is either comparable to or longer than light volatile evolution time. The major portion of light volatiles are evolved during the particle heat-up period. The diffusion time is either comparable to or shorter than the devolatilization time in most cases.

For a 100 μm particle, the zone of action ($r < 0.05$ cm) only represents approximately one-half percent of the total volume (or mass). The characteristic convective time in this region, which is estimated by

$$\tau_{conv} = \frac{\text{Length scale of the zone } (L_I)}{\text{Average convective velocity in the zone } (\bar{V})}$$

is about 0.7 ms (= 0.05/70).

The characteristic diffusion time in the zone of action, which is defined by $\tau_{Diff} = (L_I)^2/\bar{D}$, is about 2.5 ms (= $(0.05)^2/1.0$). These times are all comparatively shorter than the N_2 formation time. However, they are either shorter than or comparable to CO combustion time and much longer than either NO formation or CHN destruction time. This suggests that although NO will be formed from fuel nitrogen within the zone of action, it will not be reduced within the zone of action either.

The heterogeneous reaction times are on the order of minutes, which is too long to make heterogeneous reaction significant in NO reduction.

7.0 REFERENCES

1. Axworthy, A. E., Dayan, V. H., and Martin, G. B. "Reactions of Fuel-Nitrogen Compounds Under Conditions of Inert Pyrolysis." Fuel. Vol. 57, p. 29, 1978.

2. Blair, D. W., Wendt, J. O. L., and Bartok, W. "Evolution of Nitrogen and Other Species During Controlled Pyrolysis of Coal." Sixteenth Symposium (International) on Combustion, The Combustion Institute (1977).

3. DeSoete, G. G., "Mechanisms of Nitric Oxide Reduction on Solid Particles." Proceedings of the Fifth EPA Fundamental Combustion Research Contractors Workshop, EPA-600/9-83-001 (NTIS PB83-164483) (1983), p. 174.

4. Kobayashi, H., Howard, J. B., and Sarofim, A. F. "Coal Devolatilization at High Temperatures." Sixteenth Symposium (International) on Combustion, The Combustion Institute (1977), p. 411.

5. Chen, S. L., Pershing, D. W., Heap, M. P., and Martin, G. B. "Influence of Coal Composition on the Fate of Volatile and Char Nitrogen During Combustion." Nineteenth Symposium (International) on Combustion, The Combustion Institute (1982).

6. Pohl, J. H., and Sarofim, A. F. "Devolatilization and Oxidation of Coal Nitrogen." Sixteenth Symposium (International) on Combustion, The Combustion Institute (1977), p. 491.

7. Smith, I. W. "The Kinetics of Combustion of Pulverized Semi-anthracite in Temperature Range 1400-2200 K." Combustion and Flame, 17, 421, (1971).

8. Solomon, P. R., and Colket, M. B. "Coal Devolatilization." Seventeenth Symposium (International) on Combustion, The Combustion Institute (1979), p.131.

9. Suuberg, E. M., Peters, W. R., and Howard, J. B. "Product Compositions and Formation Kinetics in Rapid Pyrolysis of Pulverized Coal--Implication for Combustion." Seventeenth Symposium (International) on Combustion, The Combustion Institute (1979), p. 117.

10. Walker, D. L., Rusinko, F., and Austin, L. G. "Gas Reactions of Carbon." Advances in Catalysis, 11, 133 (1959).

PART 3

DATA ANALYSIS THROUGH INVERSE TECHNIQUES

Prepared by:

C. J. Kau

and

T. J. Tyson

TABLE OF CONTENTS

LIST OF FIGURES

1.0 INTRODUCTION

Due to the great volume of field data obtained from experimental combustion devices, a need has arisen to develop an analytical tool to use these data to better understand turbulence/chemistry interaction and pollutant formation. Experimental data usually concern flow field variables such as velocity components, temperature and species concentrations. It has been the environmental engineer's dream to have an analytical tool to calculate distribution of turbulent transport properties of an entire flow field. This would eventually allow calculation of the distribution of pollutant formation rates, such as NO production rate, in a flame zone. Thus, ultimately, an effective control strategy could be devised. This methodology is called "Inverse Analysis."

Generally speaking there are two types of methods that have been used. The first method is the control volume method (Ref. 1). This method requires mapping out of the streamlines to form the field data, and then subdividing the flow field into small control volumes between streamlines. The turbulent eddy diffusivity is then derived from a material balance of nonreactive tracer in the control element. Using the eddy diffusivity, the production rate of any chemical species can be calculated by balancing turbulent diffusive flux and convective flux. The drawbacks of this method are:

(i) Requiring tracer

(ii) Mapping of the flow field

The second method is a differential equation method (Ref. 2). One has to write out an entire set of the governing equations and then evaluate the evaluable terms in these differential equations from measured data. The turbulent eddy diffusivity is the only unknown in the momentum equation to be derived from measured velocity. The production rate is the only unknown in the species equation and can thus be evaluated. This method does not require tracer; however, it requires very smooth data and cannot handle recirculatory flows due to the fact that there are more unknown turbulent stress terms than the number of governing momentum equations.

The differential equation method for analyzing weakly swirling flow will be described and tested in the following sections.

2.0 ANALYSIS

2.1 Basic Equations

The vector forms of the time-averaged continuity equation, Navier-Stokes equation of motion, and mass conservation equation for a turbulent reacting flow can be written:

$$\frac{D\rho}{Dt} + \rho(\nabla\cdot\bar{u}) = 0 \tag{1}$$

$$\rho \frac{D\bar{u}}{Dt} = -\bar{\nabla}P + \bar{\nabla}\cdot\bar{\tau} \tag{2}$$

$$\rho \frac{DY_i}{Dt} = - \bar{\nabla} \bar{J}_i + \dot{\omega}_i \tag{3}$$

where $\bar{\tau}$ is a Reynolds stress tensor, $\bar{J}_i$ is the mass flux vector of the ith species, and ω_i is the chemical production rate of ith species. Y_i is the mass fraction of the ith species. Mechanical dissipation and external body forces are neglected in the above equations.

For description of a steady axisymmetric flow field, it is convenient to write the equations in a cylindrical coordinate system; i.e.,

Continuity Equation

$$\frac{\partial}{\partial z}(\rho u_z) + \frac{1}{r}\frac{\partial}{\partial r}(r\rho u_r) = 0 \tag{4}$$

Axial (z-direction) Momentum Equation

$$\rho\left(u_z \frac{\partial u_z}{\partial z} + u_r \frac{\partial u_z}{\partial r}\right) = \frac{\partial}{\partial z}(\tau_{zz}) + \frac{1}{r}\frac{\partial}{\partial r}(r\tau_{rz}) - \frac{\partial P}{\partial z} \tag{5}$$

Radial (r-direction) Momentum Equation

$$\rho\left(u_z \frac{\partial u_r}{\partial z} + u_r \frac{\partial u_r}{\partial r} - \frac{u_\theta^2}{r}\right) = \frac{\partial}{\partial z}(\tau_{zr}) + \frac{1}{r}\frac{\partial}{\partial z}(r\tau_{rr}) - \frac{\tau_{\theta\theta}}{r} - \frac{\partial P}{\partial r} \tag{6}$$

Azimuthal (θ-direction) Momentum Equation

$$\rho\left(u_z \frac{\partial u_\theta}{\partial z} + u_r \frac{\partial u_\theta}{\partial r} + \frac{u_r u_\theta}{r}\right) = \frac{\partial}{\partial z}(\tau_{\theta z}) + \frac{1}{r^2}\frac{\partial}{\partial r}(r^2\tau_{r\theta}) \tag{7}$$

Species Conservation Equation

$$\rho\left(u_z \frac{\partial Y_i}{\partial z} + u_r \frac{\partial Y_i}{\partial r}\right) = \frac{\partial}{\partial z}(J_{iz}) + \frac{1}{r}\frac{\partial}{\partial r}(rJ_{ir}) + \dot{\omega}_i \tag{8}$$

For weakly swirling flow, there are no recirculating zones in the flow field and a boundary layer type of approximation can be employed to further simplify the above equations. By invoking a boundary layer approximation, via order of magnitude argument, the above equations can be reduced to:

Continuity Equation

$$\frac{\partial}{\partial z}(\rho u_z) + \frac{1}{r}\frac{\partial}{\partial r}(r\rho u_r) = 0 \tag{9}$$

Momentum Equations

$$\rho\left(u_z\frac{\partial u_z}{\partial z} + u_r\frac{\partial u_z}{\partial r}\right) + \frac{\partial P}{\partial z} = \frac{1}{r}\frac{\partial}{\partial}(r\tau_{rz}) \tag{10}$$

$$\rho\frac{u_\theta^2}{r} = \frac{\partial P}{\partial r} \tag{11}$$

$$\rho\left(u_z\frac{\partial u_\theta}{\partial z} + u_r\frac{\partial u_\theta}{\partial r} + \frac{u_\theta u_r}{r}\right) = \frac{1}{r^2}\frac{\partial}{\partial r}(r^2\tau_{r\theta}) \tag{12}$$

Species Equation

$$\rho\left(u_z\frac{\partial Y_i}{\partial z} + u_r\frac{\partial Y_i}{\partial r}\right) - \frac{1}{r}\frac{\partial}{\partial z}(rJ_{ir}) = \dot{\omega}_i \tag{13}$$

Generally, Eqs. (9)-(13) and an equation for conservation of energy are used to predict the flow field if boundary conditions of the flow region are known and if Reynolds stresses, diffusive flux, and chemical production term can be adequately modeled. For chemically reacting turbulent flow, the physics of the interaction between turbulence and chemistry are largely unclear. It is difficult to model these terms in an adequate manner; however, when the details of the flow field are measurable, the known information (i.e. velocities, temperature, pressure, and species distributions) can be used to compute the Reynolds stresses (or turbulent viscosity) and chemical production rates by using the same set of equations.

2.2 Inverse Analysis

When the time-mean velocities, temperature, pressure and species distributions of a flow field are measurable, the ideal gas law

$\rho = \dfrac{P\sum_i M_i X_i}{RT}$ can be used to calculate the density distribution. The terms on

the left-hand side of equation (10) can readily be evaluated. Numerically integrating equation (10) in the r-direction gives the $\tau_{rz}(z,r)$ distribution. Similarly, $\tau_{r\theta}(z,r)$ can be calculated by integrating Equation (12). If pressure is known only at the outer edge of the flow field [i.e. $P(z,\infty)$], Equation (11) must be used to integrate inwardly in the r-direction for $P(z,r)$. If $U_r(z,r)$ are not given, the continuity equation [Equation (9)] can be used to solve for them.

Apparent turbulent viscosities can be defined by analogy to Newton's law of friction for laminar flow; i.e.,

$$\mu_{rz} = \frac{\tau_{rz}}{(\partial u_z/\partial r)}$$

and

$$\mu_{r\theta} = \frac{(\tau_{r\theta}/r)}{\frac{\partial}{\partial r}(u_\theta/r)}$$

Similarly, apparent species diffusivity (α_i) of turbulence can be defined by analogy to Fick's law of diffusion; i.e.,

$$J_{ir} = \alpha_i \frac{\partial Y_i}{\partial r}$$

For engineering purposes, it is generally assumed that the ratio of turbulent viscosity to turbulent mass diffusivity is approximately constant. Thus, the species flux can be evaluated from the known value of μ_{rz}, Schmidt number and measurable species distribution; thus

$$J_{ir} = \frac{\mu_{rz}}{S_{ci}} \frac{\partial Y_i}{\partial r}$$

where Schmidt number is defined as $S_{ci} = \frac{\mu_{rz}}{\alpha_i}$. Then the chemical production rate of species i can be evaluated by Equation (13).

2.3 Numerical Consideration

The experimental data are usually very crude and unsmooth. Generally, smoothing of the raw data before the inverse analysis process is not only desir-

able but also necessary since we are interested in derivatives of the data.

In the "inverse" analysis code, the experimental data are input tabularly as functions of two physical coordinates. A subroutine named SLP is used to compute the directional derivatives for the tabulated function. SLP calculates the end point derivatives by parabolic interpolation while the derivatives of the interior points are evaluated by a cubic spline fit procedure. If spatial resolution higher than the resolution of original input data is required, a subroutine named CUBIC is used to perform the cubic interpolation and generate an extended data table. The derivatives required for cubic interpolation are calculated from original data by subroutine SLP. The derivatives required for integrating the governing partial differential equation are also computed by SLP using this extended tabular function.

3.0 SAMPLE CASE

The first sample case chosen to examine the correctness of the code's arithmetic is an NH_3-doped hydrogen laminar diffusion flame. The flame parameters are:

Fuel Tube:	0.236 cm ID
	0.635 cm OD
Oxidant Tube:	5.08 cm ID
Fuel/Oxidant Ratio:	167 percent T.A.
Percent O_2 in Oxidant:	10.51 (vol)
Percent NH_3 in Fuel:	4.01 (vol)
Fuel Flow:	2178 cm/sec
Oxidant Flow:	46.14 cm/sec
Tube Wall Temperature:	353^{o}K

The fuel nitrogen conversion experiment in the diffusion flame has been physically carried out in EER's El Toro laboratory (Ref. 3); however, the flame was not probed in detail, only stake values were measured. For the purpose of program checkout, the "experimental data" of the flame is actually "simulated" in detail using EER's diffusion code (GFAP, in diffusion flame mode). The "numerical simulated experimental data" is then fed into the "Inverse Analysis" model to back out viscosity and NO production. It should be noted that the choice of laminar flame instead of turbulent flow will not affect our program checkout since laminar and turbulent flows are described by the same set of PDE.

The viscosity distribution computed from "Inverse Analysis" code is shown in Figure 1 (at two locations downstream from the exit of the fuel tube) in comparison with the "viscosity" used to simulate the "experimental data." The NO production rates obtained from the "Inverse Analysis" code are shown in Figure 2 in comparison with the experimental data "simulated." The slight deviations in both comparisons probably can be attributed to the fundamental differences between derivative evaluation methods. In inverse analysis code a cubic spline fit procedure was used to evaluate derivatives while a central differencing scheme was used in the "experimental data simulation" model.

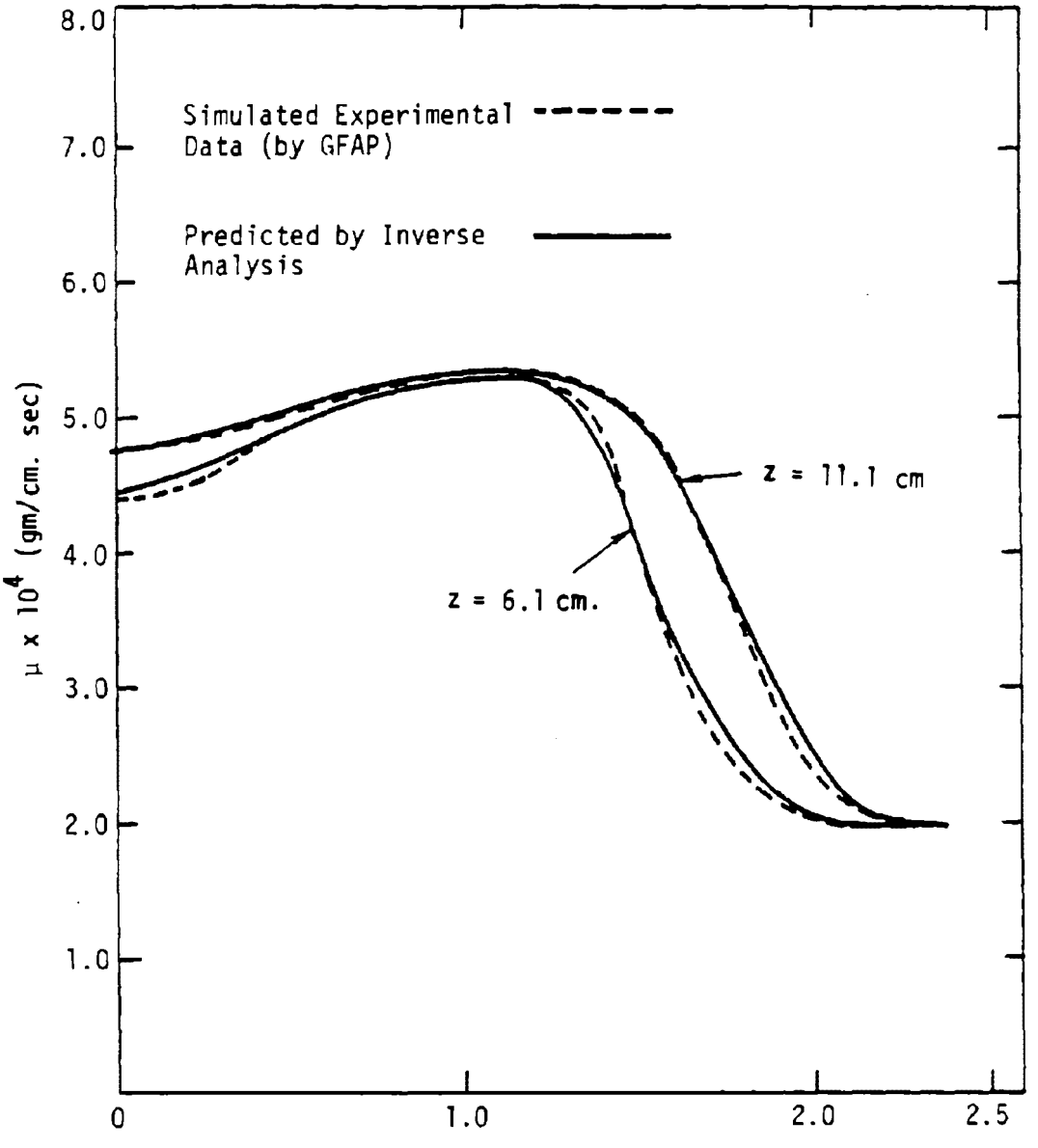

Figure 1. Comparisons of the Distribution of Viscosities.

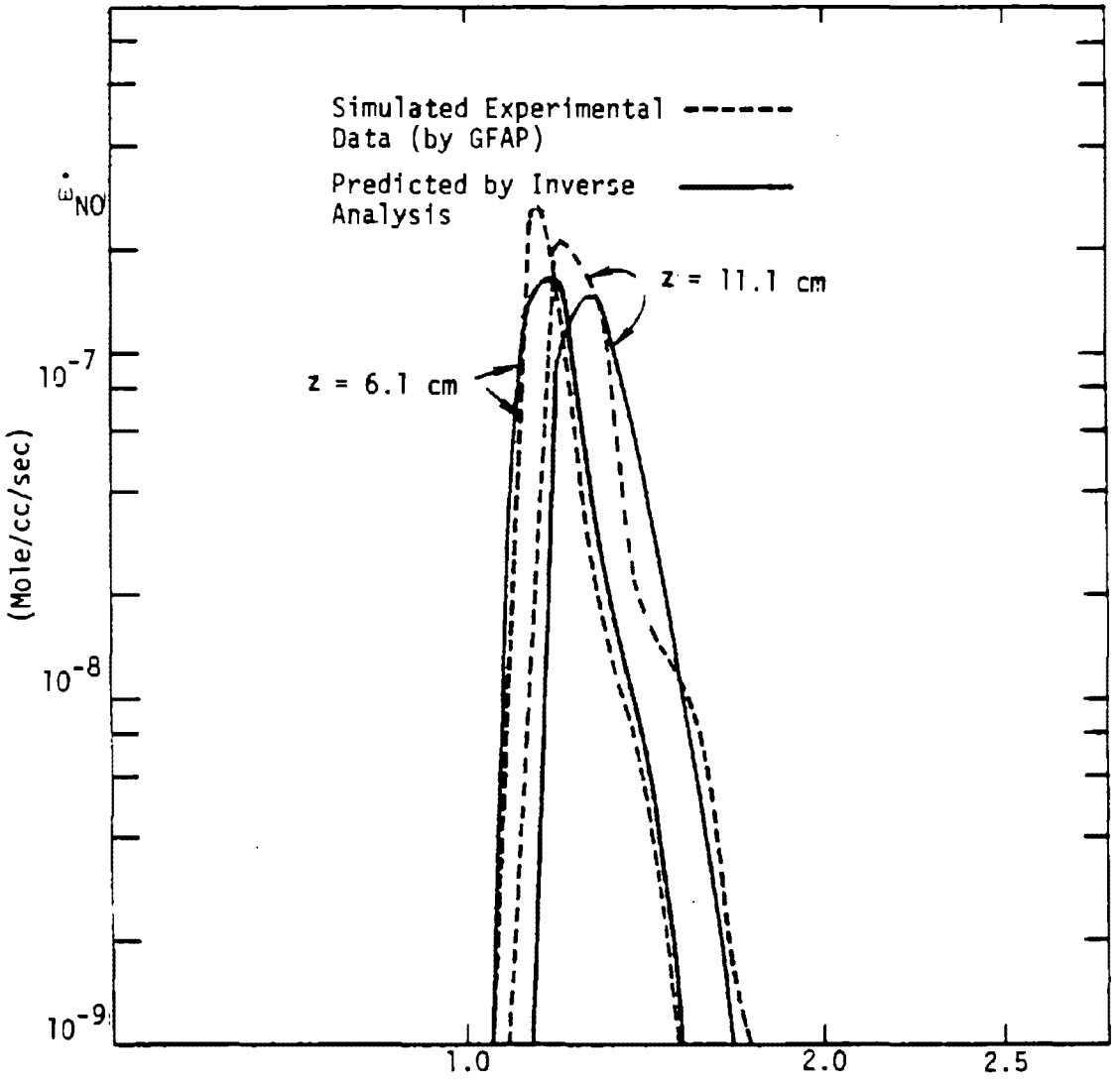

Figure 2. Comparison of the Distribution of NO Production Rates.

4.0 CONCLUSION

So far, the "Inverse Analysis" code has been successfully tested only on very smooth data (e.g., computer-generated). The tests using raw field data such as the combustion data from IFRF (Ref. 4) were unsuccessful due to extreme sensitivity of the solutions to the quality of data, due to the fact that we have evaluated the divergent terms in the equation from sparsely measured data points. Several data smoothing techniques have been tried and the results obtained are disappointing.

5.0 REFERENCES

1. Sadaka, M. and Beer, J. M. "Spatial Distribution of Nitric Oxide Formation Rate in Swirling Turbulent Methane-Air Flame." Proceedings of the Sixteenth (International) on Combustion. The Combustion Institute (1976), p. 93.

2. Lilley, D. G., and Chigier, N. A. "Nonisotropic Exchange Coefficients in Turbulent Swirling Flames from Mean value Distributions." Combustion and Flame, 16, p. 177 (1971).

3. Folsom, B. A., Courtney, C. W., Corley, T. L., and Clark, W. D., "Advanced Combustion Concepts for Low Btu Gas Combustion," Proceedings of the Third Stationary Source Combustion Symposium; Volume II, EPA-600/7-79-050b (NTIS PB292540) (1979), p. 163.

4. Michels, J., and Payne, R., "Fundamental Combustion Research Applied to Pollution Formation, Vol. IIa: Physics and Chemistry of Two-Phase Systems: Flame Combustion Processes, Part II: Detailed Measurement of Long Pulverized Coal Flames for the Characterization of Pollutant Formation," International Flame Research Foundation Report, 1982.

6.0 NOMENCLATURE

J_i : ith species flux

M_i : Molecular weight of ith species

P : Static pressure

R : Gas Constant

r : Radial coordinates

Sci : Schmidt number (ith species)

T : Temperature

t : Time

u : Velocity

X_i : Species mole fraction

Y_i : Species mass fraction

z : Axial coordinates

Greek:

ρ : Density

α : Turbulent species diffusivity

ϑ : Azimuthal coordinates

τ : Reynold stress

$\dot{\omega}_i$: Chemical production rate of ith species

μ : Turbulent eddy viscosity

Subscripts:

i : ith species

r : Radial direction

z : Axial direction

θ : Azimuthal direction

PART 4

MICROSCOPIC MIXING IN TURBULENT DIFFUSION FLAMES

Prepared by:

C. J. Kau

and

T. J. Tyson

TABLE OF CONTENTS

LIST OF FIGURES

1.0 INTRODUCTION

New information on the rate of microscopic mixing in turbulent diffusion flames discovered by re-examination of classic jet diffusion flame data obtained by Hawthorne, Weddel and Hottel (Ref. 1), and the later data by Bilger and Beck (Ref. 2) has led to the development of a simple turbulent diffusion model. The simple model postulated here consists of a well-stirred reactor and a plug-flow reactor to simulate the turbulent flamelet and flame-core in a turbulent diffusion flame. The model is used to predict NO formation in H_2/air flames. Comparisons are made against experimental data in terms of NO concentrations. Calculated peak NO concentrations for various flames show $Re^{-1/2}$ dependency, which has also been suggested in the work of Bilger and Beck (Ref. 2).

2.0 MODEL DEVELOPMENT

Considering a circular jet of fuel issuing into stationary ambient air (see Figure 1), the momentum flux based on macroscopic entrainment is:

$$J = \Pi\rho_m U_m^2 R_m^2 = \Pi\rho_o U_o^2 R_o^2$$

The mean local velocity can be expressed in terms of initial density ρ_o and velocity U_o as

$$U_m = \sqrt{\frac{\rho_o}{\rho_m}} \frac{U_o R_o}{R_m} \tag{1}$$

The mass flux per unit initial jet mass flux is

$$\left(\frac{\dot{m}_t}{\dot{m}_o}\right) = \frac{\Pi\rho_m U_m R_m^2}{\Pi\rho_o U_o R_o^2} = \sqrt{\frac{\rho_m}{\rho_o}} \left(\frac{R_m}{R_o}\right) \tag{2}$$

This expression is obtained by elimination of U_m through Equation (1).

Since the flame spreading angle is approximately independent of fuel type and jet conditions, we have:

$$R = k_2 X \tag{3}$$

where k_2 is the tangent of half jet angle. The virtue origin X = 0 is a distance ($= R_o/k_2$) upstream of the nozzle exit plane. This distance is very small in comparison with the physical dimension of the flame and can be neglected. Substituting Eq. (3) into Eq. (2) gives:

$$\left(\frac{\dot{m}_t}{\dot{m}_o}\right) = 2k_2\sqrt{\frac{\rho_o}{\rho_o}} \left(\frac{X}{D_o}\right) . \tag{4}$$

The turbulent entrainment model low-derived by Ricou and Spalding recommended k_2 = 0.16. The axial distance with a turbulent-jet-entrained stoichiometric amount of air is evaluated from

$$\frac{L_{ma}}{D_o} = \frac{1}{2k_2} \left(\frac{\dot{m}_t}{\dot{m}_o}\right)_{st} \sqrt{\frac{\rho_o}{\rho_m}} . \tag{5}$$

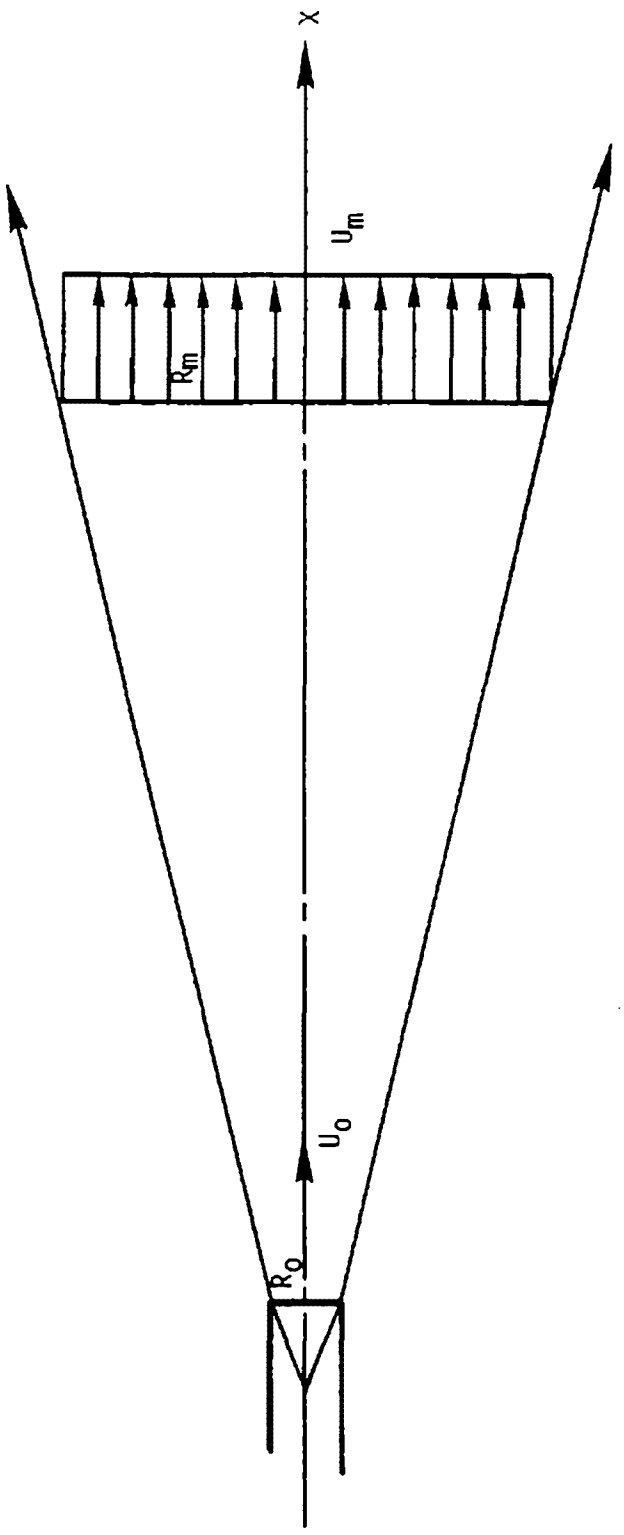

Figure 1. Schematic of Turbulent Free Jet.

Eq. (5) is plotted in Figure 2, where macroscopic mean mixture density ρ_m is taken to be $\rho_a/2$.

Recently, Broadwell (Ref. 4) has re-examined the classic turbulent-jet diffusion flame length data obtained by Hawthorne, Weddel and Hottel (Ref. 1) and has discovered that the flame length, which is a legitimate representation of the microscopic mixing distance of the stoichiometric amount of fuel and air, is also linearly proportional to $\left(\frac{\dot{m}_t}{\dot{m}_o}\right)_{st}\sqrt{\frac{\rho_a}{\rho_m}}$. Data from Hawthorne's (Ref. 1) paper and a later paper by Bilger and Beck (Ref. 2) are plotted in Figure 2. These data represent various types of fuel over small range of Richardson numbers. It is recognized that the buoyancy forces do effect flame length. The flame length here is the analytical flame length, which is the axial distance of the point of 99 percent completion of combustion (based on sample gas). The slope of the straight line best fit to the data point is 9.2 percent. Figure 2 suggests a constant ratio of microscopic mixing rate to macroscopic mixing rate; i.e.,

$$\dot{m}_{micro} = k_1 \dot{m}_{macro} ,$$

Figure 2 implies that $k_1 = 0.339$. Thus, microscopic mixing rate is approximately one-third of macroscopic mixing rate

$$\frac{L_f}{D_o} = \frac{1}{2k_1k_2}\left(\frac{\dot{m}_t}{\dot{m}_o}\right)_{st}\sqrt{\frac{\rho_o}{\rho_o}} \quad . \tag{6}$$

A logical extension of the above conclusion is that the microscopic mixing rate is linearly proportional to $\sqrt{\frac{\rho_m}{\rho_o}}\left(\frac{V}{D}\right)$; i.e.,

$$\left(\frac{\dot{m}_t}{\dot{m}_o}\right)_{micro} = k_3\sqrt{\frac{\rho_m}{\rho_o}}\left(\frac{X}{D}\right) \tag{7}$$

where $k_3 = 2k_1k_2 = 0.1085$.

The definition of velocity and Eq. (1) give

$$U_m \equiv \frac{dx}{dt} = \sqrt{\frac{\rho_o}{\rho_m}}\ \frac{U_oK_o}{k_2X}$$

Integrating the above equation with respect to t by assuming a constant mean ρ_m results in the following space-time relation:

$$\frac{X}{D_o} = \left(\frac{\rho_o}{\rho_m}\right)^{1/4}\left(\frac{U_o t}{k_2 D_o}\right)^{1/2} \tag{8}$$

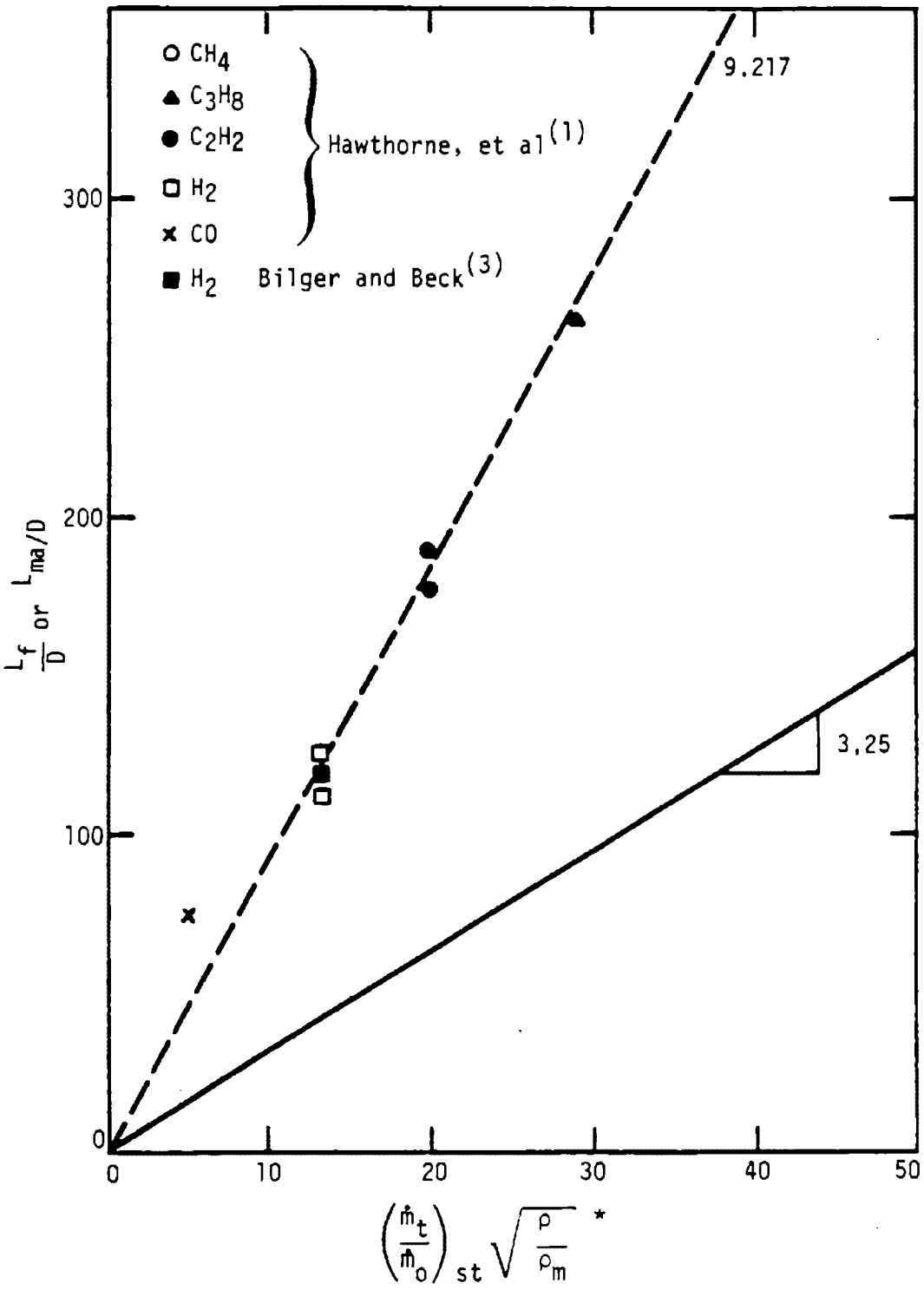

Figure 2. Flame Length vs. $\left(\frac{\dot{m}_t}{\dot{m}_o}\right)_{st}\sqrt{\frac{\rho_o}{f_m}}$

Substituting Eq. (8) into Eq. (7) results in an expression for microscopic mixing in terms of time:

$$\left(\frac{\dot{m}_t}{\dot{m}_o}\right)_{micro} = k_3 \left(\frac{\rho_m}{\rho_o}\right)^{1/4} \left(\frac{U_o t}{k_2 D_o}\right)^{1/2} \tag{9}$$

Taking the time derivative of the above equation gives microscopic air mixing rate:

$$\frac{d}{dt}\left(\frac{\dot{m}_a}{\dot{m}_o}\right)_{micro} = \frac{d}{dt}\left(\frac{\dot{m}_t}{\dot{m}_o} - 1\right) = \frac{d}{dt}\left(\frac{\dot{m}_t}{\dot{m}_o}\right)$$

$$= \frac{k_3}{2}\left(\frac{\rho_m}{\rho_a}\right)^{1/4} \left(\frac{U_o}{k_2 D_o t}\right)^{1/2} \tag{10}$$

The microscopic fuel mixing rate is

$$\frac{d}{dt}\left(\frac{\dot{m}_f}{\dot{m}_o}\right)_{micro} = \frac{1}{AF}\frac{k_3}{2}\left(\frac{\rho_m}{\rho_o}\right)^{1/4} \left(\frac{U_o}{k_2 D_o t}\right)^{1/2} \tag{11}$$

where AF is air/fuel mass ratio. The overall unburned raw fuel left in the flame per unit initial raw fuel flux is evaluated by

$$1.0 - \frac{1}{AF}\frac{k_3}{2}\left(\frac{\rho_m}{\rho_o}\right)^{1/4}\left(\frac{U_o t}{k_2 D_o}\right)^{1/2} \tag{12}$$

Experimental evidence of turbulent-jet mixing suggests that the macroscopically entrained air is first engulfed into a large coherent structure and is subsequently cascaded down to the Kolmogoroff scale and burned completely. The flame surface per unit volume of the turbulent structure is considered to be small until the Kolmogoroff scale is reached; therefore, a simple turbulent diffusion flame model is postulated which contains two major zones: a flamelet zone and a flame-core zone. The flamelet is the Kolmogoroff scale structure which contains stoichiometric (or near stoichiometric) amounts of microscopically mixed fuel and air. The flamelet structure is subsequently destroyed by the molecular diffusion process and conglomerated into the flame core structure which contains the microscopic mixture of combustion products and yet unreacted fuel. It is recommended that the flamelet structure be simulated by a well-stirred reactor with proper stoichiometry and residence time and that the flame-core zone be simulated by a plug flow reactor. The plug flow reactor is continuously fed by combustion products from the flamelet stirred reactor. A schematic of the reactors is shown

in Figure 3. The flamelet fresh air mixing rate is calculated from Eq. (10), while raw fuel mixing rate is evaluated from Eq. (11). The diluted (by combustion products) fuel mixing rate is calculated by:

$$\frac{d}{dt}\left(\frac{\dot{m}_{fd}}{\dot{m}_o}\right) = \frac{1}{AF}\,\frac{k_3}{2}\left(\frac{\rho_m}{\rho_o}\right)^{1/4}\left(\frac{U_o}{k_2 D_o t}\right)^{1/2}\left\{\frac{1 + k_3\left(\frac{\rho_m}{\rho_o}\right)^{1/4}\left(\frac{U_o T}{k_2 D_o}\right)^{1/2}}{1 - \frac{k_3}{AF}\left(\frac{\rho_m}{\rho_o}\right)^{1/4}\left(\frac{U_o t}{k_2 D_o}\right)^{1/2}}\right.$$

The proper residence time for the flamelet reactor should correspond to the molecular viscosity and the Kolmogoroff scale:

$$\tau = C_1 \frac{\lambda^2}{\nu}$$

where C_1 is proportionality constant and ν is kinematic viscosity. The Kolmogoroff scale is evaluated by

$$\lambda = C_2\left(\frac{\nu^3}{\varepsilon}\right)^{1/4}$$

where C_2 is another proportionality constant. The rate of dissipation of turbulence is estimated by

$$\varepsilon = C_3 \frac{U_m^3}{D}$$

$$\tau = \frac{C_1 C_2^2}{\sqrt{C_3}}\,\frac{\nu^{1/2} D^{1/2}}{U_m 3/2}$$

Eliminating U_m using the expression following Eq. (7), the residence time expression becomes:

$$\tau = \beta\left(\frac{\rho_m}{\rho_o}\right)^{3/4}\left(\frac{4\nu^{1/2} k_2^2 D_o^{1/2}}{U_o^{3/4}}\right)\left(\frac{X}{D_o}\right)^2 \qquad (14)$$

where $\beta \equiv C_1 C_2^2 / C_3$ is a major physical uncertainty of the model. Expressing the residence time in terms of clock time using Eq. (8) gives

$$\tau = \beta\, 4k_2\left(\frac{\rho_m}{\rho_o}\right)^{1/4}\frac{t}{\sqrt{Re_o}} \qquad (15)$$

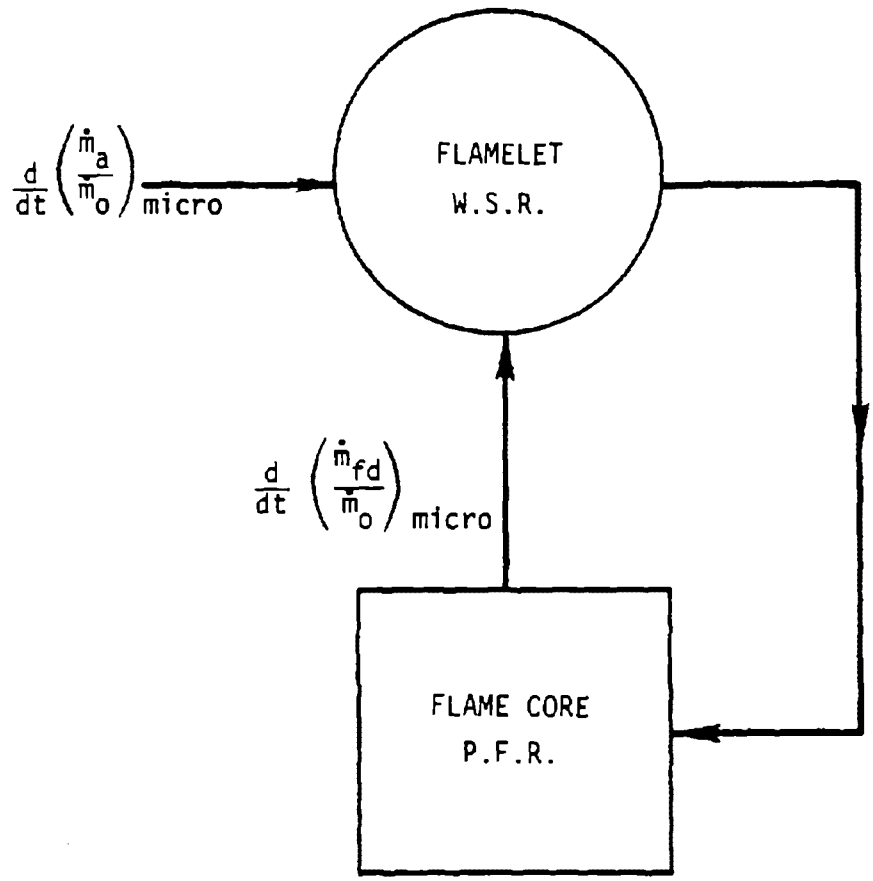

Figure 3. Schematics of Reactor Model.

where Reynolds number Re_o is defined as

$$Re_o = \frac{U_o D_o}{\nu}$$

ν here will be evaluated at some typical flame temperature instead of that of the exit plane.

3.0 NUMERICAL PROCEDURES AND PHYSICAL ASSUMPTIONS

A computer model has been developed for the interacting well-stirred reactor and plug flow reactor described in the previous section. The highlights of the physical and mathematical aspects of this code are:

1. Implicit finite-difference method is used to solve time-dependent governing equations (continuity, species and energy conservation equations and equation of state) implicitly.
2. Fully detailed kinetic mechanism with 17 species and 60 fundamental reactions for H_2/air combustion is used.
3. JANAF Table: Thermochemical properties for each species are calculated by interpolating the JANAF table.
4. Optical-thin approximation is made, which considers only gas-to-ambient radiative heat transfer.

One major uncertainty of the model is β in Eq. (15), which defines the flamelet residence time. The other major uncertainty which may effect prediction of NO is the optical-thin approximation. It is recognized that the optical-thin approximation overpredicts the rate of heat transfer, which in turn underpredicts the flame temperature, and thus underpredicts the NO formation rate.

4.0 TUNING OF THE MODEL

As a first example and check of the computational procedure, the H_u/air flame measured by Bilger and Beck (Ref. 2) is modeled. The flame is a hydrogen jet with 0.635 cm diameter and a mean exit velocity of 19323 cm/sec, which is issuing into still, 300°K air at one atmosphere. In order to compare the calculated NO concentration (mass mean of both reactors) to experimental data, it has to be multiplied by k_1. This is because the experimental data are macroscopic and the reactor data are microscopic.

The computed results, for various β values and $\alpha = 1.0$, are shown in Figure 4. α is a multiplicative factor for the gas radiative heat transfer based on the optical-thin approximation. For instance, $\alpha = 0.5$ means that the heat transfer rate considered is 50 percent of the optical heat transfer rate. When comparing the results against data in Figure 1, it can be seen that β is on the order of 10. However, the peak NO concentration point, which generally coincides with peak flame temperature, is shifting away from measured value as β increases. This is due to fact that with longer the flamelet residence time heat release occurs earlier.

If we take $\beta = 10$, the computed results for various α values are shown in Figure 5 in comparison to measurements. When $\alpha = 0.7$ the computed NO concentrations are best fitted to the experimental data.

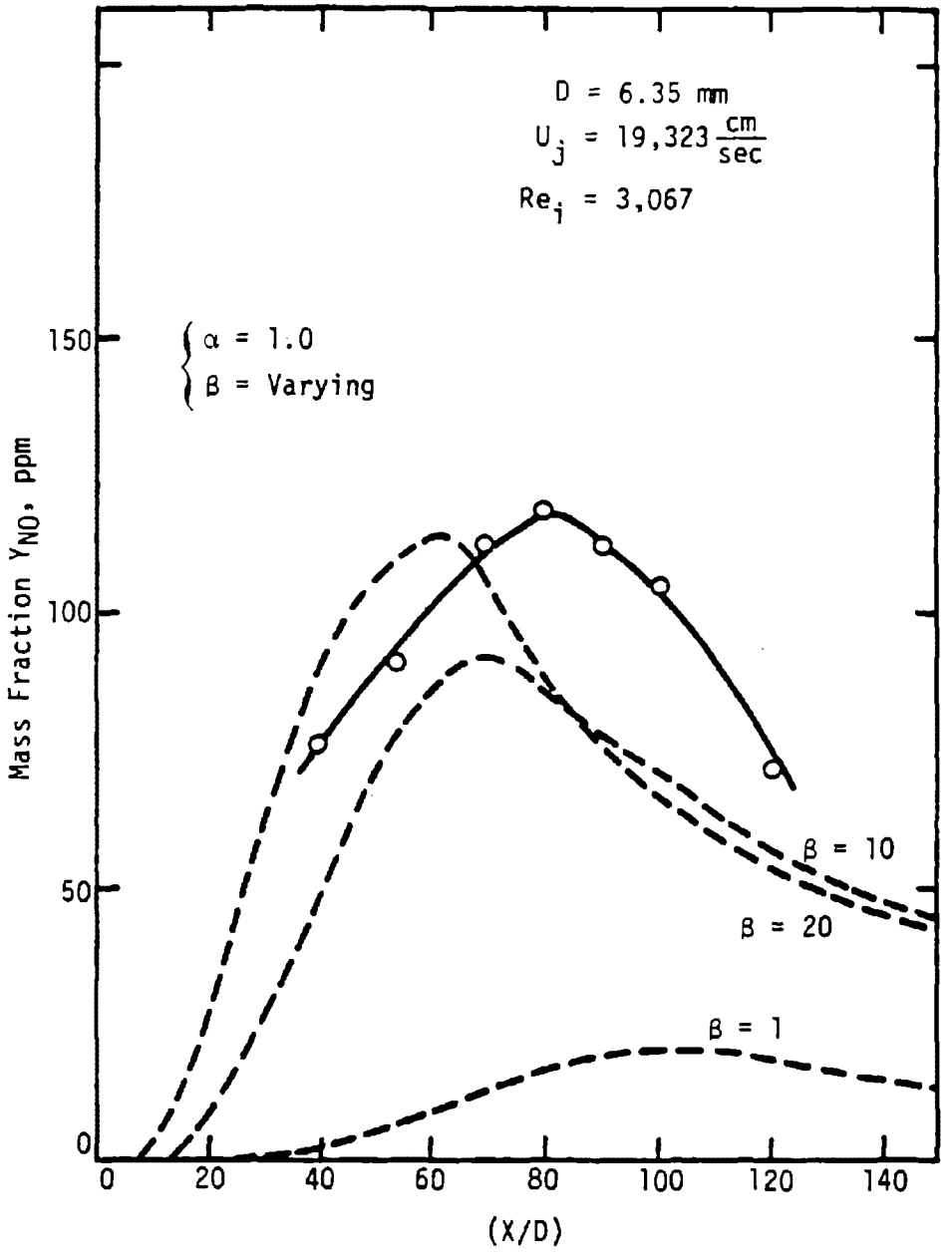

Figure 4. Effects of Uncertainty on Flamelet Residual Time β.

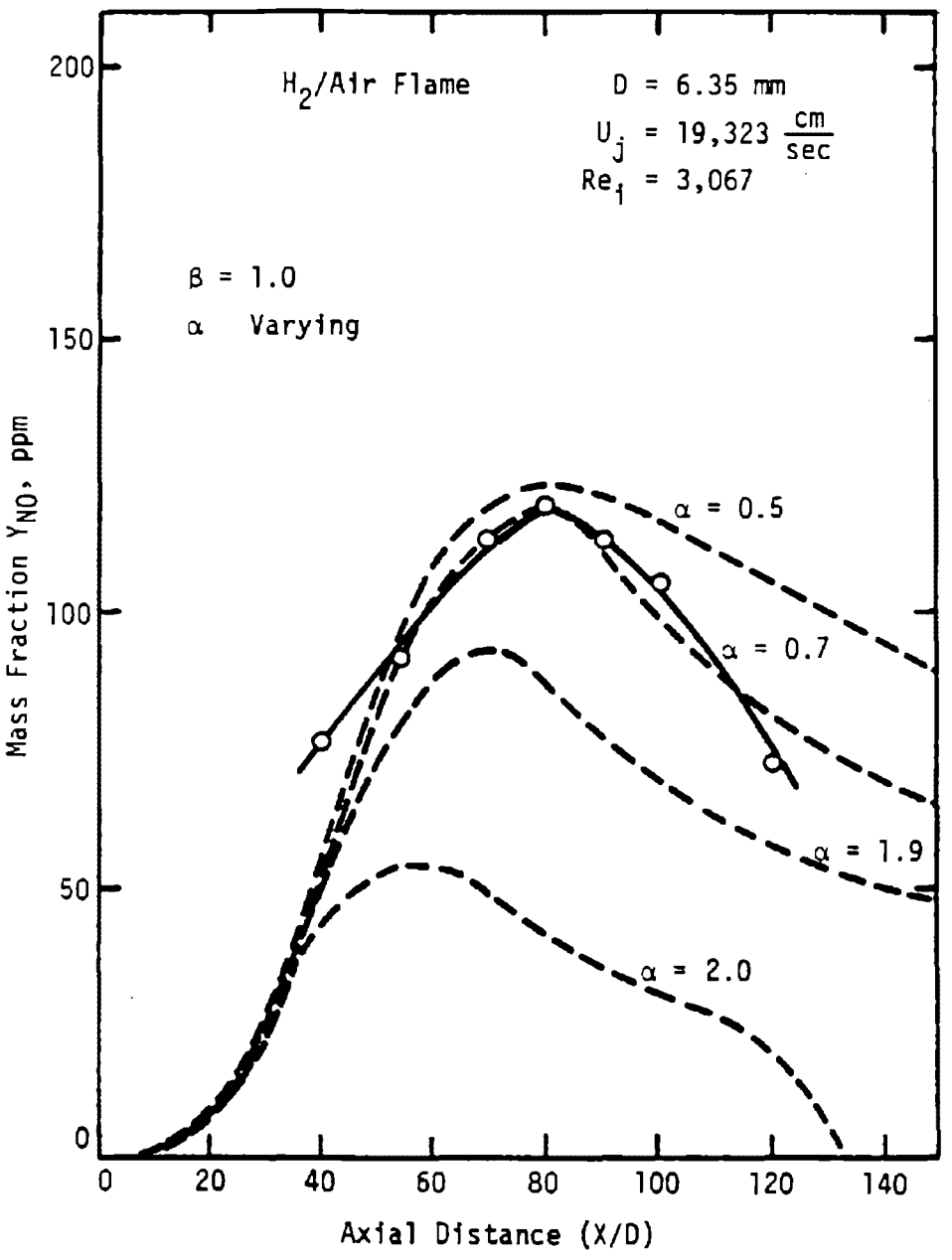

Figure 5. Fine Tuning of α and β.

5.0 REFERENCES

1. Hawthorne, W.R., Weddell, D.S., and Hottel, H.C., Third Symposium of Combustion, Flame and Explosion Phenomena, p. 266, Williams and Wilkins, 1949.

2. Bilger, R.W., and Beck, R.W., "Further Experiments on Turbulent Jet Diffusion Flames," Fifteenth Symposium (International) on Combustion, p.451, The Combustion Institute, 1975.

3. Ricou, F.P., and Spalding, D.B., J. Fluid Mech., 11, 21, (1961).

4. Broadwell, J.E., "A Model of Turbulent Diffusion Flames and Nitric Oxide Generation. Part I," TRW Document No. 38515-6001-UT-00, EERC Final Report, PO No. 18889 (1982).

PART 5

NUMERICAL MODEL
FOR
TWO-PHASE ONE-DIMENSIONAL FLOW REACTOR

Prepared by:
C. J. Kau
and
T. J. Tyson

TABLE OF CONTENTS

LIST OF FIGURES

LIST OF TABLES

1.0 INTRODUCTION

A computer model capable of analyzing various types of two-phase one-dimensional nondiffusive reacting flows (e.g., plug flows) is presented in this report. Detailed formulations and the numerical method of solution are described. The model also is applicable to zero-dimensional time-dependent flow problems and zero-dimensional steady problems with asymptotic solutions (such as well-stirred reactors).

For illustrative purposes, the detailed analyses of a gas-phase reactor (i.e., well-stirred reactor followed by a plug-flow reactor) and a coal well-stirred reactor are presented. Comparisons of calculated results to experimental data are also made.

2.0 FORMULATION

A control volume $A_x \Delta x$ is shown in Figure 1 through which fluid flows steadily. The main stream direction is the x-direction. A_x is the surface area of the reactor (or streamtube) perpendicular to the flow direction. A_x is assumed to be varying very gently and only in the x-direction. A_y is the external surface area of the reactor or streamtube through which external energy or mass is added or removed. ρ is the overall density (i.e., $\rho = \rho_p + \rho_g$). u is the convective velocity in the x-direction. $\dot{W}_{ig}$ and $\dot{W}_{ip}$ are volumetric chemical production rate of gaseous and condensed species, respectively. $\dot{Q}_p$ is the volumetric rate of heat transfer to the particles. $\dot{Q}_r$ is the volumetric heat transfer rate to the gas that is not associated with external mass flux. $\dot{q}_e$ is the energy flux to the gas that is associated with external mass flux. For example, $\dot{q}_e$ could be the heating flux of external mass before the mass enters the control volume. α_i is the species concentration of the ith species (either gaseous or condensed species) and has units of mole per gm of total mass. h is enthalpy. The subscripts "g" and "p" refer to gaseous phase and condensed phase, respectively, while the subscript "e" stands for external flux.

The conservation equations of mass and energy can be derived directly from balancing convective fluxes, as shown in Figure 1; i.e.,

outgoing flux = incoming flux + production.

In the reactors considered here, convective fluxes are assumed to be dominating and thus diffusive fluxes are neglected.

The resulting conservation equations from flux balancing are shown below:

Conservation of Mass

$$\frac{d\left(\rho u A_x\right)}{dx} \Delta x = \rho_e v_e A_y \equiv \dot{m}_e \qquad \left(\frac{gm}{sec}\right) \tag{2-1}$$

Species Conservation Equations

$$\rho u \frac{d\alpha_i}{dx} = \frac{\dot{m}_e}{A x \Delta x} \left(\alpha_{i,e} - \alpha_i\right) + \dot{w}_i \qquad \left(\frac{mole}{cc\text{-}sec}\right) \tag{2-2}$$

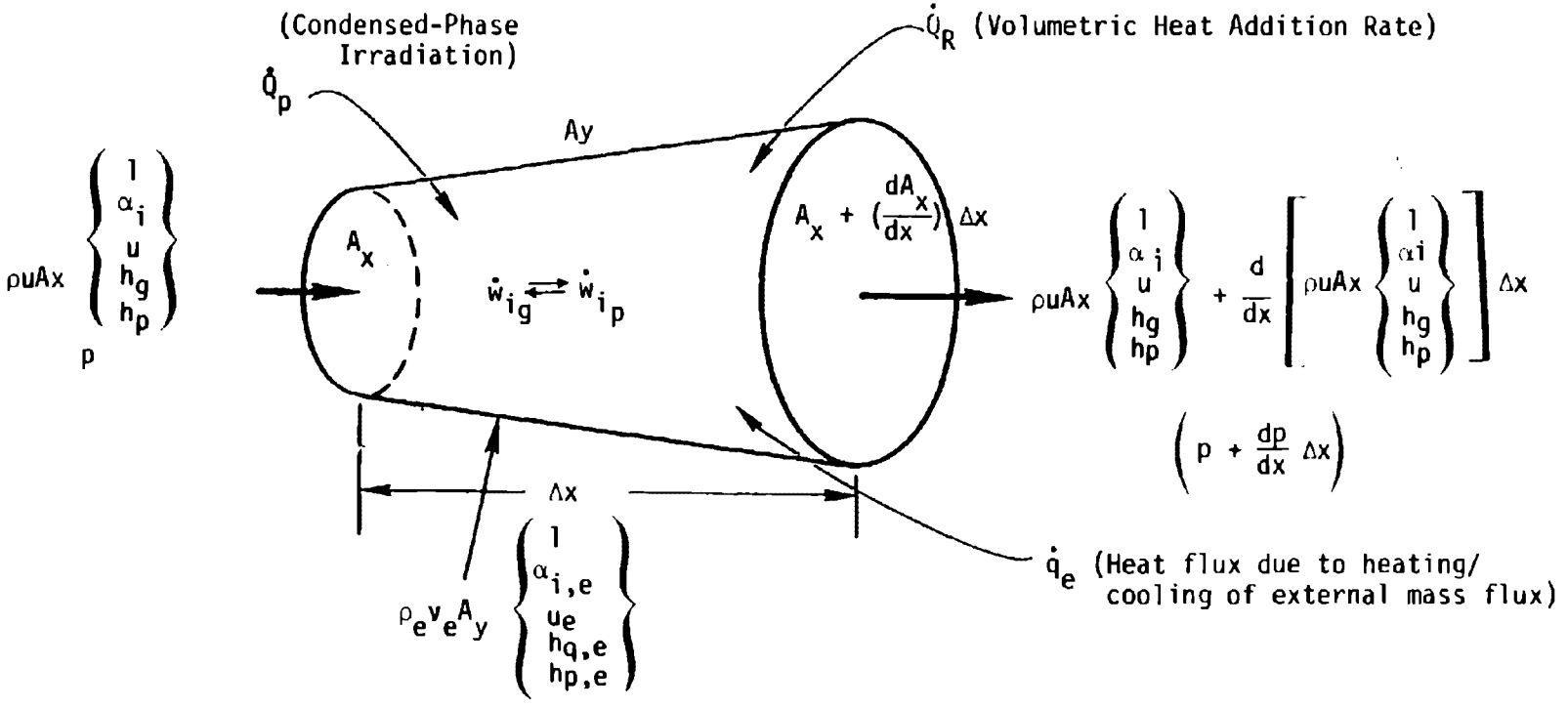

Figure 1. Heat and Mass Fluxes Balancing in a Control Volume (Flow Reactor).

Momentum Conservation Equation (Dynamic Equilibrium)

$$\rho u \frac{du}{dx} = \frac{\dot{m}}{A_x \Delta x} (u_e - u) - c_3 \frac{dp}{dx} \tag{2-3}$$

Gas-Phase Energy Conservation Equation

$$\rho u C_{pg} \frac{dT_g}{dx} = \frac{\dot{m}_e}{A_x \Delta x} \left(h_{g,e} - \sum_g h_i \alpha_{i,e} \right) - \sum_g h_i(Tg)\, \dot{w}_i - \sum_p h_i(T_p)\, \dot{w}_i + \dot{Q}_R + \left(\frac{\dot{q}_e}{\Delta V} + c_1 u \frac{dp}{dx} \right) \quad \left(\frac{cal}{cc\text{-}sec} \right) \tag{2-4}$$

Solid-Phase Energy Conservation Equation

$$\rho u C_{pp} \frac{dT_p}{dx} = \frac{\dot{m}_e}{A_x \Delta x} \left(h_{p,e} - \sum_p h_i \alpha_{i,e} \right) + \dot{Q}_p \quad \left(\frac{cal}{cc\text{-}sec} \right) \tag{2-5}$$

Equation of State

$$\rho = \frac{P M_g}{R T_g}$$

or in differential form

$$d\rho = \frac{\rho}{p} dp - \frac{\rho}{T_g} dT_g - \rho M_g \sum_g d\alpha_i \tag{2-6}$$

Auxiliary Species Conservation Equation

$$\sum_{p+g} M_i \alpha_i = 1.0$$

or in differential form

$$d\alpha_R = \frac{1}{M_R} \sum_{i \neq R} M_i d\alpha_i \tag{2-7}$$

where c_1 and c_3 are conversion factors, M_i is molecular weight of ith species and the subscript "R" refers to a reference species (usually N_2). Furthermore, it is assumed that the condensed and gaseous phases are in dynamic equilibrium (i.e., $u_g = u_p = u$) except in well-stirred reaction. However, the condensed and gaseous phases are not necessarily in thermal equilibrium ($T_g \neq T_p$), since the heat transfer mechanism (radiation) for the solid phase in particle applications is very much different from the mechanism for the gaseous phase.

Depending on the problem at hand, the set of ordinary differential equations can be solved in several ways:

- If the pressure or pressure gradient and the cross-sectional area distribution, A_x, along the reactor or streamtube are known, Eqs. (2-2), (2-4), (2-5), (2-6), and (2-7) are integrated simultaneously to solve for α_i, T_g, T_p, and , while Eq. (2-3) is integrated individually for u.
- If the cross-sectional area distribution, A_x, and the main convective velocity distribution, u, are given, Eqs. (2-2), (2-4), (2-5), (2-6), and (2-7) are integrated simultaneously to solve for α_i, T_g, T_p, and ρ while Eq. (2-3) is used to solve for p.
- If the pressure or pressure gradient and the convective velocity, u, are specified, Eqs. (2-2), (2-4), (2-5), (2-6), and (2-7) are solved simultaneously for α_i, T_g, T_p, and ρ, while Eq. (2-1) is integrated for A_x.
- If the main convective velocity, u, is set to unity, and the pressure or pressure gradient of the reactor is known (i.e., eliminating the momentum equation), the remaining set of equations can be used to describe time-dependent problems with the x-direction considered the time domain ($t = x/u$). Furthermore, this set of equations can be used to solve zero-dimensional problems with asymptotic solutions via a time-dependent iterative method. For example, well-stirred reactor simulation requires a zero-dimensional asymptotic solution.

In summary, Eqs. (2-2), (2-4), (2-5), (2-6), and (2-7), which are to be integrated simultaneously, can be rewritten in the following general form:

$$C_i \frac{dF_i}{dx} = A_i F_i + \dot{Q}_i + R_i \qquad (2\text{-}8)$$

where $F_i = \alpha_i$, T_g, T_p, and . The coefficient functions C_i, A_i, $\dot{Q}_i$ and R_i are listed in Table 1.

Table 1. Definition of C_i, A_i, $\dot{Q}_i$ and R_i for Eqn. (2-8)

F_i	C_i	A_i	$\dot{Q}_i$	R_i
α_i	ρu	$\frac{m_e}{A_x \Delta x}$	$\dot{w}_i$	$\frac{\dot{m}_e}{A_x \Delta x} \alpha_{i,e}$
Tg	$\rho u C_{pg}$	--	$-\sum_{p+g} h_i \dot{w}_i + \dot{Q}_R$	$\frac{\dot{m}_e}{A_x \Delta x}\left(h_{g,e} - \sum_{g} h_i \alpha_{ie}\right)$ $+ \frac{\dot{q}_e}{\Delta V} + c_1 u \frac{dp}{dx}$
T_p	$\rho u C_{pp}$	--	$\dot{Q}_p$	$\frac{\dot{m}_e}{A_x \Delta x}\left(h_{p,e} - \sum_{p} h_i \alpha_{i,e}\right)$
ρ	1.0		$-\frac{\rho}{T}\frac{dT}{dx} - \rho M_g \sum_{g} \frac{d\alpha_i}{dx}$	$\frac{\rho}{p}\frac{dp}{dx}$
α_R	1.0	--	$\frac{1}{M_R}\sum_{i \neq R} M_i \frac{d\alpha_i}{dx}$	--

Note: $c_1 = 0.0242$

$c_3 = 1.01325 \times 10^{+6}$

3.0 CHEMICAL REACTIONS AND THERMOCHEMICAL PROPERTIES

3.1 Chemical Reaction Rate Equations

In general form, the Kth chemical reaction can be written as:

$$\sum_i N_{i,K} Z_i \rightleftharpoons \sum_i N'_{i,K} Z_i \tag{3-1}$$

where $N_{i,K}$ and $N'_{i,K}$ are integers representing the stoichiometric coefficients of the ith species in the Kth reaction. Prime denotes products and no prime denotes reactants. Z_i is the chemical symbol (or species name) of the ith species. The net production rate (in forward direction) of the ith species in the Kth reaction is given by:

$$\dot{w}_{i,K} = (N'_{i,K} - N_{i,K}) \left[K_{f,K} \rho^{\sum_j N_{f,K}} \prod_i \alpha_j^{N_{i,j}} - \frac{K_{f,K}}{K_{e,K}} \rho^{\sum_j N'_{j,K}} \prod_i \alpha_j^{N_{i,j}} \right] E_K \tag{3-2}$$

where the forward reaction rate has Arrhenius form. The equilibrium constant, $K_{e,K}$, is calculated by:

$$K_{e,K} = \exp\left(\frac{-\Delta G_K}{RT}\right) (RT)^{-\sum_i \left(N'_{i,K} - N_{i,K}\right)} \tag{3-3}$$

where ΔG_K is net production of Gibbs free energy and is defined as:

$$\Delta G_K = \sum_i N'_{i,K} G'_i - \sum_i N_{i,K} G_i \quad . \tag{3-4}$$

The term E_K in Eq. (3-2) is the modification of reaction rate due to a third body and is defined as:

$$E_K = \begin{cases} \sum E_{K,i} \alpha_i & \text{for three body reactions} \\ = 1 & \text{for all others} \end{cases} \tag{3-5}$$

where $E_{K,i}$ is the third body efficiency of the ith species in the Kth reaction.

The overall production rate of the ith species is the sum of $\dot{w}_{i,K}$ over all K; i.e.,

$$\dot{W}_i = \sum_K \dot{W}_{i,K} \qquad (3\text{-}6)$$

3.2 Thermochemical Data

The thermochemical properties (specific heat, enthalpy and Gibbs free energy) for each species are taken directly from JANAF Thermochemical Table (Ref. 8) in tabular form as a function of temperature. Linear interpolation is used to compute the properties at local temperature.

4.0 HEAT TRANSFER

4.1 Gas Radiation

The major radiating species in a hydrogen flame is water vapor. For a hydrocarbon flame, carbon dioxide and carbon monoxide are also among major radiating species. For the optically this limit (photon mean free path is much greater than the characteristic dimension of the flame) the Planck mean absorptance coefficient of species i can be obtained from gas emittance data (Ref. 1); i.e.,

$$K_{pi} = \tfrac{1}{3}\left(\frac{\epsilon_{gi}}{L}\right)_{L \to 0}$$

where L is the characteristic dimension of the flame and ϵ_{gi} is the emittance of the ith species. The values of K_{pi} for H_2O, CO_2, and CO were calculated by Kelly and Kendall (Ref. 2) based on emittance data of Edwards and Balakrishnan (Ref.3). The Planck mean absorptance for a mixture can be estimated by:

$$K_p = \sum_i P_i K_{pi}$$

where P_i is partial pressure of the ith radiating species.

The volumetric radiative heat transfer term, $\dot{Q}_R$, in governing equation can be expressed as

$$\dot{Q}_R = -4K_p\sigma(T_g^4 - T_w^4) \qquad \frac{cal}{cm^3\text{-}sec}$$

The second term represents the radiation back from the environment (or reactor wall) having temperature T_w. σ is the Boltzmann constant.

4.2 Particle Radiative and Convective Heat Transfer

Two major modes of particle energy exchange are considered here:

- Particle and reactor wall radiative energy exchange.
- Particle and surrounding gas convective energy exchange.

Generally, the radiative energy exchange between the surrounding gas and particle is small and neglected since the surrounding gas is optically thin. Interparticle radiative exchange is usually unimportant unless the particle loading ratio is

very high. Treatment of interparticle radiation is beyond the scope of this report.

The radiative energy exchange between a reactor wall and a spherical particle surface can be expressed by:

$$\dot{q}_{Rp} = \pi d_p \varepsilon\sigma\left(T_w^4 - T_p^4\right) \quad \left(\frac{cal}{sec}\right) \tag{4-1}$$

where dp is diameter of particle in cm and ε is particle emittance.

The convective heat transfer to the particle is:

$$\dot{q}_{pg} = \pi d_p^2 h_c \left(T_g - Tp\right) \quad \left(\frac{cal}{sec}\right) \tag{4-2}$$

where h_c is convective heat transfer coefficient defined as

$$h_c = \frac{Nu\ \lambda_g}{d_p} \qquad \frac{cal}{sec\text{-}cm^3\text{-}^oK}$$

where λ_g is thermal conductivity of the surrounding gas and Nu is the Nusselt number. For a rigid spherical particle in completely quiescent surroundings or when dynamic equilibrium between the particle and the ambient fluid prevails, the Nusselt number can be shown to equal two. If particle number density is defined as the number of particles per unit volume, it can be shown that

$$n_p = \frac{6\rho_p}{\rho_s \pi d_p^3} \qquad \left(\#/cm^3\right) \tag{4-3}$$

where ρ_s is particle material density and ρ_p is mass of condensed phase per volume. Then, the total particle surface area can be calculated by:

$$n_p \times \pi d_p^2 = \frac{6\rho_p}{\rho_s d_p} \tag{4-4}$$

and the total radiative heat transfer per unit volume can be expressed by:

$$\dot{Q}_{Rp} = n_p \dot{q}_{Rp} = \frac{6\rho_p}{\rho_s d_p} \varepsilon\sigma\left(T_w^4 - T_p^4\right) \quad \left(\frac{cal}{cm^3\text{-}sec}\right) \tag{4-5}$$

Similarly, the total convective heat transfer per unit volume is

$$Q_{pg} = n_p q_{pg} = \frac{12\rho_p \lambda_g}{\rho_s d_p^2} (T_g - T_p) \qquad \left(\frac{cal}{cm^3\text{-}sec}\right) \tag{4-6}$$

The overall particle heat transfer is the sum of the convective and radiative components; i.e.,

$$\dot{Q}_p = \dot{Q}_{Rp} + \dot{Q}_{pg} \tag{4-7}$$

This allows calculation of the last term in Eq. (2-5).

For a coal particle undergoing devolatilization or combustion, the material density varies with time. If the fact that the coal particle might swell is ignored and it is assumed that the particle maintains the same size throughout the process, the instantaneous particle material density for a monosize system can be estimated by:

$$\rho_s = \frac{6\rho Y_p}{n_p \pi d_p^3} \tag{4-8}$$

where Y_p is the total mass fraction of particle phase. Ash is used as a tracer. If we further assume that the ash content in a coal particle stays constant during the process, the particle number density can be estimated from the ash content of the system; i.e.,

$$n_p = \frac{\text{Instantaneous Ash Content/Volume}}{\text{Initial Ash Content/Particle}} = \frac{6\rho\, Y_{ash}}{\pi d_p^3\, \rho_s^o\, Y_{ash}^o} \tag{4-9}$$

where Y_{ash} and Y^o_{ash} are the instantaneous and initial ash mass fractions in the coal particle, respectively. ρ_s^o is the initial particle material density of coal. Thus, from Eq. (4-8) and Eq. (4-9), the instantaneous material density can be found from:

$$\rho_s = \rho_s^o \left(\frac{Y^o_{ash}\, Y_p}{Y_{ash}}\right) \tag{4-10}$$

5.0 WELL-STIRRED REACTOR

A well-stirred reactor, also referred to as a perfectly stirred reactor, is an idealized reactor consisting of a reaction chamber, and inlet for the entry of premixed reactants and an outlet for the withdrawal of products at such a rate as to maintain steady overall mass flow through the reactor. Theoretically, a well-stirred reactor will provide an infinite mixing rate which allows the reaction to be purely chemically controlled without physical mixing limitation. Thus, the contents of the reactor are chemically and thermodynamically homogeneous throughout the reactor and are the same as those of the products leaving the reactor.

Mathematically, simulation of a well-stirred reactor is a zero-dimensional kinetic problem with a steady solution. The key parameters are reactor residence time and reactor inlet conditions. As was discussed briefly in previous sections, if u = 1.0, the set of governing equations described in Section 2 can be applied for time-dependent problems with the x-direction considered the time domain. For example, Eq. (2-2) becomes:

$$\frac{d\alpha_i}{dt} = \frac{\dot{m}_e}{\rho A_x \Delta x}\left(\alpha_{i,e} - \alpha_i\right) + \frac{\dot{w}_i}{\rho} \qquad (5\text{-}1)$$

Asymptotically $\left(\text{i.e. } \frac{d}{dt} \to 0\right)$, Eqn. (5.1) becomes:

$$\frac{1}{\tau}\left(\alpha_i - \alpha_{i,e}\right) = \frac{\dot{w}_i}{\rho} \qquad (5\text{-}2)$$

This is the steady state well-stirred reactor equation, where $\alpha_{i,e}$ is input species distribution, α_i is exit species distribution and $\dot{w}_i$ is instantaneous chemical production rate. $\tau = \frac{\rho A_x \Delta x}{\dot{m}_e}$ is defined as the residence time of a well-stirred reactor, since $A_x \Delta x$ is reactor volume, and $\dot{m}_e/\rho$ is volumetric flow rate. The residence time is defined as:

$$\tau = \frac{\text{Volume}}{\text{Volume Flow Rate}} \ .$$

In summary, we can apply the set of equations described in Section 2 to a well-stirred reactor based on the following conditions:

- Letting $\frac{\rho A_x \Delta x}{\dot{m}_e}$ be the residence time of the well-stirred reactor.
- Eliminating Eq. (2-3) by setting U = 1.0 and dp/dx = 0.0.

- Integrating time-dependent equations, Eqs. (2-2), (2-4), (2-5), (2-6) and (2-7), until a steady solution is achieved.

Practically, a well-stirred reactor model can be used to simulate a flame holder, multiburner or recirculation zone in a furnace.

6.0 NUMERICAL METHOD OF SOLUTION

Since the system involves fast finite-rate chemistry, the governing differential equations to be integrated are numerically stiff. The implicit finite difference technique is considered to be the most effective numerical method. The implicit finite difference scheme for the governing ordinary differential equation, Eq. (2-8), is expressed as follows:

$$\frac{C_i}{\Delta x}\left[F_i^{n+1} - F_i^{n}\right] = A_i F_i^{n+1} + \dot{Q}_i^{n} + \sum_j \left(\frac{\partial \dot{Q}}{\partial F_j}\right)^{n}\left(F_j^{n+1} - F_j^{n}\right) + R_i^{n} \quad (6\text{-}1)$$

where nonlinear terms in Q_i are linearized via Taylor series expansion and are truncated after the first order term. Rearranging the above equation gives:

$$\left[\left(\frac{\partial \dot{Q}_i}{\partial \alpha_i}\right)^{n} + A_i - \frac{C_i}{\Delta x}\right] F_i^{n+1} + \sum_{j \neq i}\left(\frac{\partial \dot{Q}}{\partial F_j}\right)^{n} F_j^{n+1}$$

$$= \sum_{\text{all } j}\left(\frac{\partial \dot{Q}_i}{\partial F_j}\right)^{n} F_j^{n} - \left(\frac{C_i}{\Delta x} F_i^{n} + \dot{Q}_i^{n} + R_i^{n}\right) \quad (6\text{-}2)$$

All terms on the right hand side of the equation are either known or can be evaluated at x^n station. Mathematically, Eq. (6-2) is a set of simultaneous linear algebraic equations. A Gauss-Jordan reduction algorithm (Ref. 4) with diagonal pivot strategy is used to solve these equations for all F_i simultaneously at x^{n+1} ($= x^n + \Delta x$) station.

This numerical procedure is basically noniterative. Therefore, the truncation error due to the linearization of nonlinear terms has to be carefully controlled. The error controlling strategy used is to control the error via the integration step size, Δx, since the finite difference equations asymptotically approach the ordinary differential equation they represent when $\Delta x \to 0$. The method used here is to limit the step size so that no component of solution may vary by more than a small percentage (ε_1) of its value at the last step; i.e.,

$$\Delta_{max} \equiv \max_i \left| \frac{F_i^{n+1} - F_i^{n}}{F_i^{n}} \right| \leq \varepsilon_1 \quad (6\text{-}3)$$

If this criterion was violated, the current numerical integration step would be

repeated, cutting the step size in half. The integration procedure would be repeated, continuing to halve the integration step size until criterion (6-3) was satisfied by all solution components. A lower limit (ε_2) is also set for Δ_{max}. If Δ_{max} was less than $\varepsilon_2 (< \varepsilon_1)$, the step size would be doubled for the next integration step. Based on our extensive numerical experience, ε_2 = 2 percent, and ε_1 = 5 percent are good criteria for steady-state or time-dependent problems. For the class of problems in which only asymptotic solutions are of interest, these criteria can be increased as long as solutions remain stable. For this class of problem, the computation will stop when time-wise change of all variables becomes very small; i.e.,

$$\Delta_{max} \left(\frac{u}{\Delta x} \right) < \varepsilon_3$$

where ε_3 is a small number to be input to the program externally. The value of ε_3 varies with the type of problems. For instance, ε_3 = 0.0001 gives sufficiently accurate solutions for well-stirred reactor simulations.

The computer program has been coded for CDC 7600 computer using Fortran IV language. Input to the computer program is presented in the appendix at the end of Part 5.

7.0 APPLICATIONS

The computer model can operate in the following three modes:

- Plug-flow reactor (gas-phase or two-phase)
- Well-stirred reactor (gas-phase or two-phase)
- Well-stirred reactor followed by plug-flow reactor (gas-phase only)

For illustrative purposes, here we present two sample computations:

- A gas-phase well-stirred reactor followed by an isothermal plug-flow reactor for gas-phase fuel nitrogen study
- A coal well-stirred reactor simulating the KVB coal stirred reactor (Ref. 5). Computational results are compared to experimental data.

Details of the computations are described in the following sections.

7.1 Gas-Phase Fuel Nitrogen Conversion Simulation

Conversion of fuel nitrogen in fuel-rich environments has been one of the most interesting topics in current NO_x control research. As the first example calculation, the computer model is used to predict fuel nitrogen (HCN) conversion in a fuel-rich CH_4 flame under controlled conditions (i.e., constant temperature and equivalence ratio). The reactor is an isothermal gas-phase, 10-ms, well-stirred reactor (as flame holder) followed by an isothermal plug-flow reactor. The methane is doped with 0.5 percent (by volume) HCN. Computations are made at three different reactor temperature levels and five reactor equivalence ratios:

$T = 1850^{\circ}K$, $1950^{\circ}K$, and $2050^{\circ}K$

$\phi = 1.3$, 1.5, 1.7, 1.9, and 2.1

The calculated results are plotted in Figure 2. Figure 2 shows percentage conversion of HCN to total fixed nitrogen (TFN - [NO + NH_3 + HCN]) at two different PFR exits (300 ms and 500 ms). It is noted that the minima in TFN are observed under very rich conditions and the minima are enhanced by increasing temperature.

Figure 3 shows HCN and O concentrations versus PFR time for two typical calculations; i.e.,

- $\phi = 1.7$ and $T = 1850^{\circ}K$
- $\phi = 1.9$ and $T = 1950^{\circ}K$

As can be seen in Figure 3, the HCN concentrations for both cases decay very

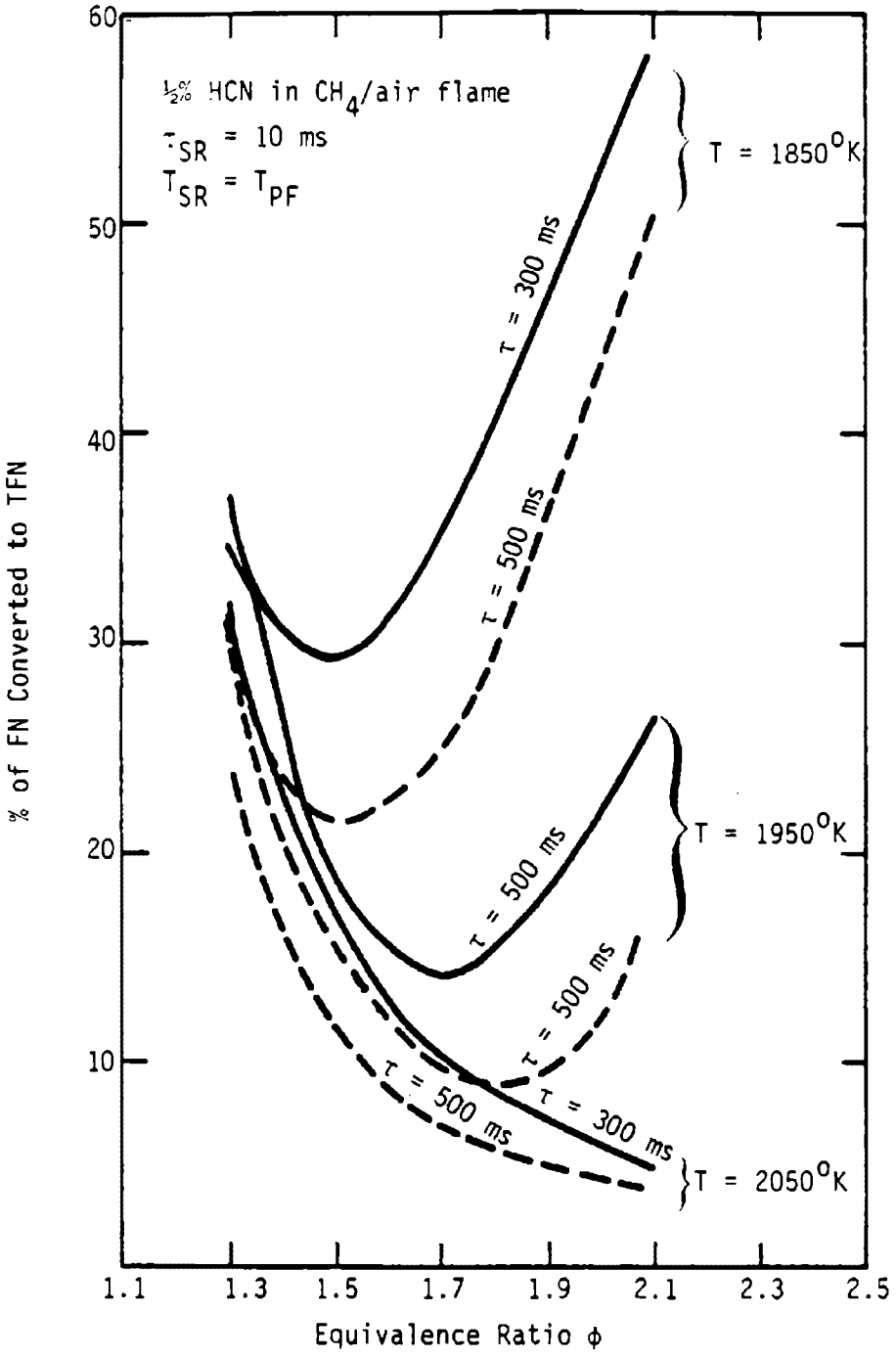

Figure 2. Percentage Fuel-N Conversion for a Premixed CH_4/air Flame at τ = 300 ms and 500 ms

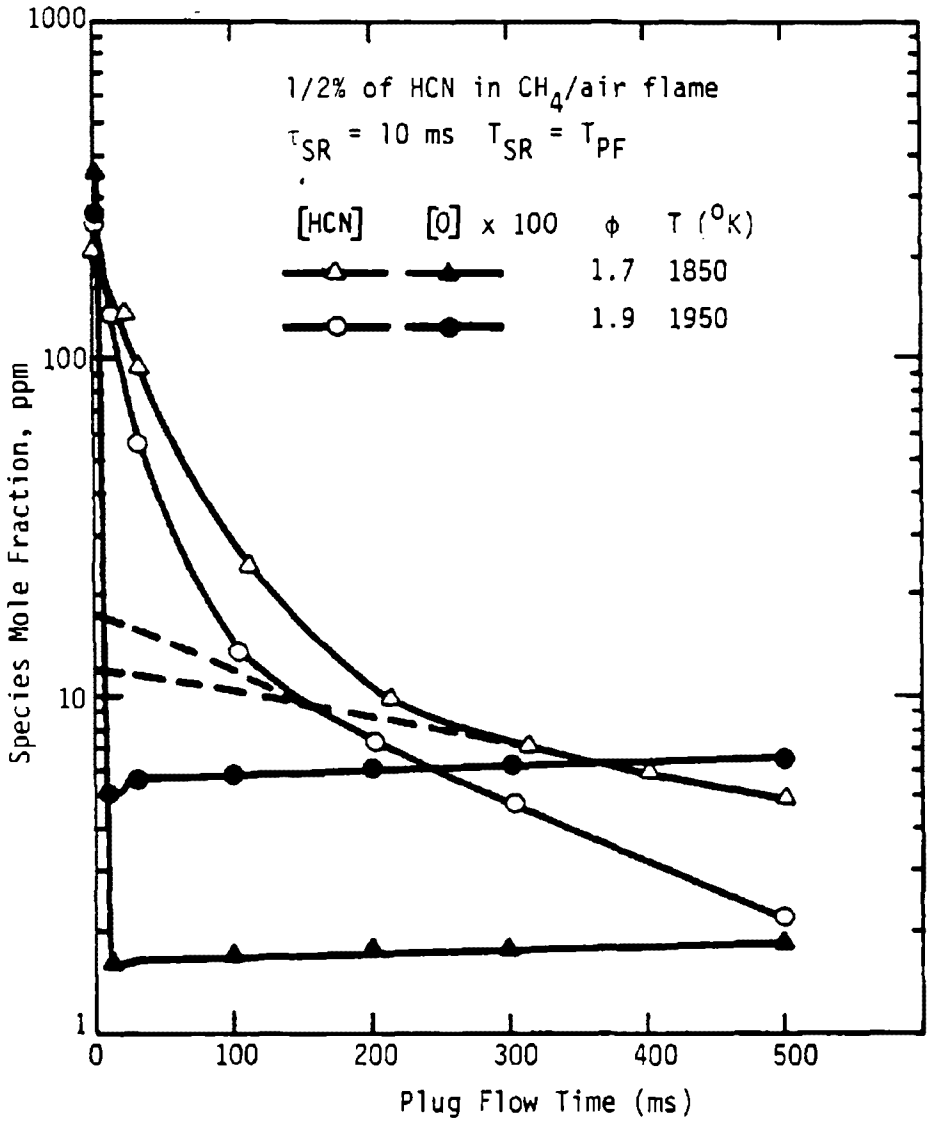

Figure 3. HCN and O Concentration in a Premixed CH_4/air Flame as a Function of Time.

rapidly in the early stages (near t = 0) and decay linearly at a later stage (t = 300-500 ms).

For the case $\phi = 1.7$ and $T = 1850^{\circ}K$, reaction rates have been screened. The screening result shows that the controlling reaction for HCN destruction in the early stage is the reverse-Zeldovich reaction; i.e.,

$$N + NO \rightarrow N_2 + O \qquad (96)$$

This reaction is responsible for about 67.2 percent of N_2 production. The net HCN destruction rate, from the screening result, at the same stage is approximately an order of magnitude greater than the N_2 production rate. Thus it can be concluded that reaction (96) is controlling and is second order. In a later stage (t = 500 ms), the HCN destruction rate is approximately one order of magnitude less than the N_2 production rate. According to the screening result, the reaction:

$$HCN + O \rightarrow CH + NO \qquad (116)$$

is responsible for 66.7 percent of HCN destruction; thus, it can also be concluded that this reaction is controlling at this stage. Reaction (116) is virtually first order since the level of O-atom is practically constant at later stages of plug flow as can be seen in Figure 3.

It is of interest to note that the conclusions derived above are qualitatively in agreement with findings of the experimental investigation recently conducted in Exxon Research and Engineering Company by Song et al. (Ref. 7).

7.2 Coal Well-Stirred Reactor

The devolatilization of coal can be considered a first-order chemical reaction (Kobayashi, et al., Ref. 7):

$$\frac{dm_i}{dt} = K_i \left(m_i - m_{i,\infty}\right) \qquad (7\text{-}1)$$

where m_i is the mass of ith component (or functional group) of coal and $m_{i,\infty}$ is the asymptotic yield of the component. The devolatilization rate constant K_i is found by the Arrhenius equation ($K_i = A_i \exp(^{-E}i/RT)$. If it is further assumed that the coal particle temperature is constant during devolatilization in a well-stirred reactor, the asymptotic yield can be considered constant. Integrating Eq. (7-1)

gives:

$$\frac{m_{i,\infty} - m_i}{m_{i,\infty}} = e^{-k_i t} \tag{7-2}$$

Thus the time rate of devolatilization can be obtained by differentiating the above equation:

$$\frac{d}{dt}\left(\frac{m_i}{m_{i,\infty}}\right) = K_i e^{-k_i t} \qquad \left(\frac{1}{sec}\right) \tag{7-3}$$

Due to the lack of experimental information on coal particle exit age distribution, an analytical exit age distribution is assumed (Ref. 9). For a reactor having mean residence time τ_{SR}, the age distribution is:

$$E(t) = \frac{1}{\tau_{SR}} e^{-t/\tau_{SR}}$$

E(t) dt is the mass fraction of coal at reactor exit having age between t and t+dt. Using this analytical age distribution expression, we can calculate the rate of devolatilization of the ith functional group as:

$$\dot{R}_i = \int_0^\infty \frac{1}{\tau_{SR}} e^{-t/\tau_{SR}} \cdot K_i e^{-K_i t} \, dt$$

$$= \frac{K_i}{K_i \tau_{SR} + 1} \qquad \left(\frac{1}{sec}\right) \tag{7-4}$$

The coal stirred reactor model is then used to simulate KVB's experiment (Ref. 5). KVB's well-stirred reactor fired pulverized Wyoming subbituminous coal. The mean particle size was approximately 50 μm and the reactor temperature reported was 1511°K. The mean reactor residence time varied from 10 ms to 50 ms. The reactor's exit NO and oxygen concentrations were measured. The computed results of the coal reactor model are plotted against KVB's measurements in Figures 4 and 5. Figure 4 shows predicted and measured NO concentrations versus mean stirred reactor residence time τ_{SR} for several overall equivalence ratios (i.e., ϕ = 2.63, 1.25, and 1.05). Figure 5 shows predicted and measured reactor exit oxygen concentrations versus mean reactor residence time. The volatile devolatilization model and gas-phase kinetics used in these calculations are taken from Part 2 of

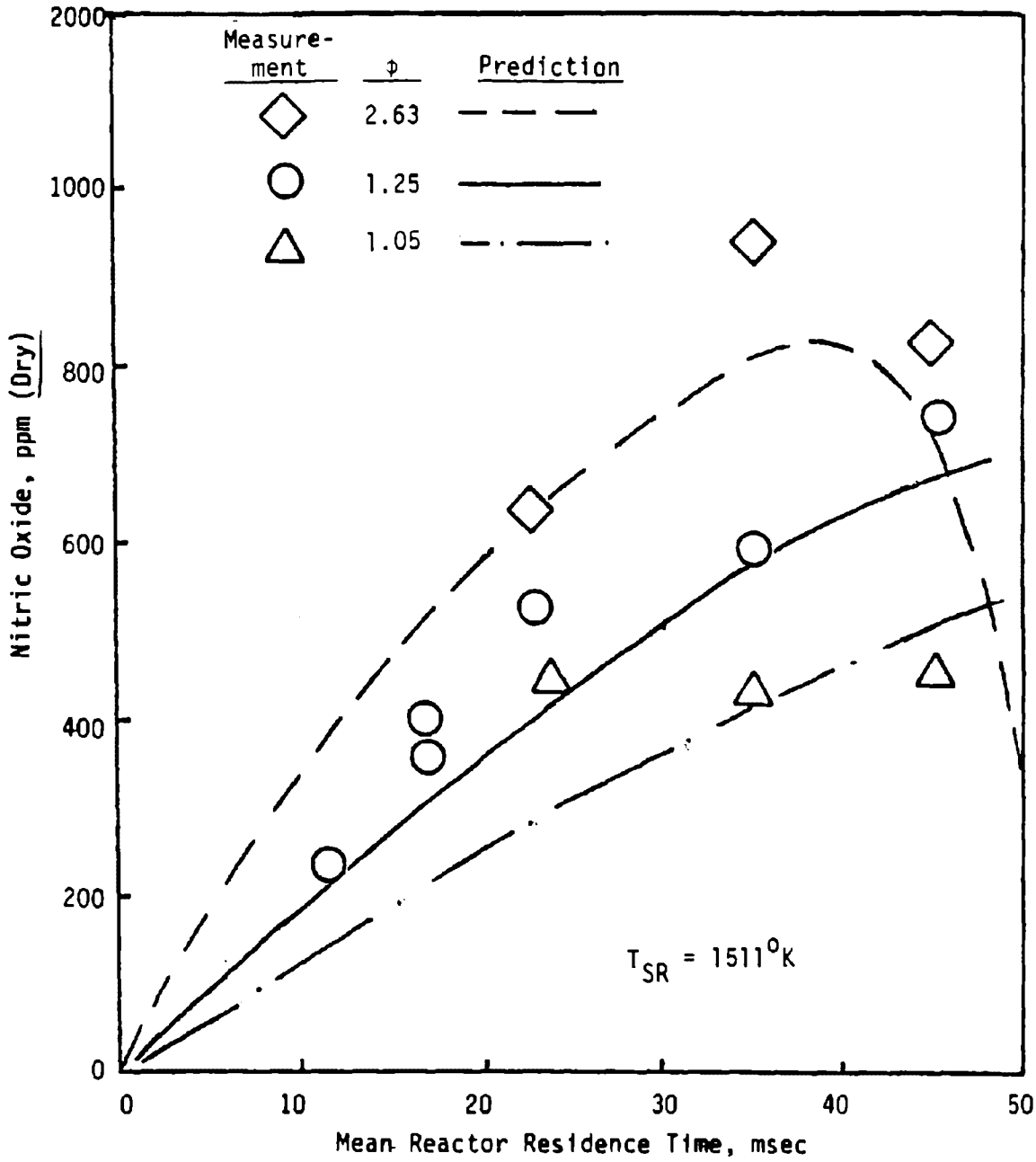

Figure 4. Comparisons of Predicted NO Concentration Against Measurement (Wyoming Subbituminous).

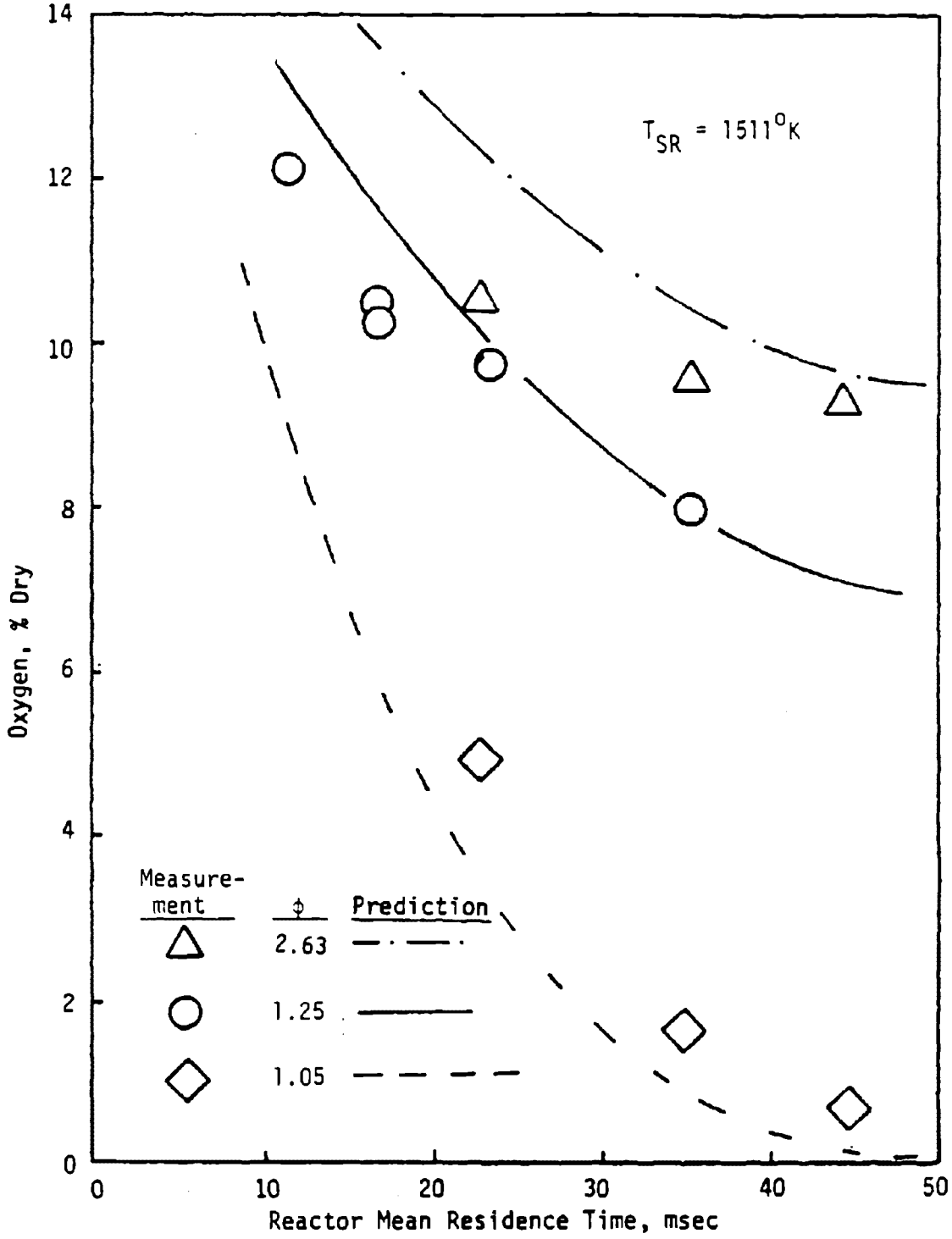

Figure 5. Comparisons of Predicted Exit Oxygen Concentration Against Measurements (Wyoming Subbituminous).

this report. The fundamental reaction rates for char oxidation and char gasification (for 50 μm particles) used in these computations are:

Oxidation

$C(s) + O_2 \rightarrow CO_2^*$ $\quad K_f = 1.08 \times 10^{10} \exp(-20{,}000/RT)$

$CO_2^* + C(s) \rightarrow CO + CO$ $\quad K_f = 1.0 \times 10^{16}$

Gasification

$C(s) + H_2O \rightarrow CO + H_2$ $\quad K_f = 9.01 \times 10^{10} \exp(-30{,}000/RT)$

$C(s) + CO_2 \rightarrow CO + CO$ $\quad K_f = 6.44 \times 10^{11} \exp(-35{,}000/RT)$

8.0 REFERENCES

1. Sparrow, E. M. and Cess, R. D., Radiation Heat Transfer, Brook/Cole Publishing Company, Belmont, California, p. 218 (1970).

2. Kelly, J. T. and Kendall, R. M., "Further Development of the Premixed One-dimensional Flame (PROF) Code," EPA-600/7-78-172a (NTIS PB286243) (1978).

3. Edwards, D. K. and Balakrishnan, A., "Thermal Radiation by Combustion Gases," Int. J. Heat and Mass Transfer, Vol. 16, p. 221 (1973).

4. McCracken, D. W. and Dorn, W. S., "Numerical Methods and Fortran Programming," Wiley, New York (1964).

5. Muzio, L. J., Maloney K. L., and Shiomoto G. H., "Nitric Oxide Formation in a Pulverized Coal Fired Jet-Stirred Reactor," presented at Coal Combustion Technology and Emission Control, CIT, Feb. (1979).

6. Kau, C. J. and Tyson, T. J., "Fundamental Combustion Research Applied to Pollution Control, Vol IV: Engineering Analysis, Part 2: Mathematical Modeling of Microscale Combustion of a Coal Particle." EERC Final Report, Contract No. 68-02-2631 (1987).

7. Song, Y. H., Blair, D. W., Siminski V. J., and Bartok, W., "Conversion of Fixed Nitrogen to N_2 in Rich Combustion," Eighteenth Symposium (International) on Combustion, The Combustion Institute, p. 53 (1981).

8. Stall, D. R. and Prophet, H., "JANAF Thermochemical Table--Second Edition," Dow Chemical Company (1970).

9. Field, M. A., Gill, D. W., Morgan, B. B., and Hawksley, P. G. W., "Combustion of Pulverized Coal," The British Coal Utilization Research Association, Leatherhead, p. 30 (1967).

APPENDIX

Program Input Data

The input data cards for One-Dimensional Flame Analysis Program are explained in this appendix. The input cards can be divided into the following groups:

I Title Card

II Namelist Cards ($INPUT)

The namelist cards are divided into the following sub-groups:

- General Input
- Well-Stirred Reactor Option
- Solid Phase Option
- Option to Specify Temperature Distribution
- Option to Specify Pressure Distribution
- Option to Specify Velocity Distribution
- Option to Specify area Distribution (Confined Flame)
- Screen Option
- Optional Table Input for External Flux
- Optional Automatic Air-Staging
- Option to Specify Oxidant/Fuel Ratio for external Flux
- Sensitivity Analysis
- Output Control
- Numerical Control

III Species Cards

IV Reaction Cards

V Namelist Cards ($COALRK)

The program is coded for CDC 7600 computer using FORTRAN IV language.

The following are the descriptions of input data for the One-Dimensional Flame Analysis Program.

I. TITLE CARD

Columns 1-70 are used for run ID

Columns 71-75 are used for continuation index which is a right justified integer indicating the number of files in the continuation tape.

II. NAMELIST ($INPUT)

The following parameters are general input.

Symbols	Descriptions	Default Value
KASE	Case No.	0
NS	Total number of species (Max. 52)	0
NR	Total number of reactions (Max. 200)	0
ICRU	Index for rate constant units	1
	= 0 molecule-cm-sec units	
	= 1 mole-cm-sec units	
ITIME	Maximum CPU time allowed for the run (sec)	
X	Current streamwise distance	-
XMAX	Maximum X to be integrated to	-
DXMAX	Maximum streamwise integration step size allowed	-
DXMIN	Minimum streamwise integration step size allowed	
DX	Initial streamwise step size	DXMIN
E3RDB(I,K)	Third body efficiency	1.0
	I = species index	
	K = reaction index	
T	Initial temperature (^{o}K)	-
U	Initial axial velocity (cm/sec)	-
ALPHA(I)	Initial species distribution (mole fraction)	-

Default

Symbols	Descriptions	Value
TKINET	Kinetic cut of temperature (^{o}K)	400
P	Current pressure (atm)	1.0
ITHEQM	= -1 constant temperature	0
	= 0 normal mode	
	= 1 thermal equilibrium between gas and solid phases	
IDRADG	≠ 0 if gas radiation is to be considered	0
	= 0 no gas radiation considered	
IDRADP	≠ 0 if solid phase is to be considered	0
	= 0 no solid phase radiation considered	
TWALL	Surrounding/wall temperature (^{o}K)	0
AREA	Initial stream-tube cross section (cm^2)	1.0
TAUSR	S.R. resident time (sec)	0
HSTATE	Enthalpy of external flux (cal/gm)	-
ALPHAF(I)	Species mole fraction distribution of external flux	-
TE	Temperature of external flux	-
VE	Cross-stream velocity of external flux	-

SOLID PHASE

For two-phase flow calculations the following parameters and variables have to be specified.

Symbols	Descriptions	Default Value
NSP	Number of solid species	0
NRP	Number of reactions including solid species	0
DIMTRP	Particle diameter (cm)	0.0
TP	Particle temperature (^{o}K)	0.0
RHOS	Current particle material density (gm/cm^3)	0.0
YSOLID	Solid phase mass fraction	0.0
RHOSO	Initial solid materials density (gm/cm^3)	0.0
YASH	Ash mass fraction in raw coal (as fired)	0.0
XNU	Particle Nusselt Number	2.0

Symbols	Descriptions	Value
YSOLDE	Solid mass fraction in external flux	0.0
ICOLSR	Coal S.R. Index	
	≠ 0 if run is coal S.R.	0
PHE	S.R. equivalence ratio (for coal S.R. only)	0
ICONPF	P.F.R. continued from S.R.	0
PHEF	P.R.F. equivalent ratio	0
IDCOAL	Coal ID	0
	= 0 not coal particle	
	= 1 bituminous	
	= 2 lignite	

Option to Specify Temperature Distribution

If the temperature of reactor is to be specified, the energy equation is by-passed. The following parameters for the T(X) table should be provided in $INPUT namelist.

Symbols	Descriptions	Default Value
NXTRTB	No. of entries for T(X) Table (Maximum 50)	0
XTRTB(I)	X Coordinate of T(X) table	-
TRTB(I)	Temperature (^{o}K) at XTRTB(I)	-

Option to Specify Pressure Distribution

If the pressure of reactor is to be specified, P(X) table has to be provided (under $INPUT) as follows:

Symbols	Descriptions	Default Value
NXPRTB	No. of entries for P(X) table (maximum 50)	0
XPRTB(I)	X Coordinate of P(X) table	-
PRPTB(2)	Pressure (ATM.) at XPRTB(2)	-
	Note: i) dp/dx will be calculated by simple differencing ii) If U(x) is constant, reactor area AREA will be calculated iii) If reactor area is defined (i.e., NXRWTB 0) U(x) will be calculated.	

Option to Specify Velocity

If reactor velocity is to be specified, U(x) table has to be provided (under $INPUT) as follows:

Symbols	Descriptions	Default Value
NXURTB	No. of entries for U(x) table (maximum 50)	0
XURTB(I)	X coordinate of U(x) table	-
URTB(I)	Velocity (cm/sec) at XURTB(I)	-

CONFINED FLAME (VARIABLE AREA)

For confined flame with variable area, stream function coordinate system must be used (i.e., IPSICD = 1). The following parameters defined the area:

Symbols	Descriptions	Default Value
NSRWTB	Number of entries for area specifying table (maximum 50)	0
XRWTB(I)	x coordinate of area table (cm)	
RWALTB(I)	r coordinate of the wall(cm)	

SCREEN

Screen option gives the reaction number and its percentage contribution (integrated over r at constant x) of production/destruction, of up to five most active reactions, for each specified species.

Symbols	Descriptions	Default Value
NSPSCN	Number of species to be screened (maximum 10)	0
ISPSCN(I)	Index of the species to be screened	0

TABLE INPUT FOR EXTERNAL FLUX

Symbols	Descriptions	Default Value
NXETB	Number of entries in external flux table (maximum 30)	0
XETB(I)	Axial coordinate for external flux table	-
XMDETB(I)	Mass flux table (gm/sec-cm)	-
AETB(I)	Species mole fraction table	-
TETB(I)	Temperature table (^{o}K)	-
QDETB(I)	Heat flux tube (cal/gm)	-

OPTIONAL AUTOMATIC AIR-STAGING

Symbols	Descriptions	Default Value
IAUSTG	Automatic air-staging index	0
	≠ 0 if automatic air-staging (cm)	
XAUSTG	Duration of automatic air-staging (cm)	-
TAUSTG	Staged air temperature (^{o}K)	-

Note: If IAUSTG is not 0 program will set NXETB = 5 and automatically calculate external flux tables (e.g., XETB, SMDETB, AETB and TETB) based on above information and PHE/PHEF

SPECIFYING OXIDANT/FUEL RATIO FOR INFLUX

Symbols	Descriptions	Default Value
IOFRSP	o/F specification index	0
	≠ if o/F ratio is specified for influx	
ALPHAA(I)	Oxidant species distribution (same unit as ALPHA)	-
ALPHAF(2)	Fuel species distribution (same unit as ALPHA)	-

Symbols	Description	Default Value
YSOLIA	Solid mass fraction in oxidant	0.0
YSOLIF	Solid mass fraction in fuel	0.0
OFRE	o/F for influx (Mass)	0.0

OUTPUT CONTROL

The following parameters are output control parameters.

Symbols	Description	Default Value
NPRT	Number of print stations in X direction (max. 30)	0
XPRINT(I)	X coordinate for output (cm)	-
IOUT1	If $\neq$ 0 print net production rates for each species	0
IOUT2	If $\neq$ 0 print	0
IOUT3	If $\neq$ 0 print forward/backward rates of each reaction	0
IPUNCH	If $\neq$ 0 store the necessary variables in tape for continuation	
IMFCHK	Will print mass flux (integrated over r at fix x) if $\neq$ 0	0
IREWIN	Will rewind continuation tape before written if $\neq$ 0	0

NUMERICAL CONTROL

The following variables are designed to gain some internal control of the accuracy of the numerical calculations.

Symbols	Description	Default Value
EPSIL	Maximum tolerable negative value (EPSIL) for species concentration which will be set to a	-1.0 E-9
EPSI	very small positive value (EPSI)	+1.0 E-16

Default

Symbols	Descriptions	Value
EPSTOP	Convergent criteria (^{o}K/ms) for time-dependent calculation	1.0
EPSIPC	Minimum solid mass fraction to be considered	1.0 E-6
DELLO	Lower limit for step size control	0.02
DELUP	Upper limit for step size control	0.05
MINNER	Maximum number of inner iterations allowed	1
NCOUPL	Number of coupling eqns.	NS+2

SPECIES CARDS

The following group of cards are the species name, molecular weight, heat of formation and parameters for laminar diffusion coefficients.

Card No.	Column	Description	Format
3.1	1-5	Name of the first species	A5
	6-10	Blank	5X
	11-20	Molecular weight	E10.3
	21-30	Heat of formation at 298.15^{o}K (kcal/mole)	E10.3
	31-40	Simplified diffusion parameter (bifurcation)	E10.3
	41-50	Stockmayer force constant ε_{o}/K (^{o}K)	E10.3
	51-60	Stockmayer force constant σ(A)	E10.3
	61-70	Stockmayer for constant δ (dimensionless)	E10.3
	71-80	Polarizability α (10^{25} cm^{2})	E10.3
3.2	1-5	Name of second species	A5

REACTION CARDS

The chemical reaction mechanism for a particular problem is input on the last set of cards, one card for each reaction. No particular order is required. The forward reaction rate constant is expressed as AT^{-N} exp(-B/RT).

Ten possible reaction types included in the program are:

Reaction Type

(1) $A + B \leftrightarrows C + D$

(2) $A + B + M \leftrightarrows C + M$

(3) $A + B \leftrightarrows C + D + E$

(4) $A + B \leftrightarrows C$

(5) $A + M \leftrightarrows C + D + M$

(6) $A + B \rightarrow C + D$

(7) $A + B + M \rightarrow C + M$

(8) $A + B \rightarrow C + D + E$

(9) $A + B \rightarrow C$

(10) $A + M \rightarrow C + D + M$

(11) $S^* + B \rightarrow C + D$ Surface reaction (soot)

(12) $A + B \xrightarrow{S^*} C + D$ Surface catalytic reaction (soot)

(13) $C^* + B \rightarrow C + D$ Surface reaction (char)

(14) $A + B \xrightarrow{C^*} D + D$ Surface catalytic reaction (char)

Card No.	Column	Description	Format
4.1	1-2	Stoichiometric coefficient of Species A	I2
	3-7	Species A	A5
	8	+ sign	
	9-10	Stoichiometric coefficient of Species B	I2
	11-15	Species B (or M)	A5
	16	+ sign	
	17-18	Stoichiometric coefficient of Species M (or 0)	I2
	19-23	Blank or M	A5
	24	= sign	
	25-26	Stoichiometric coefficient of Species C	I2
	27-31	Species C	A5
	32	+ sign (if needed)	
	33-34	Stoichiometric coefficient of Species D	I2
	35-39	Species D (or M)	A5
	40	+ sign (if needed)	

Card No.	Column	Description	Format
4.1	41-42	Stoichiometric coefficient of Species E	I2
	43-47	Species E (or M/blank)	A5
	49-50	Reaction type, 1 to 14	I2
	51	Blank	
	52-59	A, pre-exponential factor cm-mole-sec units	E8.2
	60-63	N, temperature exponent	F4.1
	64-72	B, activation energy kcal/mole	F9.1
	73-80	Comments	A8
4.2		Next reaction	

If IDCOAL ≠ 0, the namelist of $COALRK, which defined coal properties, has to be provided.

$COALRK

YC, YH, YO, YN, YS, YMOIST, YASH	Mass fraction of coal composition (C, H, O, N, S, moisture and ash) from ultimate analysis
HHVMMF	High heating value of coal (ash and mineral free) (cal/gm)
AEQ(I), ANEQ(I), EEQ(0)	Parameters for equilibrium constants which define asymptotic yield of devolatilization
ACD(I), ECD(I), ATAR, ETAR, AOLE, EOLE, AACE, EACE, ASSO, ESSO, ACH4, ECH4	Arrhenius parameters of devolatilization rate for Ith species, tar, olefins, acetylene, soot and methane
YLGTVO(I)	Mass fraction of light volatiles in coal

$END

PART 6

GENERATION OF ELLIPTIC-CODE TEST CASES

Prepared by:

C. J. Kau

and

T. J. Tyson

TABLE OF CONTENTS

LIST OF FIGURES

LIST OF TABLES

1.0 INTRODUCTION

The EPA's Fundamental Combustion Research (FCR) Program has undertaken a project to assess current capability to numerically solve the Navier-Stokes elliptic field equations, which govern a wide class of combustion behavior. The intent is to establish whether computational capability exists which could be used to develop low pollutant emission combustion systems. Numerical techniques which appear promising will be candidates for future development through FCR sponsorship.

The assessment focuses on the numerical capability of solving the differential equations, and not on the analysis of the physics and chemistry imbedded within the equations. To assess this capability, the values of all physical and chemical variables have been prescribed. The computational results will be compared with the solutions used to generate the test cases.

This section will describe how the first group of test cases are generated. The characteristics of the first group are:

- Non-Premixed Reactants
- Steady State
- One Atmosphere Nominal Pressure
- Simple Slow Chemistry
- Simple Flow Field Behavior
- Simple Diffusive Transport Model (Equivalent molecular diffusion with large "effective" coefficients).
- Boundary Conditions on Rectangular Coordinate Lines

The first group of test cases consists of 3 cases which are generated from the following two simple parabolic types of flow fields:

- Planar Opposed Jets of Fuel and Oxidizer
- Planar Co-Flowing Jets of Fuel and Oxidizer

For slow chemistry, carbon monoxide and pure oxygen are selected as the fuel and oxidizer. A simple three step reaction mechanism which includes only two carbon monoxide oxidation reactions and one oxygen dissociation step is assigned,

i.e.,

	Reaction	Rate (mole/cc-sec system)
(1)	$CO + O_2 \rightleftarrows CO_2 + O$	$k_{f1} = 6.905 \times 10^{7}\ T \exp(-34810/RT)$
(2)	$CO + O + M \rightleftarrows CO_2 + M$	$k_{f2} = 3.8 \times 10^{24}\ T^{-3} \exp(-6170/RT)$
(3)	$O + O + M \rightleftarrows O_2 + M$	$k_{f3} = 1.4 \times 10^{18}\ T^{-1} \exp(-340/RT)$

Rate constants for the above reactions are taken from EER's basic reaction set. Thermochemical properties for all four species (CO, O_2, CO_2 and O) are taken directly from JANAF Tables (Ref. 1). Turbulent eddy diffusivity and turbulent Prandtl and Lewis numbers are assumed to be constant. EER's General Flame Analysis Program (GFAP) (Ref. 2) is used for preliminary computations. The results obtained from these computations are then used to extract essential flow field parameters such as flame thickness, impingement plane displacement, etc. These parameters are then used to help define the boundary conditions analytically for the test cases.

Obtaining the exact Navier-Stokes solution for the opposed jet case is possible because the solution behavior is self-similar, leading to ordinary differential equations. After solving the equations, the solution is then skewed in the coordinate system to destroy the self-similarity, and diffusive fluxes are introduced in both coordinate directions. A problem posed in this manner is a true test of the computational capability of a Navier-Stokes code.

The second coflowing case is close to being exact. Its accuracy rests on the validity of the Prandtl boundary layer approximation for coflowing, slowly-varying mixing layers. Having generated a solution under this valid assumption, the solution is once again skewed in the coordinate system to provide a flame field where diffusive fluxes are of the same order in both coordinate directions. Although a problem posed in this fashion requires the full Navier-Stokes equations for solution, it is a considerably less severe test than the opposed jet case because of the lack of a strong upstream influence. With this type of problem it is felt that a calibration of computational capability can be obtained.

The details of this test-case generating process are described in the following sections.

2.0 OPPOSED-JET DIFFUSION FLAME

It is known that there are similitude solutions for opposed-jet flames. The self-similar solutions for temperature and species concentrations involve the similarity variable $\eta = r\sqrt{\frac{a}{\nu}}$ where a is the strain rate and ν is kinematic viscosity. Figure 1 is a schematic of an opposed-jet diffusion flame. Due to the density change caused by heat release, the impingement plane of the oxidizer jet shifts away from the plane of the fuel jet by a displacement δ . The impingement plane is an imaginary plane where the V component of potential flow goes to zero (by extrapolation).

The test case selected consists of a CO/O_2 flame with a fuel-side strain rate a_f = 30(1/sec). Prandtl and Lewis numbers both equal 0.9. The equivalent molecular viscosity, μ , equals 0.01 (gm/cm-sec). The similitude solution obtained from GFAP computations is plotted in Figures 2 through 4. Figure 2 shows the velocity profile of V versus r. The displacement δ , which is measured directly from Figure 2, is 2.29 cm. Figure 3 shows the temperature profile of the same flame. The flame thickness, t_f, measures the distance between points where temperature deviates by approximately $1^{\circ}K$ from the temperature of the unreacted jet. In this case, t_f = 6.5 cm. Figure 4 presents the species concentration distributions for O_2, CO, CO_2 and O.

The potential flow field on the fuel side is defined by:

$$V = -a_f y \tag{2-1a}$$

$$U = a_f x \tag{2-1b}$$

Thus, the displacement δ will help define the potential flow field on the oxygen side,

$$V = -a_o(y-\delta) \tag{2-2a}$$

$$U = a_o x \tag{2-2b}$$

where a_o is the oxidizer side strain rate and is related to the fuel-side strain rate by

$$a_o = a_f \sqrt{\frac{\rho_f}{\rho_o}} \tag{2-3}$$

since there is no pressure drop cross the flame (i.e. $\frac{\partial p}{\partial r} = 0$).
Due to the similarity of the solutions, the conditions

$$\frac{\partial}{\partial x}\left(\frac{U}{x}\right) = 0 \tag{2-4a}$$

$$\frac{\partial V}{\partial x} = 0 \tag{2-4b}$$

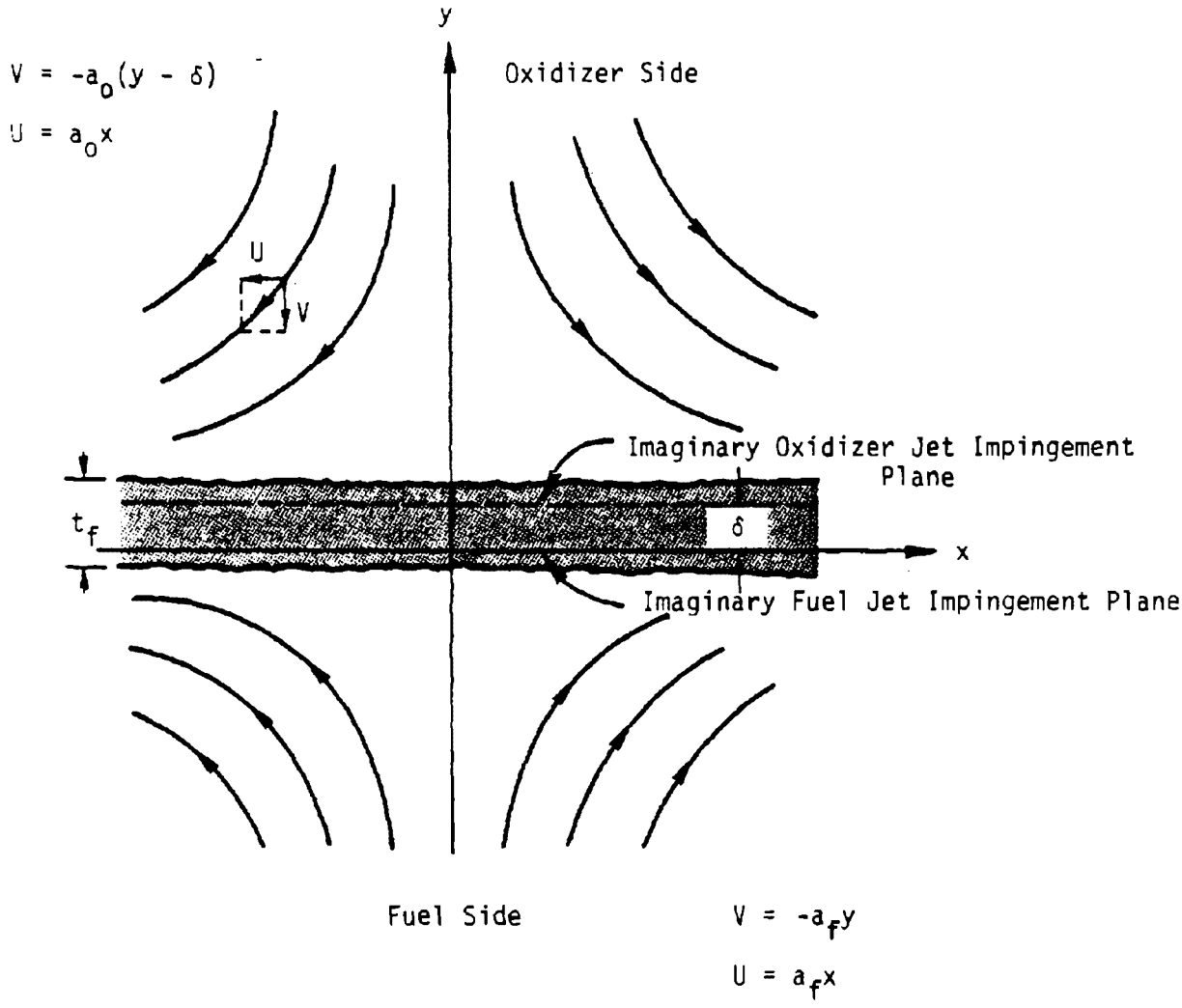

Figure 1. Schematic of Opposed-Jet Diffusion Flame.

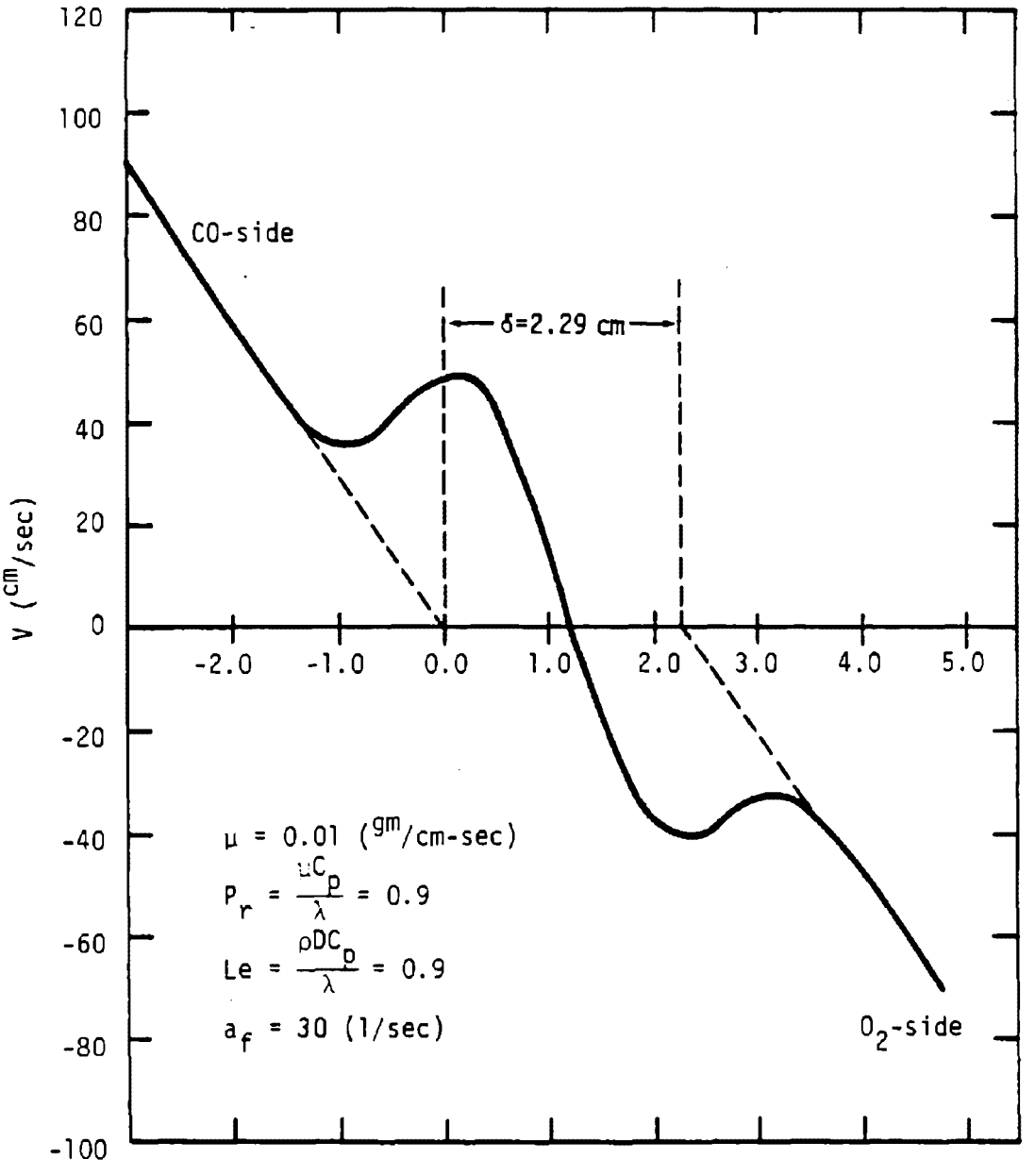

Figure 2. V Velocity of CO/O_2 Opposed Jet Diffusion Flame.

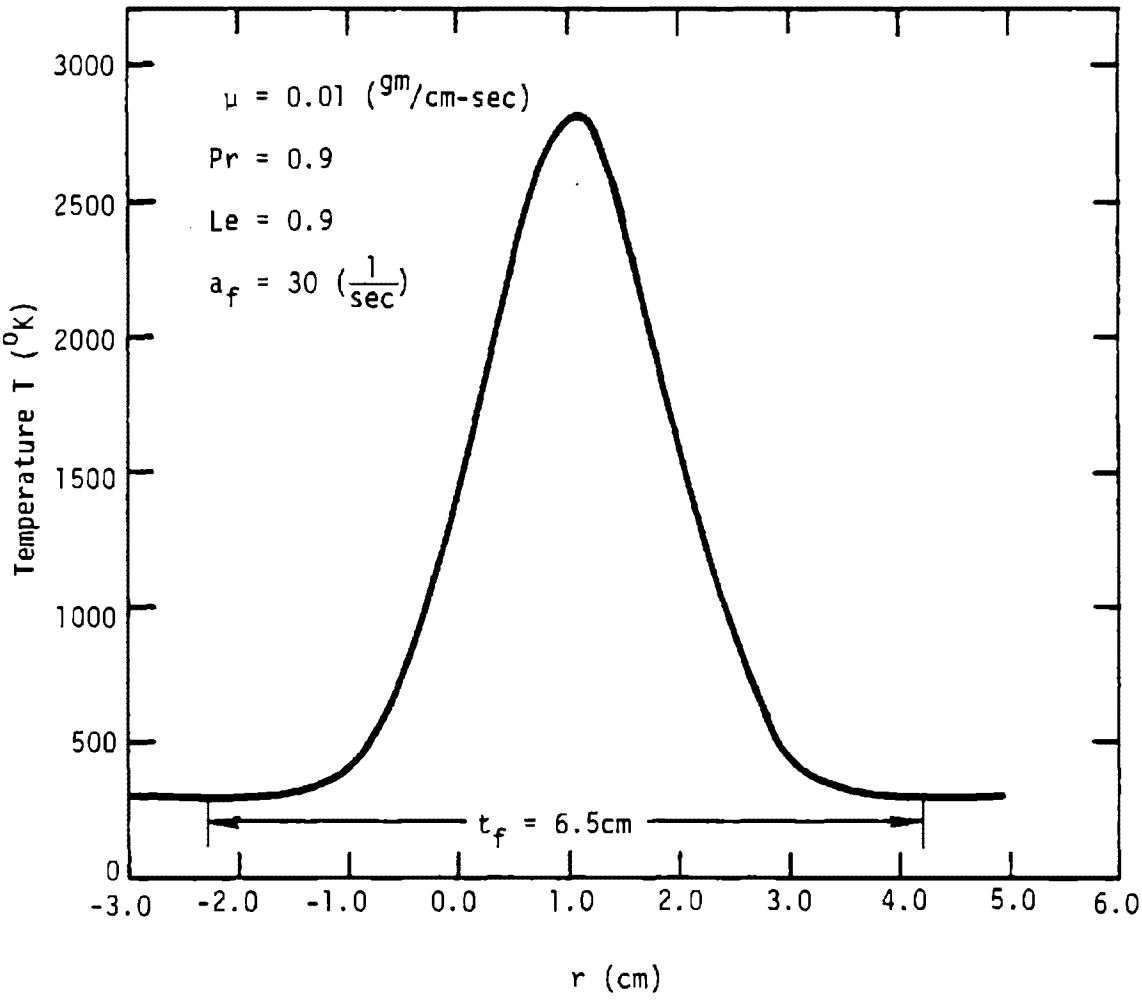

Figure 3. Temperature Profile of CO/O_2 Opposed-Jet Diffusion Flame.

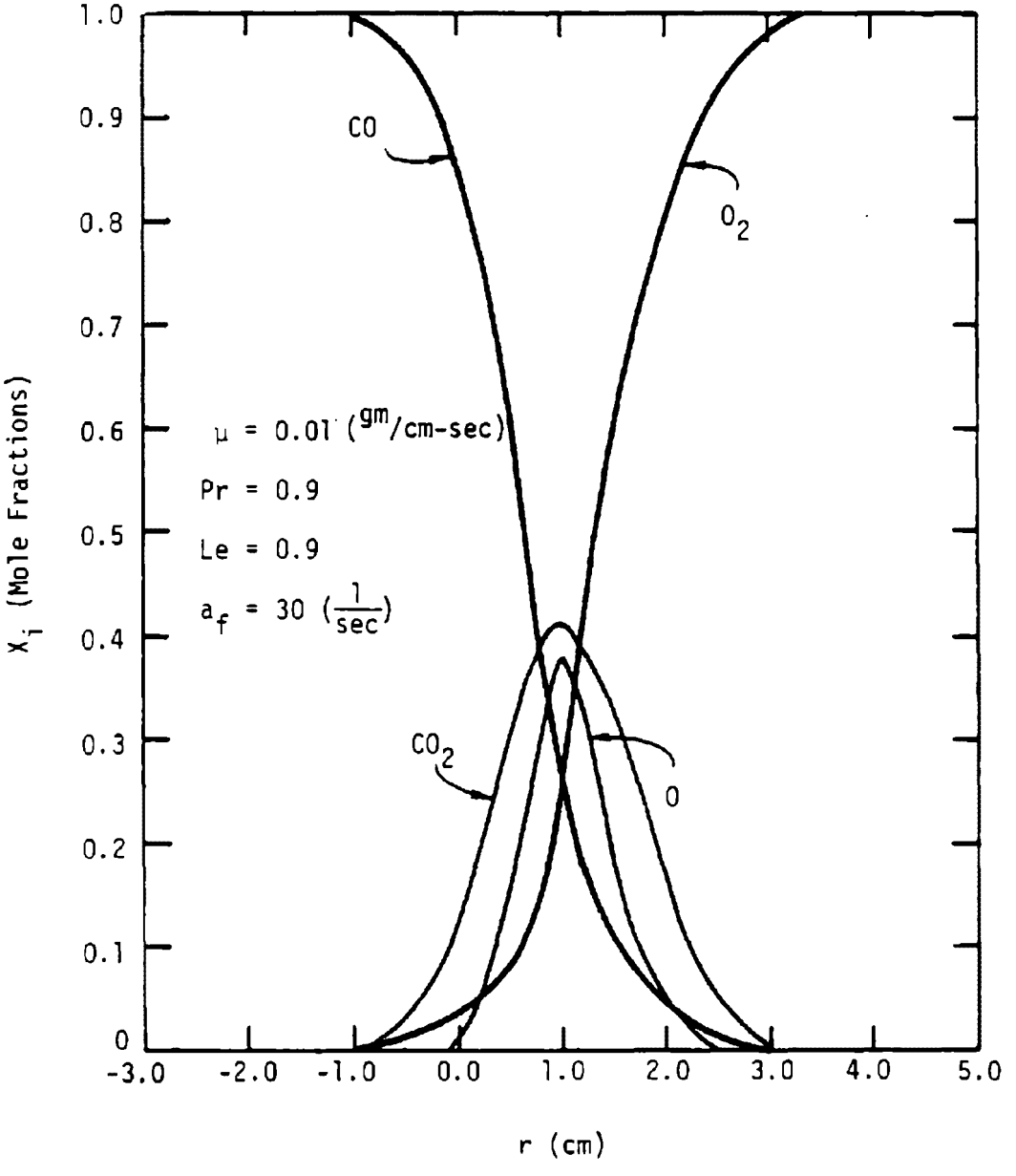

Figure 4. Species Distribution of CO/O_2 Opposed-Jet Diffusion Flame.

$$\frac{\partial X_i}{\partial x} = 0 \qquad (2\text{-}4c)$$

$$\frac{\partial T}{\partial x} = 0 \qquad (2\text{-}4d)$$

are satisfied for the entire flow field.

2.1 Coordinate Transformation

Two elliptic test cases are generated by coordinate transformation of the opposed-jet diffusion flame flow field in the following manner (see Figure 5):

(a) Rotating the coordinate axes x-y by a positive (counterclockwise) angle, to the axes x'-y' (see Figure 5a). The transformation can be expressed mathematically by the equations:

$$\begin{cases} x = x' \cos \alpha + y' \sin \alpha \\ y = -x' \sin \alpha + y' \cos \alpha \end{cases}$$

and

$$\begin{cases} U = U' \cos \alpha + V' \sin \alpha \\ V = -U' \sin \alpha + V' \cos \alpha \end{cases}$$

(b) Carving out a rectangular domain (x'_m , y'_m) to define the boundaries of the flow field (see Figure 5b). y_m is taken to be $2y_1$ (i.e. symmetric with respect to y'-axis).

(c) Translating the coordinate axes x'-y' to the axes x"-y" which have origin at the left-lower corner of the rectangular domain, the axis y" on left boundary and axis x" on bottom boundary (see Figure 5c), or mathematically:

$$x' = x'' - (x_m - x_1)$$
$$y' = y'' - (y_m - y_1)$$

and

$$U'' = U'$$
$$V'' = V'$$

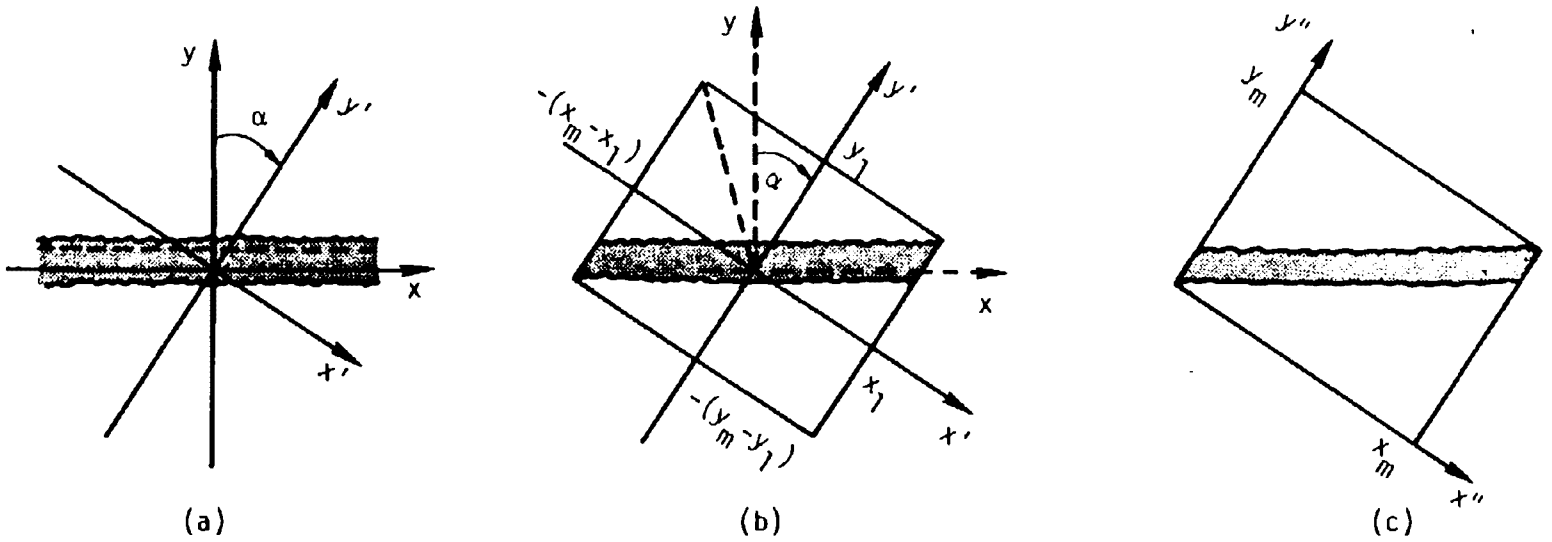

Figure 5. Schematic of Coordinate Transformation of an Opposed-Jet Diffusion Flame.

Boundary conditions for the rectangular domain are transformed according to the above equations.

2.2 Limitation of the Angle of Rotation - α

As is shown in Figure 6, inflowing conditions are physically meaningful on boundaries $\overline{AD}$ and $\overline{BC}$ (i.e. all independent variables are specified), while outflowing conditions are meaningful on boundaries $\overline{AB}$ and $\overline{DC}$ (i.e. only derivatives of the variables are specified). In order to maintain outflow conditions on boundaries $\overline{AB}$ and $\overline{DC}$, two criteria that limit the angle of rotation (i.e. α) must be satisfied:

- There is net outflow at points A and C (i.e. $\theta_2 \geq \alpha$). θ_2 is the angle between net flow direction and $\overline{AB}$.
- The flame zone does not appear on boundaries $\overline{AB}$ and $\overline{BC}$.

Geometrically (see Figure 6), the distance between point D and the intersection of $\overline{DC}$ and the x-axis is:

$$S = y_1 - x_1 \tan \alpha$$

or

$$\frac{S}{x_1} = \frac{y_1}{x_1} - \tan \alpha = \cot(\alpha + \theta_1) - \tan \alpha \qquad (2\text{-}5)$$

Assuming δ is small in comparison with the dimension of the rectangular domain, θ_2 is approximately equal to θ_1 since

$$\tan \theta_1 = \frac{x}{y}$$

and

$$\tan \theta_2 = \frac{U}{-V} = \frac{x}{y-\delta}$$

In the limiting situation in which velocity at point A is tangential to boundary $\overline{AB}$:

$$\theta_2 \simeq \theta_1 \simeq \alpha$$

and the flame is barely touching the upper boundary $\overline{AD}$.

$$\frac{S}{x_1} = \cot(2\alpha) - \tan \alpha = 0$$

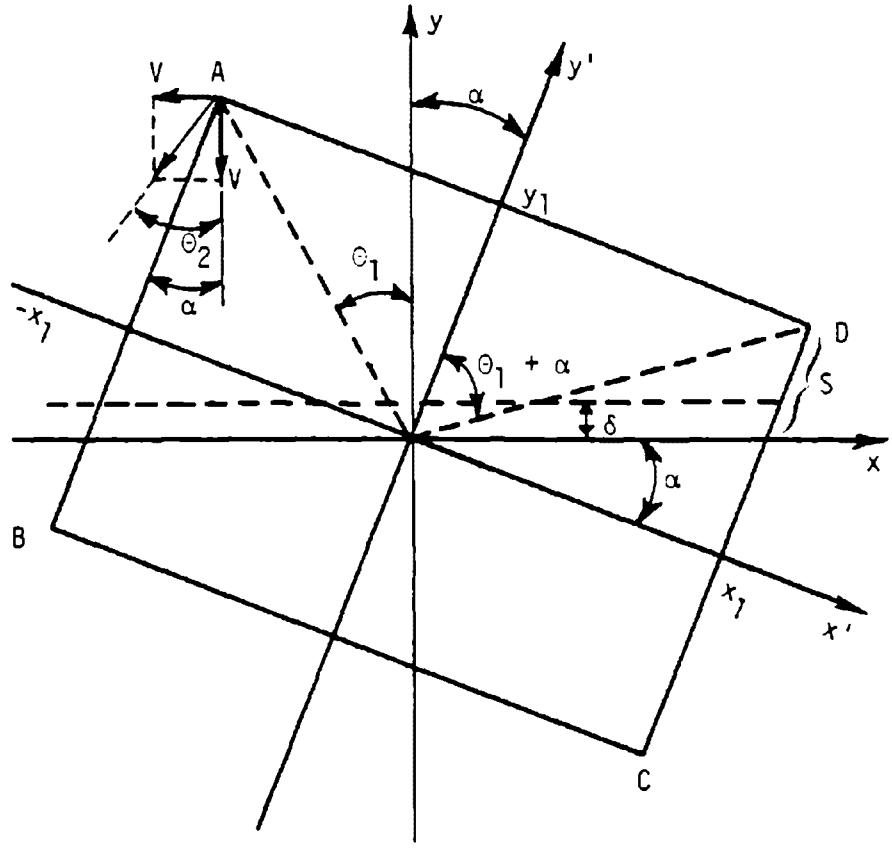

Figure 6. Limitation of the Angle of Rotation α.

Solving for gives:

$$\alpha = 30^{0}$$

which is the maximum angle of rotation. The same conclusion can also be drawn by analyzing the flow direction at point C.

2.3 Test Cases No. 1 and No. 2

The boundary conditions for test cases No. 1 and No. 2 are derived from analysis of the same opposed-jet diffusion flame which is rotated by an angle $\alpha = 25^{0}$. The only difference between case No. 1 and case No. 2 is the size of the rectangular domain. The parameters for these two cases are specified in Table 1.

The physical flame thickness is obviously the same for both cases No. 1 and 2. However, relative to the y computational domain, case No. 1 represents a thin flame and case No. 2 is a thicker flame. Numerically, a thick flame is easier to analyze since more of the available grid points may be positioned within the region of rapid change. Boundary conditions for these two cases are listed in the Appendix at the end of Part 6.

Table 1.

Parameters for Cases No. 1 and No. 2

Case No.	1	2
Domain (x_m x y_m)	52 x 38	30 x 22.5
y_1 (cm)	19.794603	11.996887
x_1 (cm)	26.0	15.0
α (deg.)	25.0	25.0
a_f ($\frac{1}{sec}$)	30.00	30.00
a_o ($\frac{1}{sec}$)	28.0685	28.0685
T_f (^{o}K)	300.00	300.00
Ta (^{o}K)	300.00	300.00
fuel type	CO	CO
oxidizer type	O_2	O_2
μ(^{gm}/cm-sec)	0.01	0.01
Pr	0.9	0.9
Le	0.9	0.9

3.0 COFLOWING-JET DIFFUSION FLAME

The coflowing planar jet-boundary diffusion flame calculation is performed using GFAP. As shown in Figure 7, the upper flow is from an oxidizer jet which contains pure O_2 at 300°K. The lower flow is from a fuel jet which contains pure CO at 300°K. The mainstream velocity of oxidizer jet is 1500 cm/sec and the fuel jet velocity is 750 cm/sec. Numerically, the cross-stream velocity on the fuel side is forced to zero at $y \leq 0$ in the coordinates shown in Figure 7, while the cross-stream velocity on the oxidizer side is left to be calculated. Figure 8 shows the edge cross-stream velocity on the upper flame boundary. Prandtl and Lewis numbers are assumed to be 0.9. Figure 7 also presents the upper and lower flame zone boundaries and the locus of peak temperature in the flame zone.

3.1 Test Case No. 3

To produce elliptic test case No. 3 the following coordinate transformations are made:

(a) Translating the origin of the coordinate system x-y to x=12.433, y=13.0, which is an arbitrarily selected point on the locus of peak temperature. The new axes are denoted by x' - y'.

(b) Rotating the coordinate axes x'-y' by a positive angle (counterclockwise) $\alpha = 25°$, to the new axes x"-y".

(c) Translating the origin of the coordinate axes x"-y" downward to x" = 0, y" = -15.0. The new coordinate axes are represented by x"'-y"'.

Figure 9 shows the flame after the transformation. Boundary conditions on all four sides of the domain (250 cm x 180 cm) are obtained in the following manner:

- The bottom (fuel-side) boundary condition can be determined analytically by
  $U"' = U \cos \alpha$
  $V"' = U \sin \alpha$
  since V = 0 is assumed on the fuel-side.
- The upper (oxidizer side) boundary condition can be obtained by
  $U"' = U \cos \alpha - V \sin \alpha$
  $V"' = U \sin \alpha + V \sin \alpha$

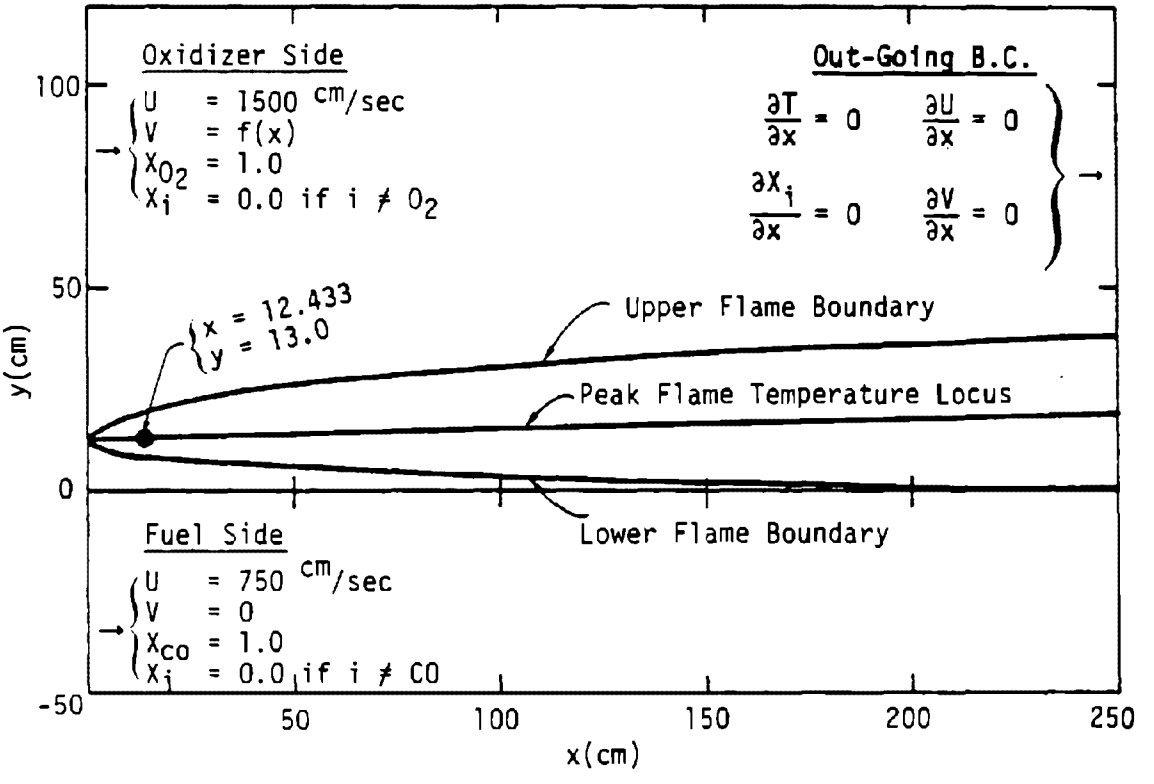

Figure 7. Planar Co-Flowing Jet Diffusion Flame of CO/O_2 (in original coordinates).

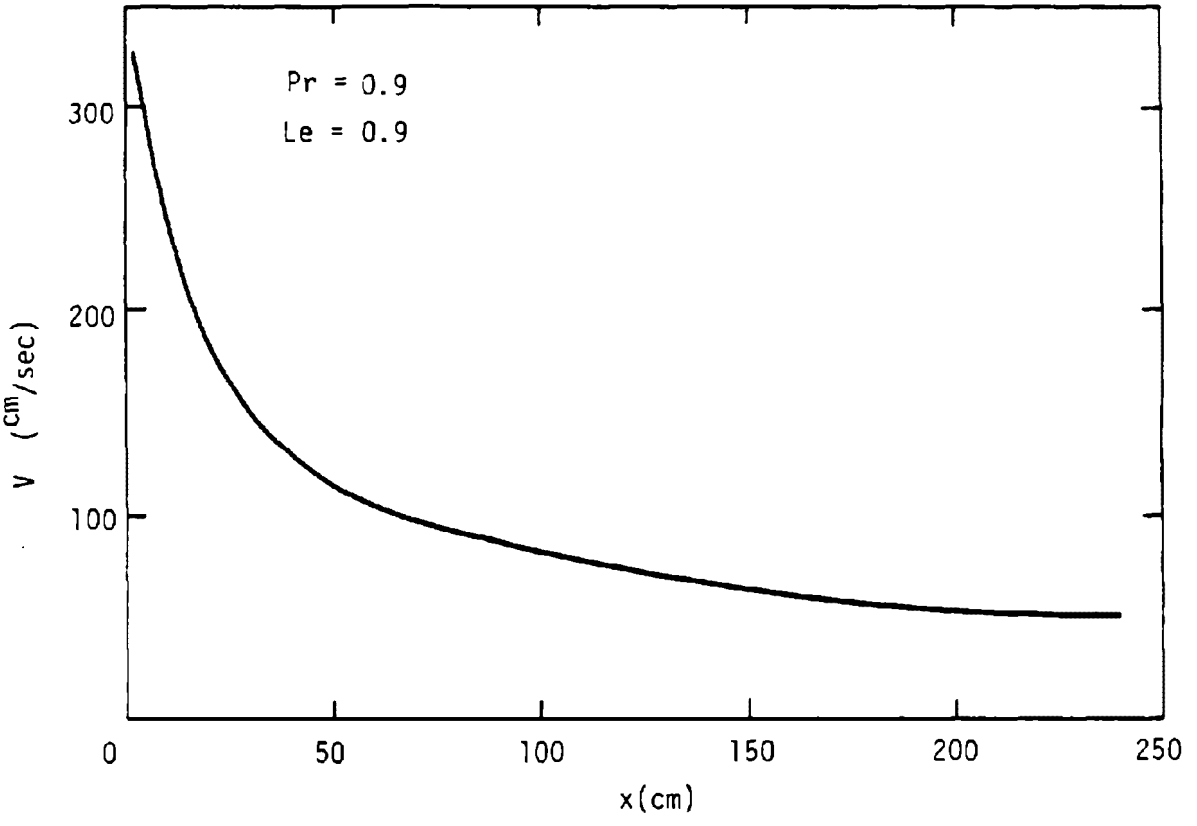

Figure 8. Edge Velocity on Upper Flame Boundary (in original coordinates).

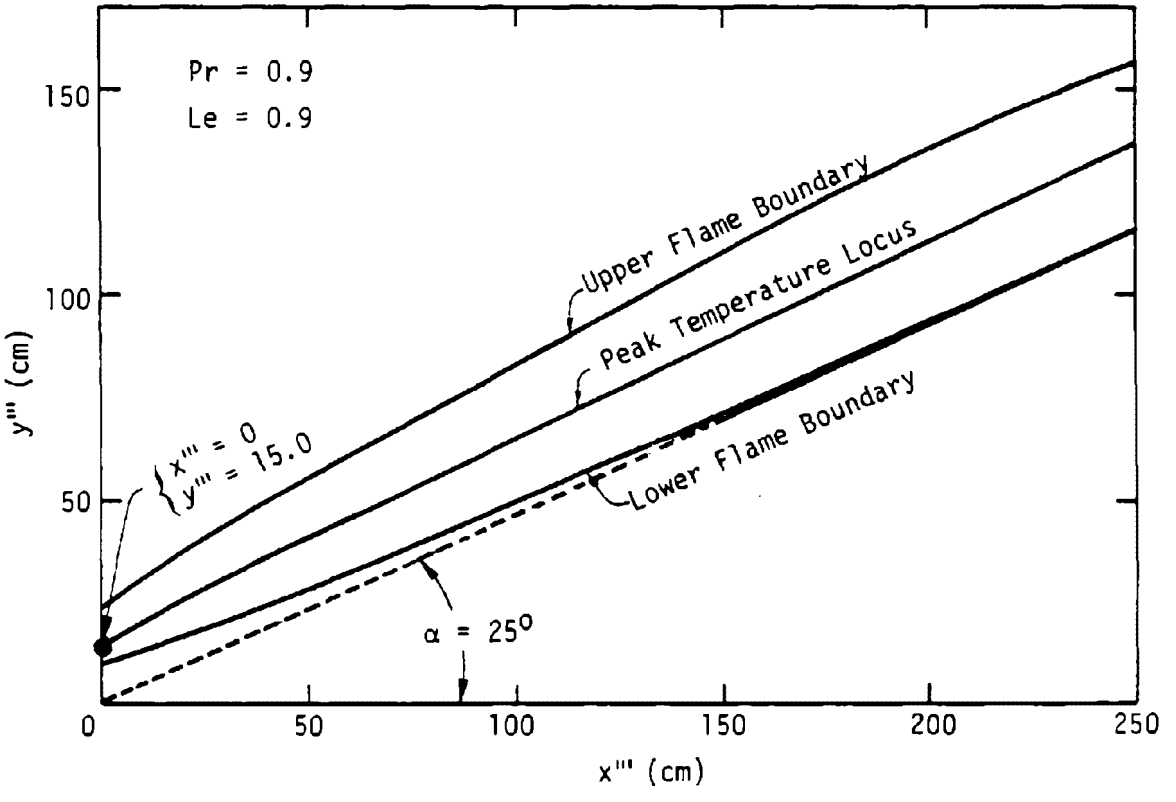

Figure 9. Planar Co-flowing Jet Diffusion Flame of CO/CO_2 (in transformed coordinates).

where V is obtained by curve fitting the numerical result (Figure 8).

- The left-hand side ($x''' = 0$) boundary condition can be divided into three portions:
  1. The region from the coordinate origin to the lower flame boundary ($y''' = 10$ cm): The boundary condition in this portion is the same as that of the bottom boundary.
  2. Flame zone ($h''' = 10$ cm to 20 cm): The boundary condition is provided by the fine plots from the numerical results of GFAP code.
  3. The portion above the flame zone ($y''' > 20$ cm): The boundary condition in this portion is the same as that of the upper boundary.
- The right-hand side ($x''' = 250$) boundary condition is the transformed outgoing boundary condition.

The complete details of the boundary conditions can be found in the Appendix.

4.0 REFERENCES

1. Stull, D. R., and Prophet, H., "JANAF Thermochemical Tables - Second Edition," NSRDS-NBS37, Dow Chemical Co. (1979).

2. Kau, C. J., and Tyson, T. J., "Fundamental Combustion Research Applied to Pollution Control, Vol IV: Engineering Analysis, Part 1: A Computer Program for General Flame Analysis," EERC Final Report, Contract No. 68-02-2631 (1987).

APPENDIX

The boundary conditions for all three cases of the first group of elliptic-code test cases are presented in this appendix. For simplicity, the superscripts (i.e. " ' ", " " ", and " "' ") which were used to differentiate variables in different coordinate systems during coordinate transformation are all dropped in this section.

TEST CASE NO. 1

1. Geometry: Planar with boundary conditions on rectangular coordinate lines

2. Species Present: CO, CO_2, O_2, O (All thermodynamic properties from JANNAF tables)

3. Reaction Mechanism:

Reaction	Rate (mole-cc-sec system)
$CO + O_2 \rightleftarrows CO_2 + O$	$k_f = 6.905 \times 10^7 \, T \exp(-34810/RT)$
$CO + O + M \rightleftarrows CO_2 + M$	$k_f = 3.8 \times 10^{24} \, T^{-3} \exp(-6170/RT)$
$O + O + M \rightleftarrows O_2 + M$	$k_f = 1.4 \times 10^{18} \, T^{-1} \exp(-340/RT)$

4. Transport Properties:

Constant Equivalent Molecular Viscosity: $\mu = 0.01$ gm/cm-sec
Constant Prandtl No.: Pr = 0.9
Constant Lewis No.: Le = 0.9

5. Pressure: P = 1.0 atm at (x = 0, y = 0)

6. Boundary Conditions:

(I) at y = 0, ($0 \leq x \leq 52$ cm)

$T = 300^{o}K$

$\begin{cases} X_{CO} = 1.0 \\ X_i = 0 \text{ if } i \neq CO \end{cases}$

$U = 19.2836x - 919.75789$ ($^{cm}/_{sec}$)

$V = 22.98133x - 246.44847$ ($^{cm}/_{sec}$)

(II) at y = 38 cm, ($0 \leq x \leq 52$ cm)

$T = 300^{o}K$

$\begin{cases} X_{O_2} = 1.0 \\ X_i = 0 \text{ if } i \neq O_2 \end{cases}$

$U = 18.04084x - 70.64078$ ($^{cm}/_{sec}$)

$V = 21.501718x - 857.9259$ ($^{cm}/_{sec}$)

(III) at $x = 0$, $(0 \leq y \leq 38\ cm)$

$$\frac{\partial T}{\partial x} + 0.4663 \frac{\partial T}{\partial y} = 0$$

$$\frac{\partial X_i}{\partial x} + 0.4663 \frac{\partial X_i}{\partial y} = 0$$

$$\frac{\partial U}{\partial x} + 0.4663 \frac{\partial U}{\partial y} + \left(\frac{2.1445}{73.9625 - y}\right)U + \left(\frac{1}{73.9625 - y}\right)V = 0$$

$$\frac{\partial V}{\partial x} + 0.4663 \frac{\partial V}{\partial y} + \left(\frac{1}{73.9625 - y}\right)U + \left(\frac{0.4663}{73.9625 - y}\right)V = 0$$

(IV) at $x = 52\ cm$, $(0 \leq y \leq 38\ cm)$

$$\frac{\partial T}{\partial x} + 0.4663 \frac{\partial T}{\partial y} = 0$$

$$\frac{\partial X_i}{\partial x} + 0.4663 \frac{\partial X_i}{\partial y} = 0$$

$$\frac{\partial U}{\partial x} + 0.4663 \frac{\partial U}{\partial y} - \left(\frac{2.1445}{37.5517 + y}\right)U - \left(\frac{1}{37.5517 + y}\right)V = 0$$

$$\frac{\partial V}{\partial x} + 0.4663 \frac{\partial V}{\partial y} - \left(\frac{1}{37.5517 + y}\right)U - \left(\frac{0.4663}{37.5517 + y}\right)V = 0$$

7. Steady State

8. Solve for Ignited Solution

TEST CASE NO. 2

1. Geometry: Planar with boundary conditions on rectangular coordinate lines

2. Species Present: CO, CO_2, O_2, O (All thermodynamic properties from JANNAF tables)

3. Reaction Mechanism:

Reaction	Rate (mole-cc-sec system)
$CO + O_2 \rightleftarrows CO_2 + O$	$k_f = 6.905 \times 10^7 \, T \exp(-34810/RT)$
$CO + O + M \rightleftarrows CO_2 + M$	$k_f = 3.8 \times 10^{24} \, T^{-3} \exp(-6170/RT)$
$O + O + M \rightleftarrows O_2 + M$	$k_f = 1.4 \times 10^{18} \, T^{-1} \exp(-340/RT)$

4. Transport Properties:

   Constant Equivalent Molecular Viscosity: $\mu = 0.01$ gm/cm-sec
   Constant Prandtl No.: $Pr = 0.9$
   Constant Lewis No.: $Le = 0.9$

5. Pressure: $P = 1.0$ atm at $(x = 0, y = 0)$

6. Boundary Conditions:

   (I) at $y = 0$, $(0 \leq x \leq 30$ cm)

   $T = 300^{o}K$

   $\begin{cases} X_{CO} = 1.0 \\ X_i = 0 \text{ if } i \neq CO \end{cases}$

   $U = 19.2836x - 530.6299$ (^{cm}/sec)

   $V = 22.98133x - 142.1818$ (^{cm}/sec)

   (II) at $y = 22.5$ cm, $(0 \leq x \leq 30$ cm)

   $T = 300^{o}K$

   $\begin{cases} X_{O_2} = 1.0 \\ X_i = 0 \text{ if } i \neq O_2 \end{cases}$

   $U = 18.04084x - 39.8421$ (^{cm}/sec)

   $V = 21.501718x - 480.6995$ (^{cm}/sec)

(III) at $x = 0$ $(0 \leq y \leq 22.5 \text{ cm})$

$$\frac{\partial T}{\partial x} + 0.4663 \frac{\partial T}{\partial y} = 0$$

$$\frac{\partial X_i}{\partial x} + 0.4663 \frac{\partial X_i}{\partial y} = 0$$

$$\frac{\partial U}{\partial x} + 0.4663 \frac{\partial U}{\partial y} - \frac{U}{(0.4663y - 19.8976)} - \frac{0.4663\ V}{(0.4663y - 19.8976)} = 0$$

$$\frac{\partial V}{\partial x} + 0.4663 \frac{\partial V}{\partial y} - \frac{0.4663\ U}{(0.4663y - 19.8976)} - \frac{0.2174\ V}{(0.4663y - 19.8976)} = 0$$

(IV) at $x = 30$ cm $(0 \leq y \leq 22.5 \text{ cm})$

$$\frac{\partial T}{\partial x} + 0.4663 \frac{\partial T}{\partial y} = 0$$

$$\frac{\partial X_i}{\partial x} + 0.4663 \frac{\partial X_i}{\partial y} = 0$$

$$\frac{\partial U}{\partial x} + 0.4663 \frac{\partial U}{\partial y} - \frac{U}{(0.4663y + 10.1023)} - \frac{0.4663\ V}{(0.4663y + 10.1023)} = 0$$

$$\frac{\partial V}{\partial x} + 0.4663 \frac{\partial V}{\partial y} - \frac{0.4663\ U}{(0.4663y + 10.1023)} - \frac{0.2174\ V}{(0.4663y + 10.1023)} = 0$$

7. Steady State

8. Solve for Ignited Solution

TEST CASE NO. 3

1. Geometry: Planar with boundary conditions on rectangular coordinate lines

2. Species Present: CO, CO_2, O_2, O (All thermodynamic properties from JANNAF tables)

3. Reaction Mechanism:

Reaction	Rate (mole-cc-sec system)
$CO + O_2 \rightleftarrows CO_2 + O$	$k_f = 6.905 \times 10^7\ T \exp(-34810/RT)$
$CO + O + M \rightleftarrows CO_2 + M$	$k_f = 3.8 \times 10^{24}\ T^{-3} \exp(-6170/RT)$
$O + O + M \rightleftarrows O_2 + M$	$k_f = 1.4 \times 10^{18}\ T^{-1} \exp(-340/RT)$

4. Transport Properties:

Constant Equivalent Molecular Viscosity: $\mu = 0.01$ gm/cm-sec
Constant Prandtl No.: $Pr = 0.9$
Constant Lewis No.: $Le = 0.9$

5. Pressure: $P = 1.0$ atm at $(x = 0, y = 0)$

6. Boundary Conditions:

(I) $y = 0,\ (0 \leq x \leq 250$ cm)

$U = 679.73$ (cm/sec)
$V = 316.90$ (cm/sec)
$T = 300^oK$
$X_{CO} = 1.0$
$X_i = 0$ if $i \neq CO$

(II) $y = 180$ cm $(0 \leq x \leq 250$ cm)

$U = 1323.09 + 0.1472x - 2.5301 \times 10^{-4} x^2$ (cm/sec)
$V = 711.72 - 0.3126x + 5.3508 \times 10^{-4} x^2$ (cm/sec)
$T = 300^oK$
$X_{O_2} = 1.0$
$X_i = 0$ if $i \neq O_2$

(III) $x = 250$ cm $(0 \leq y \leq 180$ cm$)$

$$\frac{\partial T}{\partial x} + 0.4964 \frac{\partial T}{\partial y} = 0$$

$$\frac{\partial X_i}{\partial x} + 0.4964 \frac{\partial X_i}{\partial y} = 0 \quad \text{for all } i$$

$$\frac{\partial U}{\partial x} + 0.4964 \frac{\partial U}{\partial y} - \frac{U}{(x + 0.4964y)} - \frac{V}{(2.0145x + y)} = 0$$

$$\frac{\partial V}{\partial x} + 0.4964 \frac{\partial V}{\partial y} - \frac{(0.4964)U}{(x + 0.4964y)} - \frac{(0.4964)V}{(2.0145x + y)} = 0$$

(IV) $x = 0$

(i) $0 \leq y \leq 10$ cm

$U = 679.73$

$V = 316.90$

$T = 300^{o}K$

$X_{CO} = 1.0$

$X_i = 0.0$ if $i \neq CO$

(ii) 10 cm $\leq y \leq 20$ cm

See Figures A1-A6 for U, V, T, X_{CO}, X_{O_2}, X_O and X_{CO_2}

(iii) 20 cm $\leq y \leq 180$ cm

$U = 1254.39 + 0.7622y - 2.114 \times 10^{-3} y^2$

$V = 859.38 - 1.642y + 4.565 \times 10^{-3} y^2$

$T = 300^{o}K$

$X_{O_2} = 1.0$

$X_i = 0.0$ if $i \neq O_2$

7. Steady State

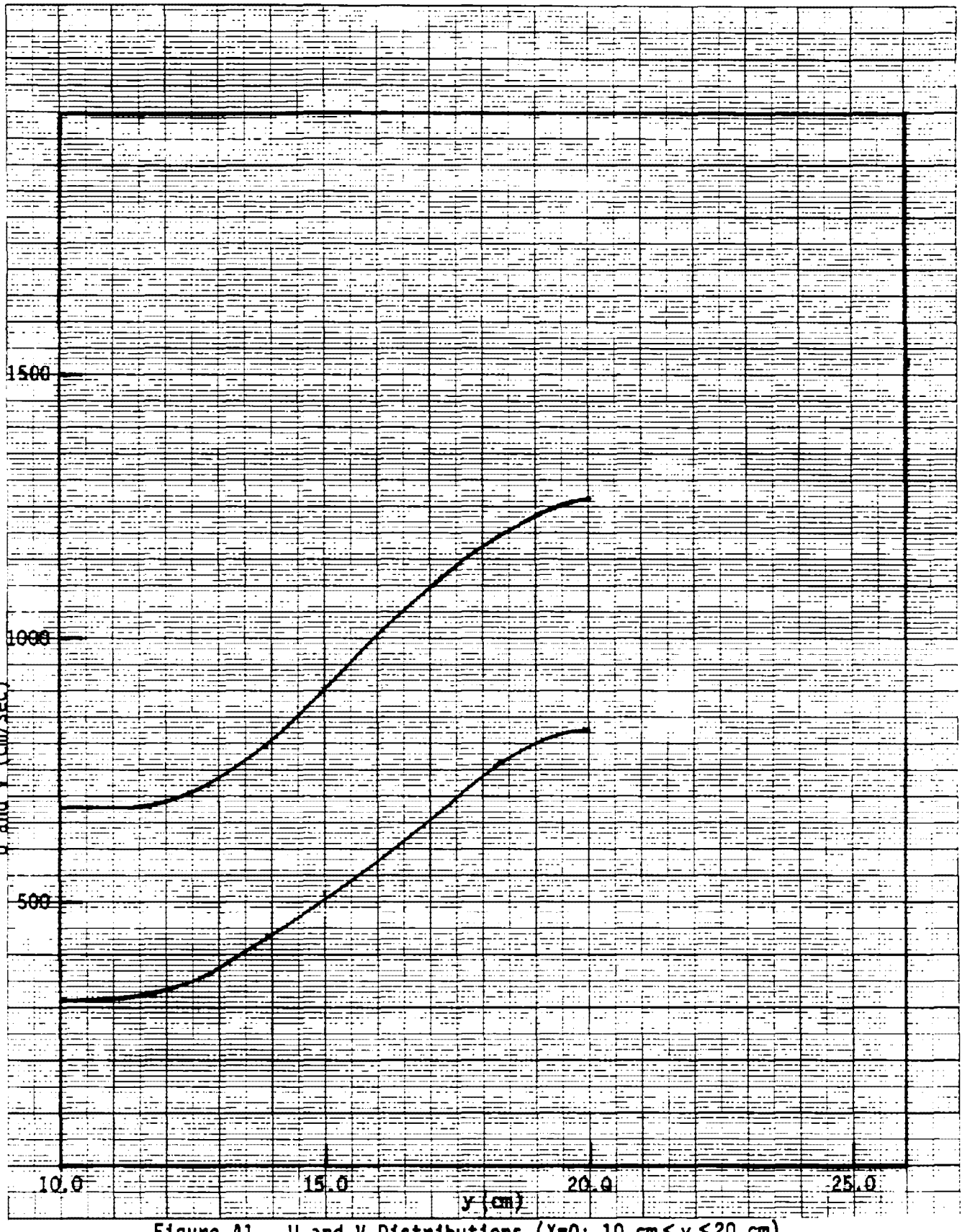

Figure A1. U and V Distributions (X=0; 10 cm ≤ y ≤ 20 cm).

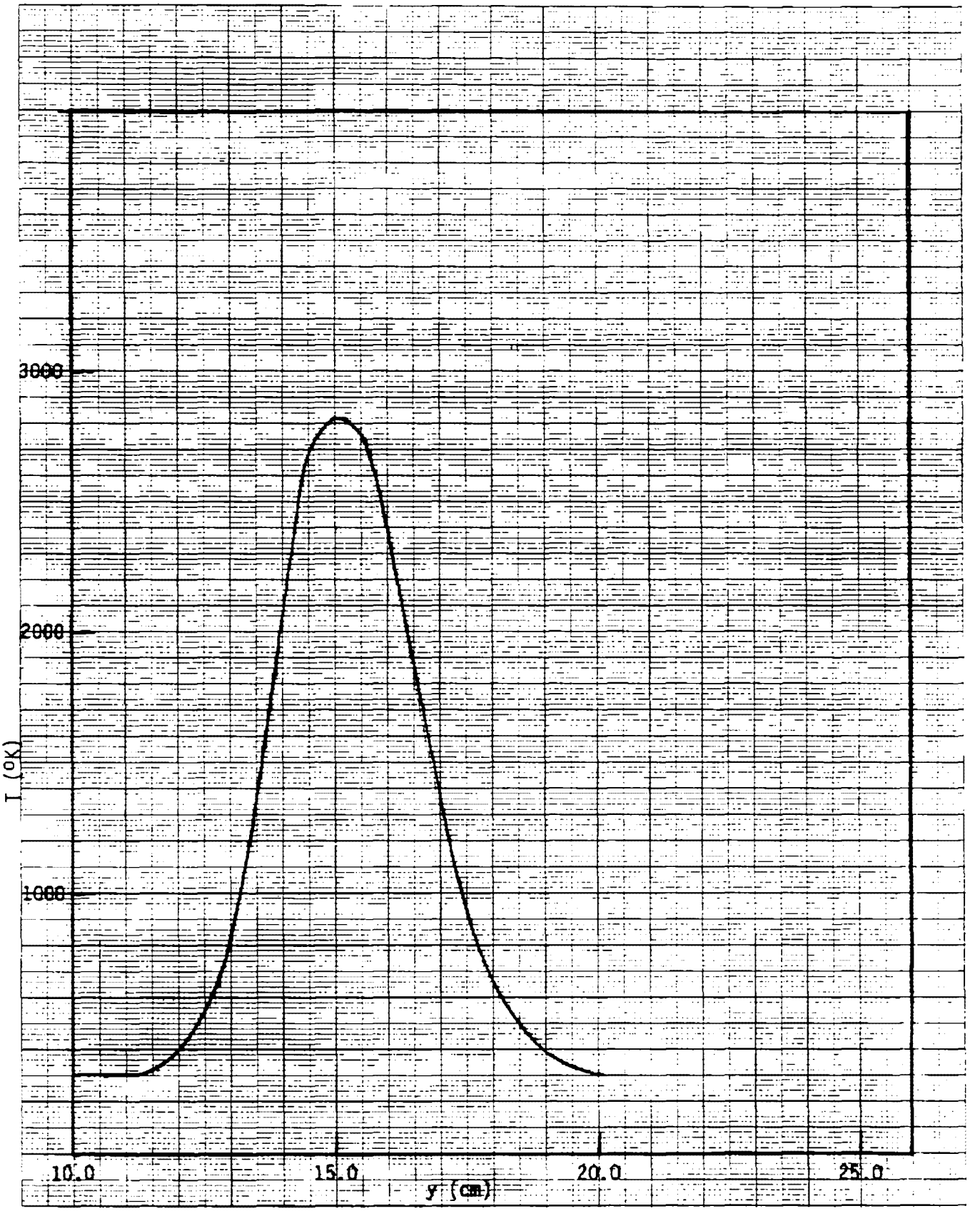

Figure A2. Temperature Distribution (X=0; 10 cm ≤ y ≤ 20 cm).

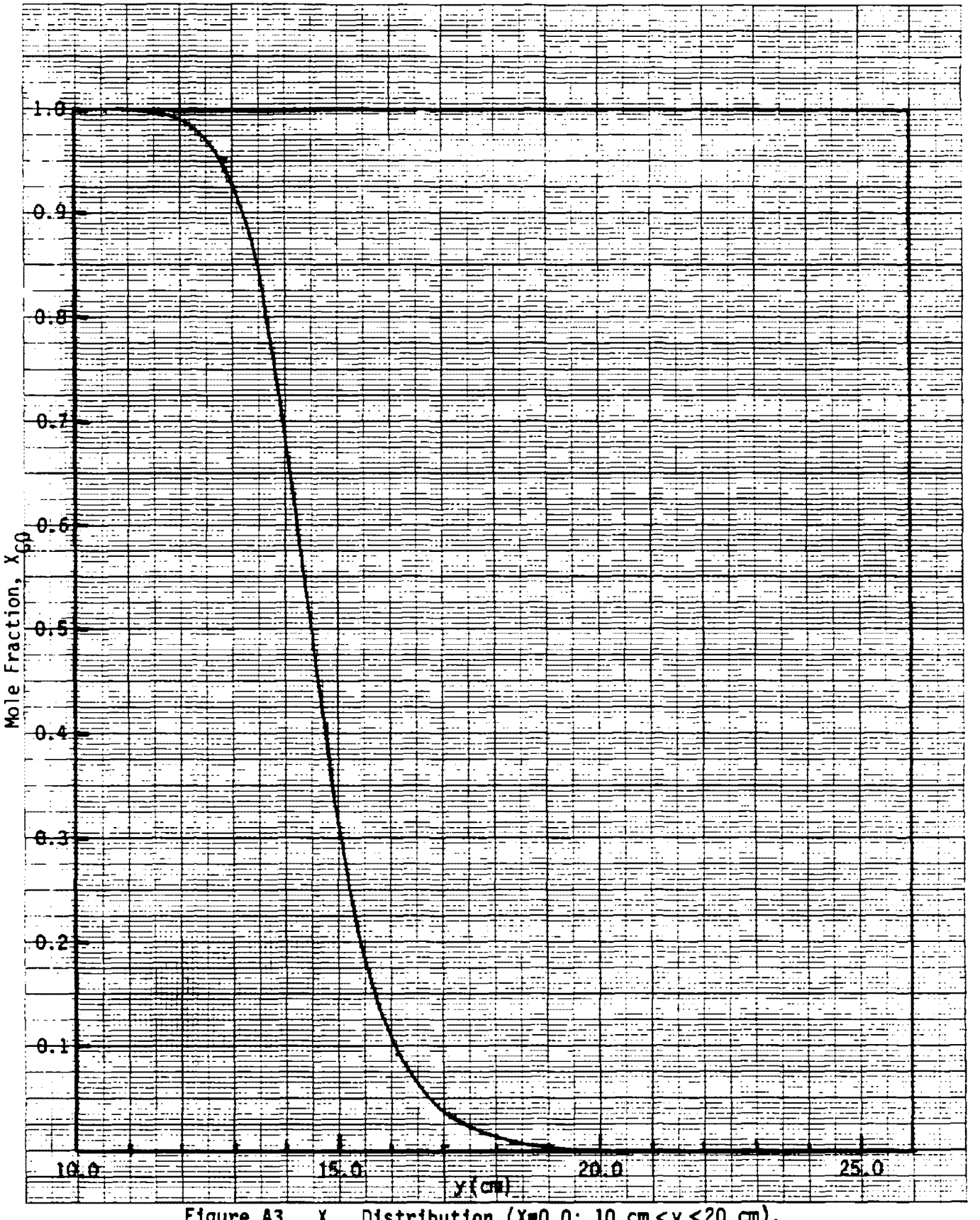

Figure A3. X_{CO} Distribution (X=0.0; 10 cm ≤ y ≤ 20 cm).

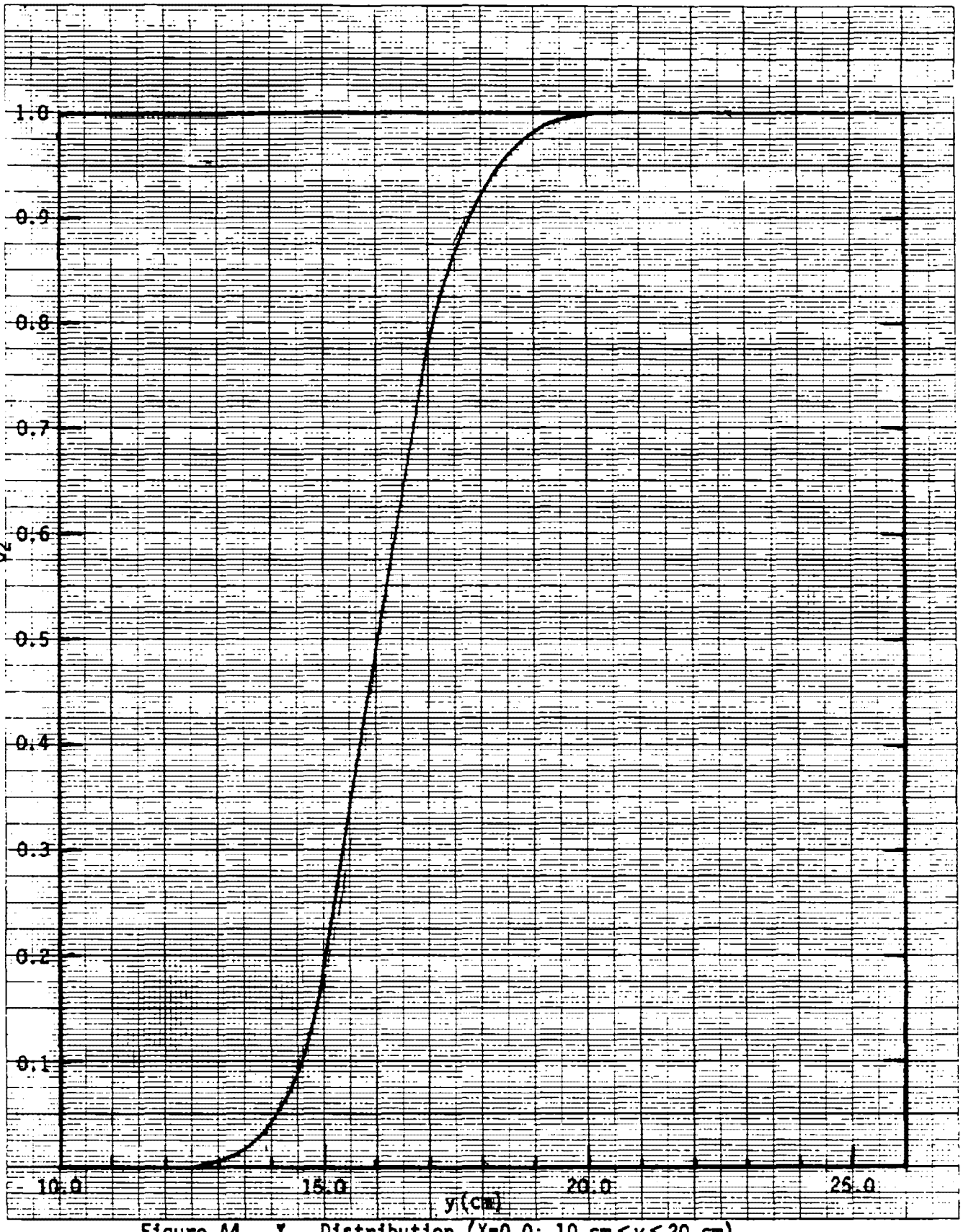

Figure A4. X_{O_2} Distribution (X=0.0; 10 cm ≤ y ≤ 20 cm).

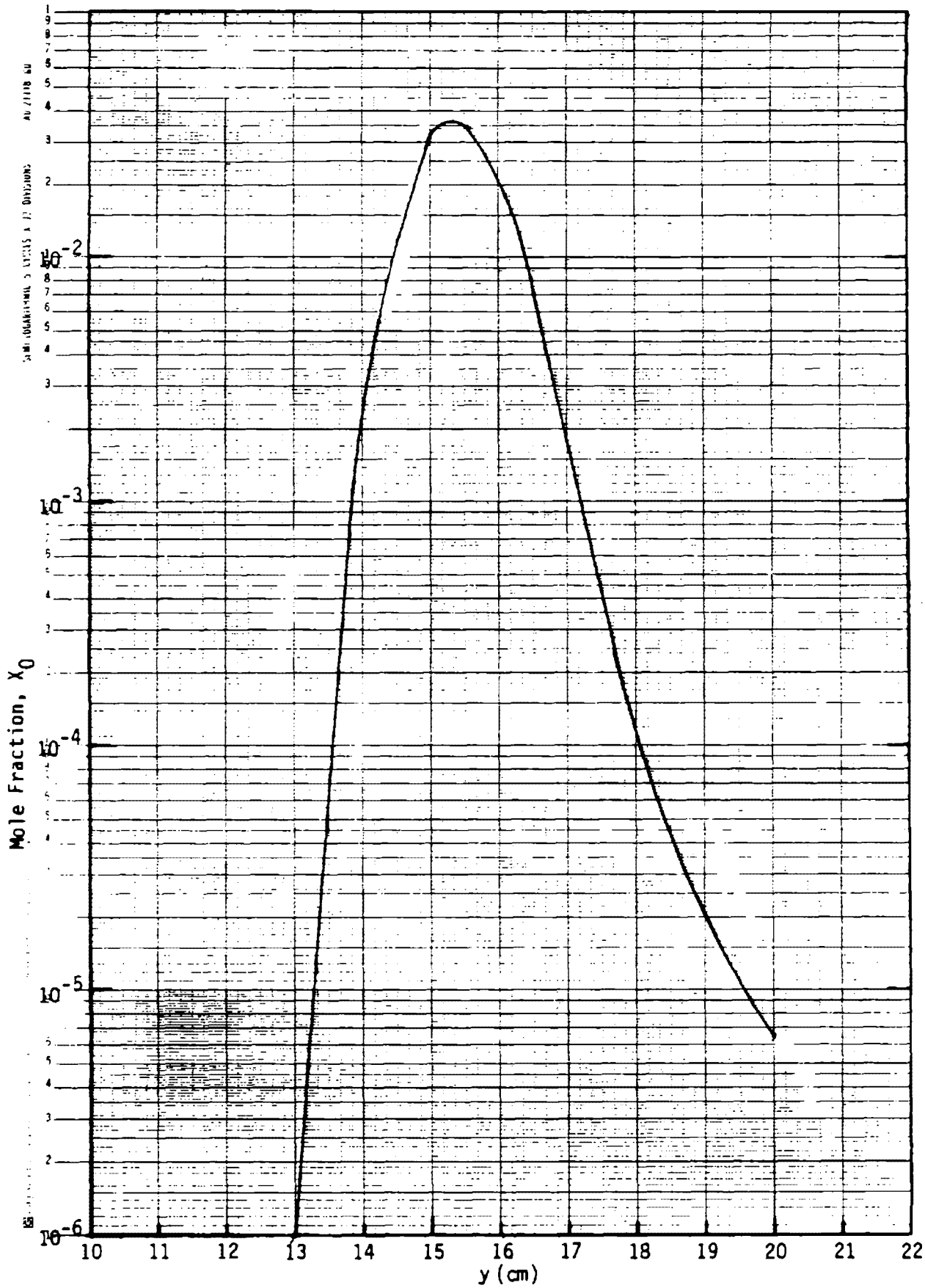

Figure A5. X_0 Distribution (X=0.0; 10 cm ≤ y ≤ 20 cm).

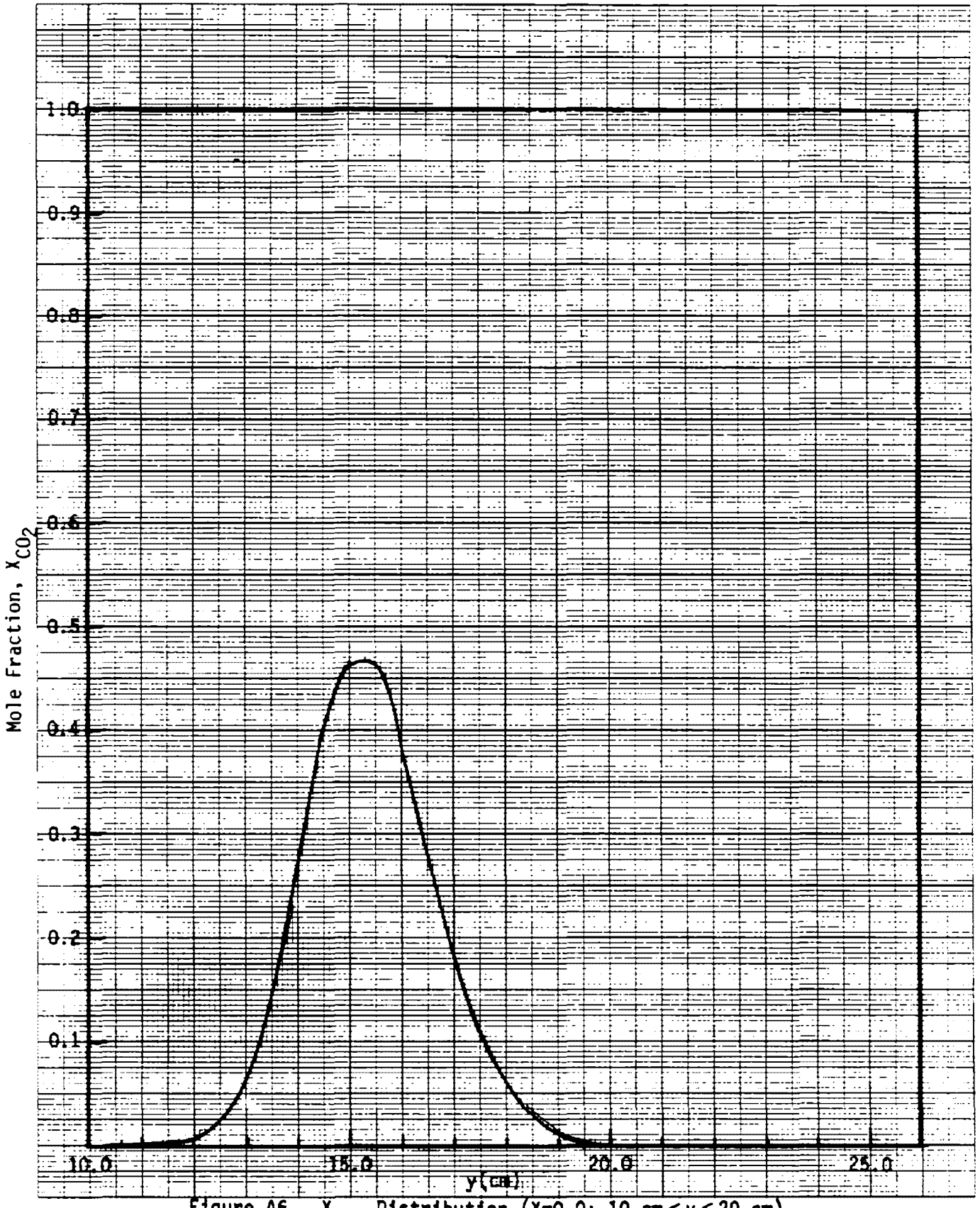

Figure A6. X_{CO_2} Distribution (X=0.0; 10 cm ≤ y ≤ 20 cm).